



**HAL**  
open science

# Monitoring artificial structures construction layers using microwave methods

Sergei Sulavko

► **To cite this version:**

Sergei Sulavko. Monitoring artificial structures construction layers using microwave methods. Materials. Le Mans Université; Rostovskij gosudarstvennyj universitet, 2021. English. NNT: 2021LEMA1016 . tel-03515132

**HAL Id: tel-03515132**

**<https://theses.hal.science/tel-03515132>**

Submitted on 6 Jan 2022

**HAL** is a multi-disciplinary open access archive for the deposit and dissemination of scientific research documents, whether they are published or not. The documents may come from teaching and research institutions in France or abroad, or from public or private research centers.

L'archive ouverte pluridisciplinaire **HAL**, est destinée au dépôt et à la diffusion de documents scientifiques de niveau recherche, publiés ou non, émanant des établissements d'enseignement et de recherche français ou étrangers, des laboratoires publics ou privés.



# THESE DE DOCTORAT DE

LE MANS UNIVERSITE

ECOLE DOCTORALE N° 596

*Matière, Molécules, Matériaux*

Spécialité : « *Département de physique* »

**« Monitoring artificial structures construction layers using microwave methods »**

Par

**« Sergei SULAVKO »**

Thèse présentée et soutenue à « **Université Fédérale du Sud** », le « **19 mai 2021** »

Unité de recherche : **Département de physique**

Thèse N° : 2021LEMA1016

## Rapporteurs avant soutenance :

Adrei Kochur PROFESSEUR DES UNIVERSITÉS, Université d'état des transports Rostov

Philippe Daniel PROFESSEUR DES UNIVERSITÉS, LE MANS UNIVERSITÉ

Vyacheslav Zemlyakov Professeur des Universités, Université Fédérale du Sud

## Composition du Jury :

Président : Adrei Kochur

Examineurs : Albane Saintenoy

Florent Calvayrac

Vyacheslav Zemlyakov

Galina Yalovega

Dir. de thèse : Viktor Yavna

Co-dir. de thèse : Philippe Daniel

Professeur des Universités, Université d'état des transports Rostov

MAITRE DE CONFERENCES UNIVERSITÉ PARIS-SACLAY

PROFESSEUR DES UNIVERSITÉS, LE MANS UNIVERSITÉ

Professeur des Universités, Université Fédérale du Sud

Professeur des Universités, Université Fédérale du Sud

Professeur des Universités, Université d'état des transports Rostov

PROFESSEUR DES UNIVERSITÉS, LE MANS UNIVERSITÉ

---

**Titre :** Surveillance des couches de construction de structures artificielles à l'aide de méthodes microondes

**Mots clés :** Propagation du rayonnement micro-ondes; supports multicouches, méthodes optiques et de résonance pour déterminer les propriétés électriques des supports, simulation informatique, effet de la salinité et de la température sur les propriétés électriques des supports, corrélation des propriétés électriques et mécaniques.

**Résumé :** Dans cette étude, une méthode de détermination des propriétés électrophysiques des sols basée sur la méthode GPR combinée à des approches optiques et des mesures de résonance a été développée. Dans le cadre de l'électrodynamique classique, une méthode a été développée pour déterminer les indices de réfraction absolus des couches structurales et les coefficients d'atténuation correspondants dans la gamme des micro-ondes de 1200 à 1700 MHz, basée sur le traitement quantitatif des données GPR. La méthode développée de traitement des données GPR est basée sur l'utilisation d'amplitudes d'ondes réfléchies ; il permet de déterminer les constantes diélectriques et les conductivités électriques des couches structurales avec une erreur ne dépassant pas 10-15%.

Des méthodes de détermination de la constante diélectrique complexe et de l'humidité par la méthode GPR, étalonnées par des mesures en laboratoire, sont proposées et évaluées. L'approche développée permet un diagnostic rapide de l'état des objets étendus, car elle combine les avantages de la méthode GPR à grande vitesse avec un nombre limité de mesures d'étalonnage. Les dépendances de la constante diélectrique et de la conductivité spécifique vis-à-vis de l'humidité ont été étudiées dans un certain nombre de bentonites avec différentes compositions d'ions échangeables. Une corrélation entre ces grandeurs électrophysiques et la plasticité des bentonites est établie.

---

**Title :** Monitoring artificial structures construction layers using microwave methods

**Keywords :** Propagation of microwave radiation; multilayer media, optical and resonance methods for determining the electrical properties of media, computer simulation, salinity and temperature effect on the electrical properties of media, of electrical and mechanical properties correlation.

**Abstract :** In this study, a method for determining the electrophysical properties of soils based on the GPR method combined with optical approaches and resonance measurements was developed. In the framework of classical electrodynamics, a method has been developed for determining the absolute refractive indices of structural layers and corresponding attenuation coefficients in the microwave range of 1200–1700 MHz, based on the quantitative processing of the GPR data. The developed method of processing the GPR data is based on the use of amplitudes of reflected waves; it makes it possible to determine dielectric constants and electrical conductivities of structural layers with an error of not more than 10-15%.

Methods for determining the complex dielectric constant and moisture by the GPR method, calibrated by laboratory measurements, are proposed and assessed. The developed approach allows rapid diagnosing the state of extended objects, since it combines the advantages of the high-speed GPR method with a limited number of calibration measurements. The dependences of the dielectric constant and specific conductivity on the moisture have been investigated in a number of bentonites with different composition of exchangeable ions. A correlation between these electrophysical quantities and the plasticity of bentonites is established.

## Contents

	Introduction	5
1	Chapter 1. Literature review	11
1.1	GPR method	11
1.1.1	GPR equipment	14
1.1.2	Bibliometric analysis	17
1.1.3	Patent analysis	18
1.1.4	GPR on transport	19
1.1.5	Monitoring the density of soils of the railway road bed by GPR	23
1.1.6	GPR method in the construction of subgrade	24
1.2	Direct methods for measuring the electrophysical properties of soils	25
1.2.1	Quasi-optical (in free space) methods	26
1.2.2	Waveguide methods	26
1.2.3	Resonance methods	27
1.3	Conclusions	28
2	Chapter 2. Application of GPR for determining electrophysical properties of structural layers and materials	29
2.1	Method of experimental studies	29
2.2	Theory of the method	31
2.2.1	Determination of structural layers' refractive indices: general case	31
2.2.2	Additional equations for the determination of refractive indices	34
2.2.2.1.	GPR images of local objects	34
2.2.2.2.	Contact of the rigid base and the invert	38
2.2.2.3.	Equations for calculating the absolute refractive indices of the leveling layer and the invert	39
2.3	Numerical procedures for determining the coefficients of attenuation of the electromagnetic field and refractive indices	40
2.3.1	The use of traces to determine the attenuation coefficients for an example of industrial water	40
2.3.2	The use of traces to determine the attenuation coefficients of tunnel structural layers	44
2.3.3	Using the amplitude of the signal reflected by the interface of the structural layers of variable thickness to determine the attenuation coefficient of the leveling layer	47
2.4	Determination of the absolute refractive indices of structural layers	48
2.5.	Selection of refractive indices using phase analysis of radar-grams	52
2.6	Determination of the attenuation coefficient in the leveling layer by the amplitudes of the signals reflected by its boundaries	53
2.7	Results and Discussion	53
2.7.1	Verification of GPR results using alternative methods	51
2.7.2	Contrast of construction layers	55

2.8	Conclusions	57
3	Chapter 3. Resonance method for determining the electrophysical properties of soils and materials	59
3.1	Objectives of the study	59
3.2	Soils model	60
3.3	Analytical models of dielectric constant in soils	61
3.3.1	Water in soils	61
3.3.2	Analytical dielectric permittivity models related to the porosity parameter	64
3.3.3	Models of effective dielectric constant	65
3.4	Designing a cavity resonator for measuring the properties of materials taken from the core	66
3.4.1	Creating a computer model of a cavity resonator, in accordance with the prototype, in the software CST Studio Suite	69
3.5	Software and hardware device for experimental studies of the electrophysical properties of samples	71
3.5.1	Determination of the resonance frequency of electromagnetic waves transmitted through reference samples with known dielectric constant values	73
3.6	An integrated study of the dielectric properties of soils of different moistures by volume resonator method and simultaneous GPR measurements at frequencies of 1.4 GHz.	73
3.7	Determination of the real part of dielectric constant and the conductivity of soil-forming minerals using GPR calibrated method	77
3.8	Determination of sample moisture using calibrated GPR data	80
3.9	Conclusions	81
4	Chapter 4. The effect of soil salinity on the depth of GPR surveys	83
4.1	Materials used	84
4.1.1	Cohesionless materials	84
4.1.2	Cohesive materials	86
4.2	Electrophysical properties of sand	89
4.2.1	Electrophysical properties of wet sand	89
4.2.2	Electrophysical properties of wet saline sand	90
4.2.3	Electrophysical properties of wet saline sand at low temperatures	94
4.3	Some properties of the samples used	95
4.3.1	Electrophysical properties of bentonite "Dusch"	97
4.3.1.1	Determination of the accuracy of the measurements of electrophysical quantities	97
4.3.1.2	The effect of salinity on the electrical properties of the bentonite	99

	of type "Dusch"	
4.3.1.3	Electrical and mechanical properties correlation	102
4.3.1.4	Correlation of electrical properties and temperature	103
4.3.2	Electrophysical properties of the "Kutch" bentonite	104
4.3.3.	Electrophysical properties of bentonite "Zir"	106
4.4	Comparison of electrophysical properties of bentonites	108
4.5	Electrophysical properties of kaolinite "KZHV"	109
4.6	Comparison of the electrophysical properties of bentonites, kaolinite, and sand	111
4.7	Conclusions	115
	General conclusions	118
	References	120

## **Introduction**

Modern large-scale construction of roads and railways, renovation of housing and urban development has led to the active development and use of ground penetrating radar (GPR) technologies. Currently, the method of subsurface survey or georadilation is one of the most widely used and rapidly developing methods of non-destructive testing, providing all necessary information about the state of the surveyed environment. At the same time, the efficiency of the method increases significantly when combined with other non-destructive or laboratory methods. The use of reliable values of dielectric constant and specific conductivity of the medium allows calibrating georadars and creating software and hardware complexes for monitoring engineering infrastructure objects, determining thickness of structural layers and other important characteristics, such as moisture, density, etc.

Analysis of the existing physical methods for measuring the electrical properties of the materials in the microwave range showed that to solve the above mentioned problems, the most promising alternative method for integration with GPR is the resonance method which allows obtaining dielectric constants and specific-conductivities of materials and soils with their structure undisturbed.

In this regard, this thesis is devoted to theoretical and experimental study of the propagation of electromagnetic radiation in multilayer environments, the creation of a set of GPR-based methods and the resonance method for determining the dielectric constant and conductivity of materials and soils. In particular, in this thesis, for the frequency of 1700 MHz:

- The possibility of using the GPR method for determining the electrophysical parameters of materials and soils is assessed;
- The methods for designing the resonators for measuring dielectric constants and conductivities are developed;
- The method for determining the dielectric constant and conductivity is developed;
- The equipment and technology for measuring the dielectric constant and specific conductivity of samples are created.

**Relevance of the research topic.** Physical and geophysical methods for studying multilayer inhomogeneous media (soils) have recently become more and more widely used in engineering. This is primarily due to the fact that the destructive methods used today (penetration, soil sampling by drilling, etc.) do not allow obtaining information about the surveyed medium in the required volume, and are associated with significant time, labor and material costs.

Practically important results for materials and soils used in the construction and maintenance of infrastructure facilities can be obtained by combining these methods with non-destructive testing methods, i.e. GPR, seismic prospecting, electrical sounding, etc. Among geophysical methods, GPR has advantages in speed, and efficiency of use. However, in spite of the obvious attractiveness, there are certain difficulties in its application. For example, when determining the position of the interfaces between medium layers from the reflected GPR signal, the main factor affecting the accuracy of the method is the accuracy of the dielectric constant set during the survey as an external parameter. In addition, the depth of the GPR method is limited by the specific conductivity of the media, the value of which it is desirable to know before starting the survey.

In this regard, the development of methods for measuring the dielectric constant and specific conductivity of media is an important task. Thus, it seems relevant to further study the electrophysical properties of soils by GPR and resonance methods in practically important multilayered moist inhomogeneous media.

In this work, in order to improve the accuracy of the GPR measurements, a resonator (tunable split coaxial resonator with a shortening capacitance) was designed and created for measuring the dielectric constant and conductivity of samples of materials and soils with undisturbed structure at frequencies close to 1700 MHz.

Measurements of electrophysical parameters performed in the work were accompanied by computer simulation of the electric field in the resonator cavity containing samples of materials and soils.



The results of these studies will increase the efficiency and reliability of solving specific applied problems by using the method of subsurface sounding.

**The main goals of the work:**

- study of the effect of the structure and electrophysical properties of structural layers of artificial structures on the results of the GPR diagnostics;
- development of methods for measuring the electrophysical properties of soils for the refinement of GPR data.

To achieve these goals, the following **scientific problems were solved in the thesis:**

- a method for quantitative processing of GPR data is developed;
- a method for determining the electrophysical properties of soils is developed;
- electrophysical properties of soils with different degrees of moisture and salinity are investigated;

**Scientific novelty of the work. Scientific results for the defense**

1. In the framework of classical electrodynamics, a method has been developed for determining the absolute refractive indices of structural layers and corresponding attenuation coefficients in the microwave range of 1200–1700 MHz, based on the quantitative processing of GPR data. The developed method of processing the GPR data is based on the use of amplitudes of reflected waves; it makes it possible to determine dielectric constants and electrical conductivities of structural layers with an error of not more than 10-15%. This makes it promising for the use in software systems for the automatic processing of GPR information when monitoring the state of extended sections of roads and railways.

2. Methods for determining the complex dielectric constant and moisture by the GPR method, calibrated by laboratory measurements, are proposed and assessed. The developed approach allows rapid diagnosing the state of extended ob-

jects, since it combines the advantages of the high-speed GPR method with a limited number of calibration measurements.

3. The dependences of the dielectric constant and specific conductivity on the moisture have been investigated in a number of bentonites with different composition of exchangeable ions. A correlation between these electrophysical quantities and the plasticity of bentonites is established.

**Reliability of the results** obtained is determined by the use of modern, reliably developed ideas of electromagnetic radiation theory in theory and practice of GPR, by application of modern methods of computing and data processing, and by the use of libraries of approved computer algorithms. All theoretical conclusions and the results obtained are confirmed by laboratory and field tests.

**Scientific and practical significance** of the work is in developing of a set of methods, including GPR and resonant measurements, for determining electrophysical values of materials and soils; these methods are effective for practical application. The developed approaches are aimed at the quantitative processing of the results of the GPR measurements at frequencies close to 1700 MHz.

**Approbation of the work.** Principal results of this thesis are reported and discussed at a number of All-Russian and International conferences:

1.V. Yavna, A. Kasprgitsky, G. Lazjrenko, A. Kochur, S.Sulavko. Rapid method of determining the physical properties of clay soils according to infrared spectroscopy. Abstract book: 3rd International Conference on Railway Engineering: Construction and Maintenance of Railway Infrastructure in Complex Environment (ICRE2014), 2-3 august, 2014, Beijing, China. – Beijing: China Railway Publishing House. – P. 114-117.

2. V.A. Yavna, A.S. Kasprzhitsky, G.I. Lazorenko, S.N. Sulavko. Determination of the limits and the plasticity number of clay soils using infrared spectroscopy. Ab-

- stracts of the tenth scientific-practical conference and exhibition "Engineering Geophysics-2014", Gelendzhik, April 2014. DOI: 10.3997 / 2214-4609.20140358
4. Khakiev ZB, Okost MV, Kasprzhitsky AS, Sulavko S.N., Indicative method for estimating seasonal changes in the moisture of the road bed according to GPR data. Abstracts of the eleventh scientific-practical conference and exhibition "Engineering Geophysics-2015", Gelendzhik, April 2015. DOI: 10.3997 / 2214-4609.201412259
5. Z.B. Khakiev, V.A. Yavna, S.N.Sulavko, K.Yu. Kislitsa. Determination of complex dielectric constant and soil moisture by GPR. Abstracts of the twelfth scientific-practical conference and exhibition "Engineering Geophysics-2016", Anapa, April 25-29, 2016 April 2016. DOI: 10.3997 / 2214-4609.201600315
6. Victor Yavna, Zelimkhan Khakiev, Georgiy Lazorenko, Anton Kasprzhitskii, Sergey Sulavko. Quantitative GPR inspection of quasi-homogeneous ground layers. MATEC Web Conf. **Volume** 251, 14 December 2018, VI International Scientific Conference "Integration, Partnership and Innovation in Construction Science and Education" (IPICSE-2018). <https://doi.org/10.1051/mateconf/201825102025>

**The dissertation materials are published in the following papers:**

1. A.S. Kasprzhitsky, G.I. Lazorenko, S.N. Sulavko, V.A. Yavna, A.G. Kochur. Study of the interaction of water and kaolinite by the methods of IR spectroscopy. *Optics and Spectroscopy*, 2016, Vol. 121, No. 3, pp. 387–394.
2. A.S. Kasprzhitsky, G.I. Lazorenko, S.N. Sulavko, V.A. Yavna, A.G. Kochur. Investigation of the structural and spectral characteristics of free and bound water in kaolinite. *Optics and spectroscopy*. - 2016, vol. 121, No. 3, p. 28–34.
3. Vladimir Shapovalov, Victor Yavna, Andrei Kochur, Zelimkhan Khakiev, Sergey Sulavko, Philippe Daniel, Alexander Kruglikov. Application of GPR for determining electrophysical properties of structural layers and materials. *Applied Geophys.* 2019 (paper sent to the journal after recommended revision)

### **Personal contribution of the author of the thesis**

- analysis of the state of problems and setting research objectives (together with the scientific co-advisors V.A. Yavna and P. Daniel);
- performing laboratory and field tests and studies;
- theoretical studies applied to GPR practice (together with the scientific co-advisors V.A. Yavna and P. Daniel);
- theoretical studies of the characteristics of the propagation of electromagnetic waves in inhomogeneous media of different moisture and salinity (together with the scientific co-advisors V.A. Yavna and P. Daniel);
- systematization and generalization of results (together with the scientific co-advisors V.A. Yavna and P. Daniel).

## **Chapter 1. Literature review**

### **1.1. GPR method**

The GPR method belongs to non-destructive methods that are widely used to examine the subsurface space when solving a wide range of engineering problems. In Russia, the use of the GPR method is regulated by normative documents [1-5].

The GPR method is based on the emission of broadband pulses of electromagnetic radiation and recording of signals reflected by media separation interfaces or objects placed in a ground or in structural layers of artificial structures [6, 7]. The interlayer interfaces in the media under study are, for example, the contact between dry and moisture-saturated soils (groundwater level), contacts between rocks of different lithological composition, between rock and material of artificial construction, between frozen and thawed soils, between bedrock and sedimentary rocks, etc.

GPR pulse contains harmonics whose spectrum depends on the pulse duration. In GPR, the spectrum contains frequencies in the range from 10 to 5000 MHz.

A wave propagating in a medium can experience reflection and refraction on the interfaces between the media layers with different relative dielectric constant, diffract on objects whose dimensions are smaller than the prevailing wavelength, decay due to angular divergence and absorption in the medium.

Important characteristics of media that affect the description of the propagation of electromagnetic pulses are propagation velocity and attenuation coefficient. Electromagnetic waves propagation speed depends on the relative dielectric and magnetic permeabilities. For the most of media encountered in practice the relative magnetic permeability differs little from unity. Therefore, the speed of wave propagation in the medium is determined by the formula:

$$V = \frac{C}{\sqrt{\varepsilon}},$$

where  $C$  is the speed of light in vacuum or air, and  $\varepsilon$  is the relative dielectric constant of the medium.

Wave attenuation is associated with the presence of charge carriers in the medium, and their mobility. The higher the frequency of the applied field, the fewer are the obstacles to the movement of charges. Therefore, the specific electric conductivity of the medium increases with increasing frequency; this causes an increase in the attenuation coefficient of the medium and a restriction on the use of GPR in some types of soil [6,8].

Another important characteristic of GPR is resolution. The resolution of the GPR antenna unit is the ability to distinguish two closely located objects. The resolution of the GPR is determined by the wavelength and is usually taken to be equal to its fourth part.

GPR survey is most often used in GPR profiling mode when the distance between the receiving and transmitting antennas does not change [6,7]. In the process of moving, the transmitting antenna emits electromagnetic pulses that, propagating in the medium, are reflected from the contrasting interfaces of the soil layers or local objects and get into the receiving antenna. At each point, a signal is recorded, i.e. the direct passage signal from the transmitting antenna to the receiving one, and the secondary signal scattered by medium inhomogeneities. In this case, inhomogeneity is understood as the interface between media with different dielectric permeabilities  $\varepsilon_1$  and  $\varepsilon_2$ .

Moving the antenna module above the heterogeneity surface leads to the fact that a hyperbole is observed on the GPR section (also called radargram, see Figure 1.1), which is described by the following equation:

$$t(x) = \frac{2L}{V} = \frac{2\sqrt{x^2 + h^2}}{V},$$

where  $L$  is the path traveled by the wave,  $V$  is the speed,  $h$  is the depth of the object,  $x$  is the displacement of the GPR unit from the projection of the inhomogeneity onto the boundary of the half-spaces.

Figure 1.1 shows the GPR images of localized underground objects.

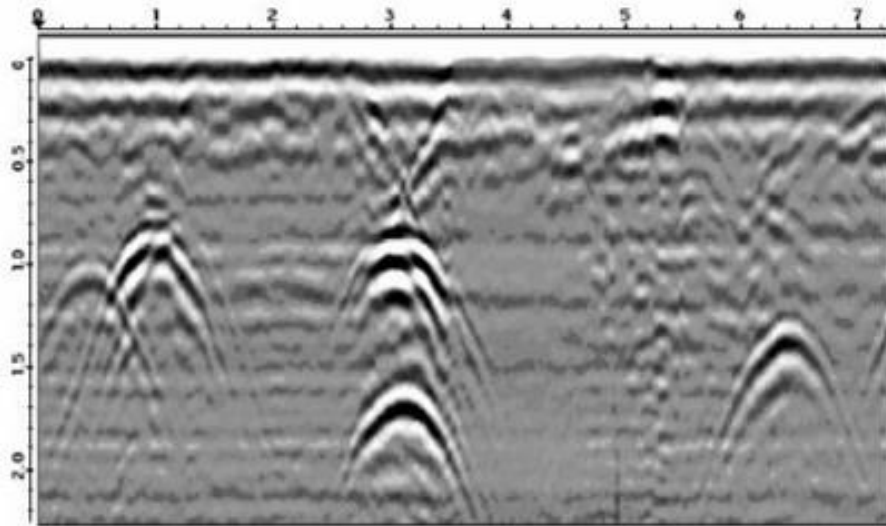


Figure 1.1. Localization of underground communication lines on the radarogram.

The use of GPR method has several reasons. The first reason is the ability to perform studies of the internal spatial structure of soil layers with relatively high resolution (up to about 1 cm), which is related to the frequency range used in this method. In addition, the GPR method allows obtaining continuous information on the surveyed environment, which makes this method promising for creating software and hardware methods for monitoring the subsurface space and searching for communication lines and their networks [9-14].

The effectiveness of the GPR equipment and technology are related to the type of antenna design. There are three main types of antennas: "butterfly", horn and dipole [15-18].

Butterfly-type antennas make it possible to obtain a sufficiently high resolution, which is necessary for accurate positioning of subsurface objects and media interface boundaries [19–20]. The use of a horn-type design allows one to generate narrowly directed and more intense radiation.

Suppression of external interference is possible by using the screen [15] made of metal attenuating external electromagnetic radiation.

To improve the quality of information, phased antenna arrays have recently been used [20-22]. Another direction to increase the effectiveness of the GPR method is the use of combinations of several operating frequencies [23-24].

GPR sections (radargrams) obtained during the survey are the sets of single tracks recorded for individual points of the GPR unit position [8,10].

Engineers apply various methods of processing radargrams based on the use of standard object patterns [25], neural networks and fuzzy logic [26-29], pattern recognition [30]. Least square approximations [31,32] in fitting the GPR patterns by hyperbolas [33-36] are used to determine the geometry and dimensions of cylindrical objects. In [37], the authors use a new method of three-dimensional complete inversion of the wave field in the frequency domain to determine both the geometric parameters of a cylindrical object and its dielectric properties. The latter allows determining the type of material.

### 1.1.1. GPR equipment

Currently, most of the domestic market is represented by the equipment of the following manufacturers:






LLC "LOGIS" (Russia), LLC "VNIISMI" (Russia), LLC "Timer" (Russia), HTP "SENSOR" and FSUE "RosdorNII" (Russia), FSUE SKB IRE RAS (Russia), LLC "GEOLOGORAUTH" (Russia), Transient Technologies Ltd. (Ukraine), Spetsavtomatika LLC (Ukraine), GSSI (USA), Sensor and Software Inc. (Canada), Era Technology (England), MALA (Sweden), Radar Systems Inc (Latvia), Ingegneria Dei Sistemi (IDS) (Italy).

Table 1.1 presents the GPR equipment and the frequencies of the antenna units used.

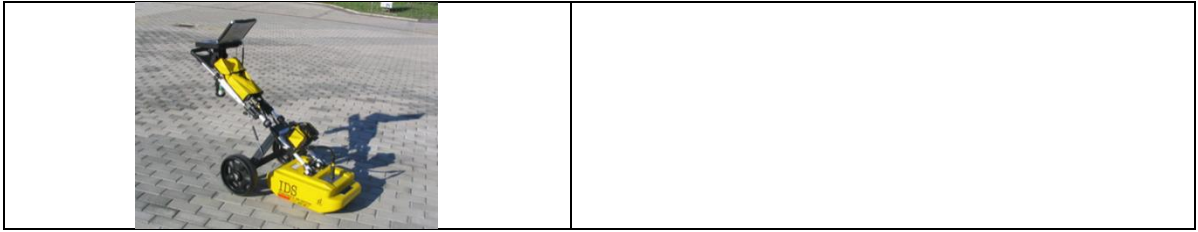
Table 1.1 - The main characteristics of ground penetrating radars

Manufacturer, device name	Antenna unit frequencies, MHz
LLC LOGIS, OKO-3	2000, 1700, 1200, 2500, 1000, 400, 900, 700, 250, 150, 90, 100, 50



	
<p>LLC VNIISMI, LOZA</p> 	<p>25, 50, 100, 300 Non-scrinned (dipolar)</p>
<p>LLC Timer, GROT</p> 	<p>15-150, 50-1000 Non-scrinned (dipolar)</p>
<p>HTP TENSOR and FSUE RosdorNII, DRL</p> 	<p>250, 1000, 2000</p>
<p>FSUE SKB IRE RAS, GERAD</p> 	<p>250, 500, 1000</p>
<p>LLC GEOLOGORAZVEDKA, TR-GEO</p> 	<p>20-30, 120-150, 150-200, 150-250, 1000, 1500</p>
<p>Transient Technologies LLC, VIY</p>	<p>70, 125, 300, 500, 700</p>

	
<p>LLC Specavtomatika, EASYRAD GPR</p> 	<p>20-400, 500-2000</p>
<p>GSSI</p> 	<p>1600, 2000, 2300, 2600, 900, 800, 400, 350, 300, 270, 200, 100</p>
<p>Sensor and Software Inc</p> 	<p>12,5-1000</p>
<p>MALA</p> 	<p>25-3200</p>
<p>Radar Systems Inc, «ЗОНД-12С»</p> 	<p>25-2000</p>
<p>Ingegneria Dei Sistemi (IDS)</p>	<p>25-2500</p>



### 1.1.2. Bibliometric analysis

The GPR method is used to solve a wide class of geophysical and engineering problems. To assess its demand, we will limit ourselves to solving only one task, namely, we will consider publications on the use of engineering methods for determining the location and depth of existing underground networks. The search was performed in the Scopus database. Dynamics of the distribution of scientific publications by year, country, scientific research areas is shown in Figure 1.2.

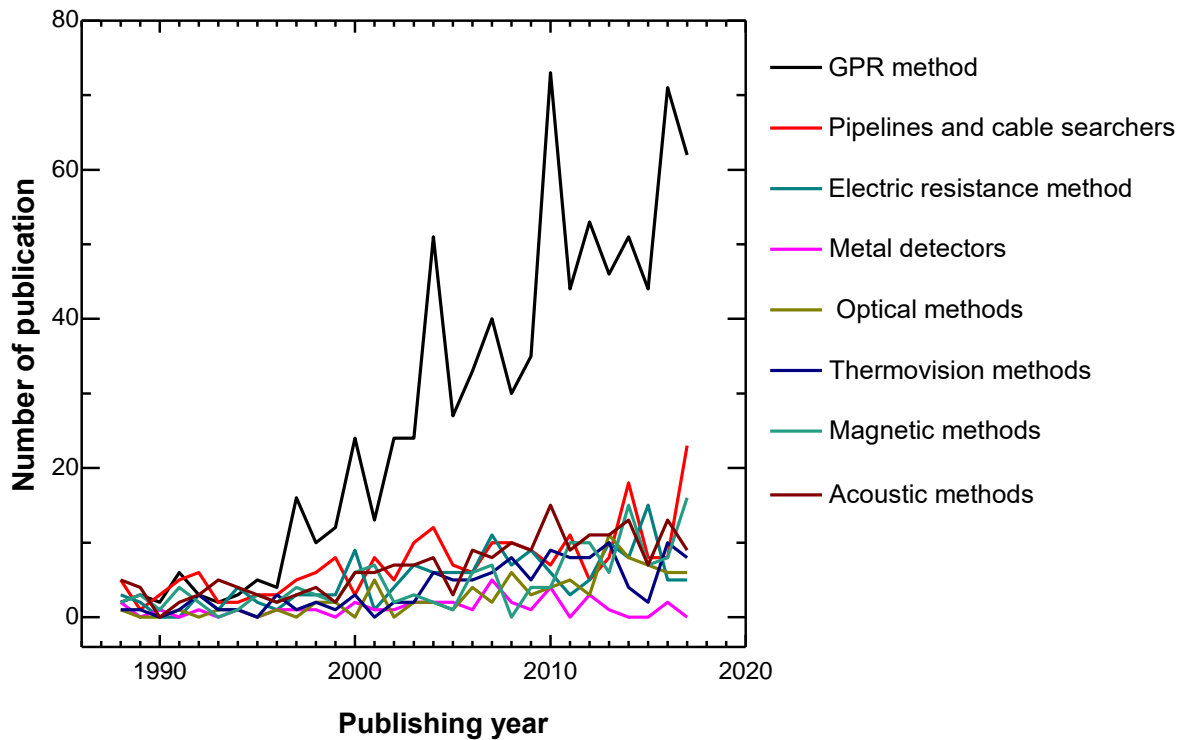


Figure 1.2. Dynamics of publication activity in the field of technologies and technical solutions for determining the location and depth of existing underground networks of engineering and technical support by non-destructive methods for the last 30 years according to the Scopus bibliographic database as of August 2018.

The figure shows that the intensive growth in the number of publications in solving the problem under consideration by non-destructive methods began around 1996 and is associated with the progress of GPR technologies. The number of publications on georadiolocation for the search for underground communications has increased over the past 20 years, about 5 times and remains at the level of 50-70 papers per year.

### 1.1.3. Patent analysis

The distribution of patent applications according to the methods and technologies for solving the engineering problem selected for analysis (determining the location and depth of existing underground networks of engineering and technical support by non-destructive methods) was determined for the period from 1988 to 2018 and is presented in Figure 1.3.

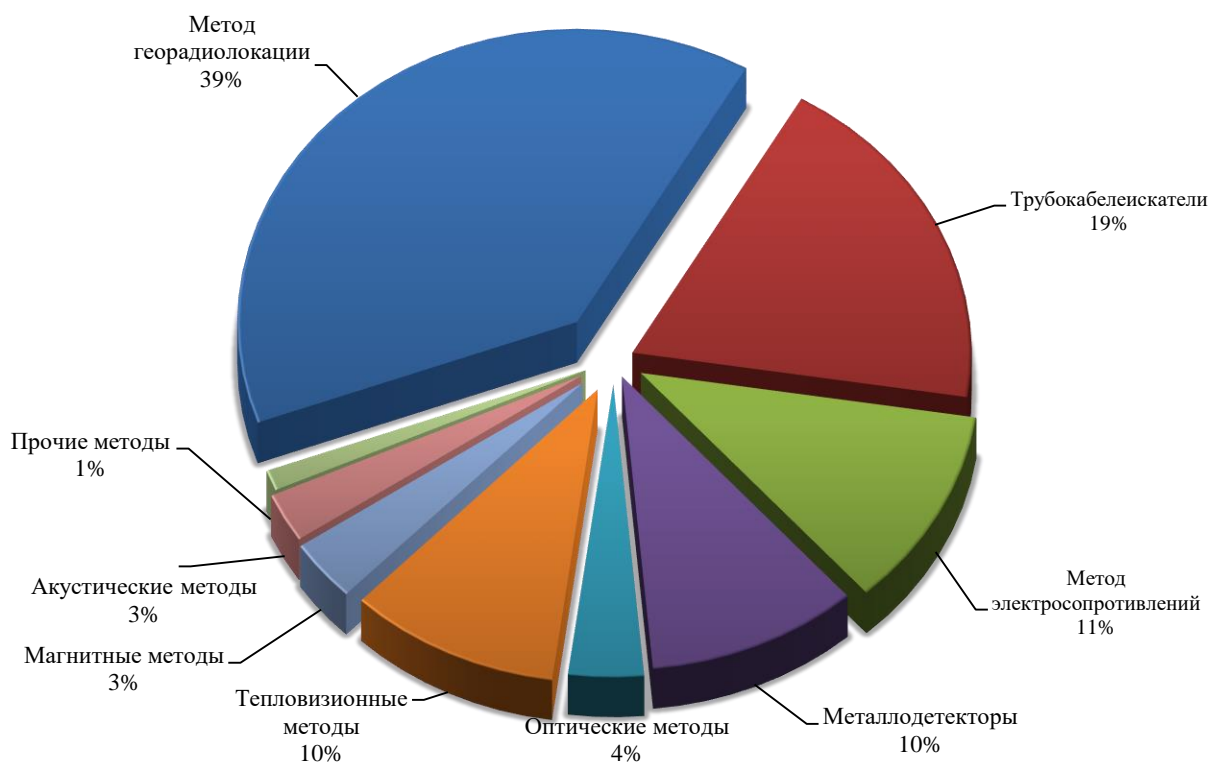


Figure 1.3. Distribution of patents by methods in the period 1988-2018 according to the database esp@cenet

It can be seen From figure 1.3 that the greatest number of inventions is related to the GPR- based method, 39%.

#### **1.1.4. GPR on transport**

The method of broadband GPR [6,10,38,39] is currently used to survey the state of the railway track and engineering infrastructure facilities. Infrastructure transport objects are sources of secondary scattered electromagnetic waves, therefore, the use of GPR for their survey sets additional requirements for the interference protection of receiving and transmitting antennas, and increasing the overall information content in the subsequent mathematical processing of measurement results.

Chapters of the monograph [40] are devoted to the problem of antenna design for GPR. Research in this direction is carried out constantly. In [41], interference from the infrastructure, increasing the depth and resolution of surveys was achieved *via* the use of a horn design of the receiving and transmitting antennas; refs. [17.42] discuss the possibilities of using Vivaldi antennas for examining the state and determining the electrical properties of infrastructure objects. In [43], experimental and theoretical studies of the effect of the distance between the antenna units on the accuracy of determining the thickness of pavement layers were performed.

Improving the informativity of the GPR method is significantly related to the progress of mathematical methods for processing radargrams; these are being developed in several directions. In recent years, significant progress in interpreting the data has been achieved using neural networks. In [44], this approach was used to control the density of the asphalt-concrete pavement, and the study [45] demonstrated the applicability of the approach for solving the problem of identifying hidden cracks. Another direction in the mathematical processing of radargrams is the automation of their interpretation [46]. Such methods lead to the creation of computer codes that work as part of hardware and software systems used in the diagnostics of extended transport infrastructure objects. Relevant technologies are developed by the following organizations and firms: U.S. Federal Railroad Admin-

istration (USA), Safe Rail System (Germany), Zetica Rail (ZARR) United Kingdom, Roadscanners Oy (Finland), IDS (Italy), GSSI (USA).

World experience of using GPR on railways has shown their high efficiency when examining the ballast layer and the road bed. As a rule, railway track surveys are carried out by multichannel GPR systems combined with global positioning and video recording systems [47]. Ref. [48] introduced a six-channel GPR complex mounted on a mobile unit and used to survey the tunnel lining at speeds up to 175 km/h.

Several studies report on determining the parameters of the materials used for ballasting the railway track by the GPR method. The work [49] is devoted to determining the informativeness of the amplitude and frequency analysis of the GPR signals reflected from the soil surface. It is shown that the methods based on the amplitude analysis of a signal are more informative than those using frequency characteristics. In [50], the dependence of the dielectric constant of the contaminated ballast material on the chemical composition of the pollutants was carried out, and [51] investigated the dependence of the dielectric constant of the ballast on the concentration of the pollutant (silty soil). In [52], the analysis of the scatter of the GPR waveforms was used to predict the ballast pollution index.

Attention to the inspection of roadbeds of roads and railways the foundations of artificial structures is caused by the danger of deformations of the upper structure of roads and buildings. To solve the problem of diagnostics of subgrade, the authors of [53] developed a method for determining the refractive index and conductivity of structural layers of artificial structures using the results of GPR surveys. The developed methods were successfully used to monitor seasonal changes in the structural layers on several sections of railway. The authors of [54] developed a method for estimating seasonal changes in moisture of the structural layers of a railway track. In [55], the GPR method is combined with the resonance method for determining the electrophysical properties of soils. The method allows, in a short time interval, to diagnose the condition of extended objects as it combines the advantages of the high-speed GPR method with a limited number of veri-

fying measurements of the dielectric constant by the resonant method, and the measurements of moisture content by laboratory methods.

Ref. [56] is devoted to the determination of the anomalous zones of the subgrade by the method of GPR and load tests. The results showed good agreement between the two methods of non-destructive testing (GPR and load tests) in identifying the anomalous zones. In [57], the correlation between the density of soil and the results of GPR surveys is established. It is noted that the dielectric constant of the soil in its natural state depends on the water content, and an increase in the bulk density of the soil usually reduces its content. Thus, the process of changing the density of the soil, occurring during the construction of artificial structures or the current maintenance of artificial structures, affects the speed of propagation of electromagnetic radiation and can be studied by GPR.

Technogenic development of the territory with unfavorable conditions led to the study of properties of permafrost soils [58] the degradation of which can cause significant damage to transport communications. In addition, numerous freeze-thaw cycles lead to a change in the geometry of the railway track due to frost heaving of the soil, which can lead to a limitation of the speed of trains and reduce the intensity of the turnover. In [59], for planning preventive maintenance in areas with frost heaving, a technique was proposed for examining the road bed of railways in order to identify frost-sensitive sub-ballast and ground layers using frequency-based GPR analysis techniques.

In recent years, research has been intensively developing to apply the GPR method to diagnose the state and determine the physical properties of quasi-homogeneous finely dispersed media (concrete structures and asphalt-concrete road surface coverings). Such studies are aimed at monitoring the quality of construction work and monitoring the state of objects, which is necessary for determining their residual life. The GPR method was employed in [60] to measure the density of asphalt-concrete mixtures. In [61], according to laboratory experiments and simulation analysis, a theoretical method was proposed for determining the degree of compaction and delamination at the interfaces between structural layers.

Field tests showed its satisfactory accuracy. Work [62] is devoted to the study of the density of the material of the asphalt pavement with drainage properties, and the identification of the presence of moisture in the layer under study by antennas operating at frequencies of 1.0 and 2.0 GHz. In [63], a library of radargrams obtained from coatings with different types of cracks was created, and a method for detecting local cracks was developed. Detection of cracks in the early stages of their development seems to be quite an important task because they contribute to the accumulation of moisture and chemical compounds, corrosion of reinforcement, weakening of the concrete monolith due to periodic processes of freezing and thawing of water. In refs. [64-65] high efficiency of the GPR method for solving the problem of determining the geometric dimensions of layers and positioning the reinforcement cage in reinforced concrete structures is noted. In [66], a GPR method was proposed for automatic localization of reinforcement in reinforced concrete structures, based on a modified hyperbolic model of image formation. The method allows estimating the thickness of the protective layer with an average accuracy of up to 3.12%. The problem of positioning pipes in a multilayer medium was solved in [67].

In [68,69] the studies are carried out to identify cracks and determine corrosion of reinforcement in concrete structures of bridges using broadband georadars, and ref. [70] is devoted to identifying cracks in road pavement (asphalt, concrete) using georadars at frequencies of 250 and 1000 MHz. Various types of cracks were simulated which allowed to describe their features in the GPR data.

Ref. [71] presents the results of laboratory experiments aimed at identifying GPR signs of corrosion of reinforcement in concrete. It is shown that the growth of corrosion leads to an increase in the amplitude of the reflected signal in the time domain, but does not change the frequency of the peak in the frequency domain; pollution with chlorides weakens the signal and lowers the frequency of the peak. In [72], the corrosion of reinforcement was accelerated in laboratory conditions, which was accompanied by GPR studies; this made it possible to propose a method for determining the corrosion rate by measuring the maximum amplitude of the



GPR signal.

An important direction of GPR research is the refinement of the values of the electrophysical parameters of the structural layers. Measurements of the dielectric constant of asphalt concrete pavements in the frequency range 1.7–2.0 MHz were carried out in refs [73, 74], and the behavior of the dielectric constant of various bitumen materials was investigated depending on weather conditions [73]. The service life of reinforced concrete structures is directly related to water permeability, because almost all destructive reactions, such as corrosion of reinforcement and concrete, require the presence of liquid water or water vapor. The correlation between the depth of water penetration into concrete and the characteristics of the GPR wave pattern was studied in [75, 76], and the gradient of the mass of water absorbed by concrete structures through capillaries was studied in [77]. Since the parameters of the wave GPR picture of the medium are significantly dependent on the presence of water, the method for determining its concentration during the formation of concrete structures was proposed in [78]. In that work, the degree of correlation between the values of dielectric constant and strength was studied on the example of 45 samples of three types of concrete.

#### **1.1.5. Monitoring the density of soils of the railway road bed by GPR**

The normative state of the roadbed of roads and railways should provide uniform elastic and dissipative properties under the action of loads from automobiles and railway rolling stock, respectively. During the operation of roads and railways, residual deformations should be absent, and elastic deformations should not exceed 30% of the total elastic deformation of the railway track [79].

To assess the possibility of using the GPR method for determining the strength characteristics of soils, a set of field and laboratory work was performed in [80], which allowed the GPR method to be calibrated to determine the density of soil.

In [81], the density of soils in the body of a railway embankment was estimated from seismic data. The authors proposed a method for obtaining the value of

density of soils from the measured values of the propagation velocity of seismic longitudinal and transverse waves. In [82], the dependences of the average frequency of the maximum of the reflected GPR signal with a center frequency of 400 MHz on the type of soil were obtained. In [83], GPR field and laboratory studies to determine the strength properties of sedimentary and intrusive rocks were carried out. The dependences of the speed of propagation and attenuation of electromagnetic radiation on the strength of granite, dolomite and sandstone are obtained. The authors of [84] performed experiments to determine the effect of soil type on the shape of the reflected GPR signal. The velocities and amplitudes of the signal in various media, including multilayer ones, have been studied. The effect of density, moisture and soil mineralization on the formation of the reflected signal is estimated.

In [85], the authors proposed methods for determining the propagation velocity of electromagnetic radiation in a medium and associated it with the density of frozen materials. The problems of determining the dielectric constant and reflection coefficient from the change in the signal amplitude were considered.

#### **1.1.6. GPR method in the construction of subgrade**

During the construction of the roadbed of roads and railways, it is necessary to observe the geometrical parameters of the structure, as specified by the standards and laid down in the project, and to ensure uniform distribution of the strength characteristics of soils along the path under construction and into its depth. According to the norms, the compaction of the subgrade soil is carried out layer by layer at optimum moisture making a certain number of passes of sealing machines along the same track. It is known that soils are three-phase systems consisting of a soil skeleton and pores filled with water or air.

Porosity and soil moisture affect soil's condition, and with a decrease in porosity due to mechanical compaction of the soil, the strength and stability of the subgrade increases. Due to the importance of the density of the soil during the con-

struction of the embankment norms the control of its values during construction is obligatory. In this regard, it is necessary to quickly monitor the density of a given profile to obtain continuous information. Such information will allow achieving a uniform compaction in accordance with the desired density values in the entire volume of the roadbed and to prevent leaving under- or overcompacted areas.

One of the methods that can be applied to solve such a problem is the GPR method [6-10]. In [86], the possibility of using GPR to determine the density of the subgrade soil of a railway under construction was studied.

## **1.2. Direct methods for measuring the electrophysical properties of soils**

Methods for studying the properties of materials and soils using radio wave technology are sufficiently studied and tested. According to [87], they can be classified as waveguide, resonance, and free space methods. The choice of measurement method is determined by a number of factors, which include the frequency range, phase composition and properties of the material under study, temperature, etc. When choosing a method, it is important to take into account the range of variation of values since methods for measuring samples with low permeability may not be suitable for samples with high dielectric constant and dielectric loss tangent. A detailed description of the theoretical concepts on the dielectric properties of substances, analysis of methods for calculating the principal dispersion parameters (relaxation time, distribution coefficient of relaxation times, thermodynamic functions, etc.), description of various methods for measuring dielectric constant and dielectric losses are given in monographs and review articles [89 -92].

In the tasks set in the dissertation research, it is assumed to obtain materials and soils with undisturbed structure obtained by boring. To substantiate the choice of methods for measuring the electrophysical parameters of the samples in the microwave range, we briefly describe the main methods for determining the dielectric constant.

### **1.2.1. Quasi-optical (in free space) methods**

When using the quasi-optical method to determine the complex dielectric constant, the sample is located between the horn emitting and receiving antennas. During measurements, propagation characteristics of electromagnetic waves are recorded, such as attenuation and phase of the wave. The advantage of the quasi-optical method is that it is a non-destructive non-contact measurement methods. Using these methods does not impose strict requirements on the size, accuracy and roughness of the samples.

### **1.2.2. Waveguide methods**

When using waveguide methods, the sample of the material under study is placed inside a coaxial or rectangular segment of the waveguide. The shape of the sample must exactly match the profile of the waveguide, which in the case of soils is difficult to implement, and leads to errors. When measuring in a coaxial waveguide, the samples should be cylindrical with a through hole in the center. The diameter of the coaxial waveguide is small compared with the diameter of the sampler. To measure in this waveguide, the selected samples must be crushed, which leads to disruption of the soil structure. The dielectric constant of the soil, as a complex multi-phase material, depends on the dielectric properties of the mineral composition of the solid, chemical nature, structure and composition of soil particles, their shape and size, as well as on the dielectric features of porous air and moisture. Each of the phases — solid, liquid, and gaseous — by entering in various combinations and ratios into the volume of the soil, contributes to the value of the effective dielectric constant of the soil as a whole complex of elements. To measure and calculate the dielectric constant of the system, knowledge of the structure, density, dispersion, porosity, moisture, chemical and mineralogical composition is necessary. In addition, it is necessary to understand the nature and the character of electrical interactions and bonding forces between atoms and molecules of soil material. It should be remembered, as noted earlier, that there are all kinds of conductivity in the soil: weak electronic (for well-conducting components of the solid phase),

dielectric (for poorly conducting elements of the mineral part of the soil) and especially ionic (for soil solution). As a result of the above factors it can be seen that the violation of the structure of the soil leads to a change in the dielectric constant and conductivity. When the waveguides are filled with a sample to be measured, another problem arises: the waveguide mismatch, which leads to additional reflections and dissipated energy.

Waveguides of this type are connected according to two schemes (depending on the type of the wave, reflected or transmitted) “for reflection”, and “for passage”.

### **1.2.3. Resonance methods**

In the resonance method, the sample under study is placed in a microwave resonator. A resonator is a volume completely enclosed by metal walls containing two small communication holes, through one of which electromagnetic fields are excited in the resonator. The dependence of the amplitude of the electromagnetic field on the frequency of the incident radiation characterizes the resonant curve of the resonator. This curve has maxima at the resonant frequencies of the resonator. When measuring, the resonance curve is recorded first without a sample, and then with the sample. In the presence of a sample, a shift of the maxima of the resonance curve towards lower frequencies and a change in the shape of the resonance curve is observed. It becomes wider and lower in comparison with the resonant curve of an empty resonator. The shift of the resonance frequency and the widening of the resonance curve caused by the presence of the sample are used to calculate its complex permittivity [18]. Measurements are possible for samples in the form of cylinders and discs. The advantage of the resonance method is the possibility of measuring the soil samples with undisturbed structure, high moisture and salinity ( $W$  up to 20%).

### 1.3. Conclusions

The above methods for determining the electrophysical properties of soil materials significantly expand the capabilities of the GPR method. The introduction of these methods in the practice of diagnostics of soil and structural layers of artificial structures will allow developing of an indicator method for GPR into a geophysical measurement method.

However, these techniques require refinement, comprehensive testing and admission in the prescribed manner to use in geophysical surveys. *In this regard, in this study, the aim is to create a GPR method for determining the electrophysical properties of soils based on the use of optical approaches.*

Comparison of the wave and resonance methods for determining the complex dielectric constant showed that resonance methods are preferable for evaluating the dielectric constant and conductivity of cylindrical core samples of large diameter. Of greatest interest is the method of a volumetric tunable resonator with a shorting capacitance, in which the directly recorded parameters are the shift of the resonant frequency and quality factor.

In this regard, this study develops a method for determining the electrophysical properties based on the resonance method of core samples of soil materials. Compared with the waveguide method, it has the following advantages:

- the resonance method requires small volumes of the investigated soil, the technology of preparation of which for measurements has been developed;
- the use of ditches with the test soil speeds up the measurement process;
- the internal dimensions of the resonator coincide with the internal dimensions of the sampler, which allows preparing samples for electrophysical measurements with minimal deformation of their natural internal structure and preservation of natural humidity.

*In this regard, this study aims to create a GPR method for determining the electrophysical properties of soils based on the use of optical approaches and resonant measurements.*

## **Chapter 2. Application of GPR for determining electrophysical properties of structural layers and materials**

Organization of timely implementation of anti-deformation and repair work in tunnels and other objects of transport infrastructure requires a detailed analysis of the physical state of structures and their individual elements. In recent years, a non-destructive ground penetrating radar (GPR) method has been increasingly used for this purpose. In this Chapter I present the results of GPR determination of electrophysical characteristics (refractive indices and attenuation coefficients for electromagnetic radiation averaged within structural layers) of the highway road concretes in the tunnel using 1200-1700 MHz microwave radiation. The method of processing the GPR data is based on classical electrodynamics and, for practical implementation, it does not require additional integration with other geophysical or destructive methods. When performing calculations of electrophysical parameters of structures' concretes, various approaches are implemented, this made it possible to estimate the errors of the computational schemes and approximations. The results obtained are applied to clarify the dimensional parameters of the layers and determine the volumetric moisture content of structures' concretes.

### **2.1 Method of experimental studies**

GPR tracking measurements were performed using the "OKO" georadar at a frequency of 1700 MHz after removal of the asphalt pavement from the roadway of the tunnel. Technical parameters of the equipment and the software for registration and primary GPR signal processing are given on the website of the manufacturer of the equipment: <http://www.logsys.ru>. According to the information of the equipment manufacturer, this radar provides the depth of examination up to 1 m with a resolution of up to 0.03 m. During the survey, the receiving antenna was kept in contact with the surface of the rigid base (the first concrete structural layer), the scanning time discrimination was chosen equal to 24 ns, and averaging over 16 independent measurements was performed during the registration of traces. It is known that the number of independent measurements in the registration of traces

significantly affects the signal-to-noise ratio, which determines the depth of measurement and the quality of the GPR data. In this study, the selection of 16 independent measurements for recording the traces is optimal for the conditions and speed of the GPR measurements. Positioning of the GPR traces was carried out in manual mode by making marks on the radargrams through each meter of the trajectory.

The processing of experimental GPR sections obtained in this work was performed in the same manner as it is done in the Geoscan32 computer software package developed by Logis Ltd. The processing included the following steps. Initially, a part of the GPR section of interest was selected from the experimental material. To increase the contrast of the anomalies of the examined structure, the average trace determined on the section of 100 traces including the current one, was subtracted from the trace of the GPR section. Then, using direct and inverse Fourier transforms, low frequencies of up to 0.5 MHz were suppressed in the frequency spectrum of the traces. At the final stage of processing, the amplitudes of the trace ( $E_{\text{exp}}(\tau)$ ) were subjected to exponential amplification:  $E(\tau) = E_{\text{exp}}(\tau)e^{\alpha\tau}$ , where  $\tau$  is the time of recording the point of the path, and  $\alpha$  is the gain parameter chosen from the condition of the best representation of GPR information.

A general view of thus processed radargram obtained at 1700 MHz in the transverse direction of the carriageway is shown in Fig. 2.1 after applying a low frequencies filtering procedure (up to 0.5 MHz).



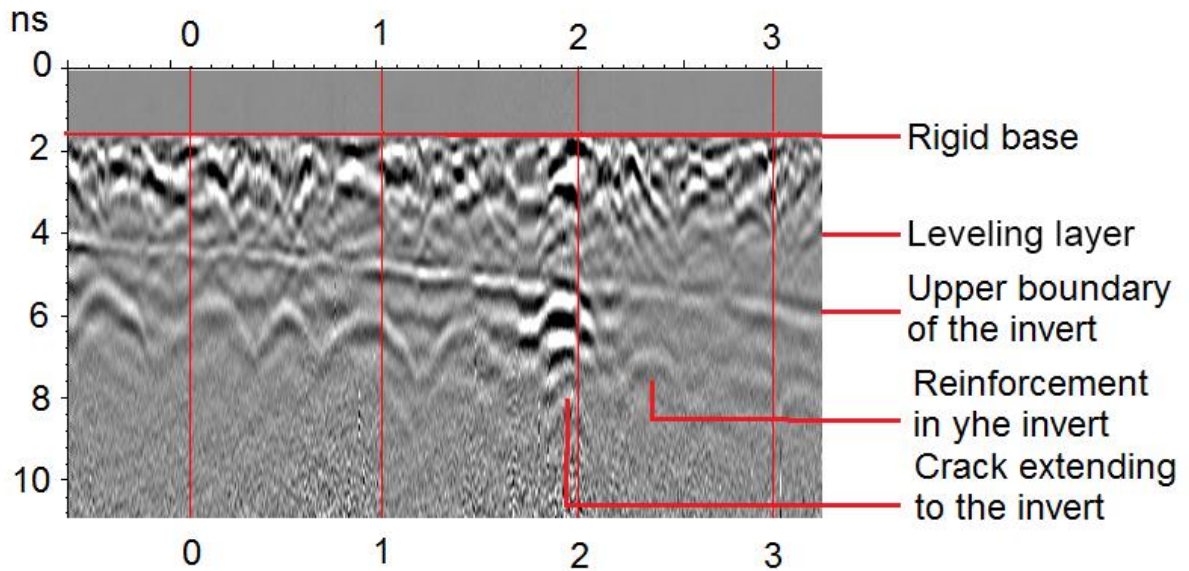


Figure 2.1. Patterns of the objects and the cracks in the body of the roadway

The following structural elements are seen in the Fig. 2.1: a rigid base plate; a leveling layer determining the slope of the rigid base plate, an upper boundary of the invert; reinforcement rods in the body of the invert. In addition, there is a set of closely lying hyperbolic lines at 2.1 m which can be assigned to a deep crack extending through all structural layers.

## 2.2. Theory of the method

### 2.2.1. Determination of structural layers' refractive indices: general case

Here we confine ourselves to considering the normal incidence of electromagnetic radiation on the boundary of the upper structural layer (incidence at  $\alpha = 0$ ), as in Fig. 2.2 for the general case.

The application of the approximation of normal incidence of the GPR pulse is valid in the case when the aperture of the antenna is substantially smaller than its distance from the boundaries of the structural layers.

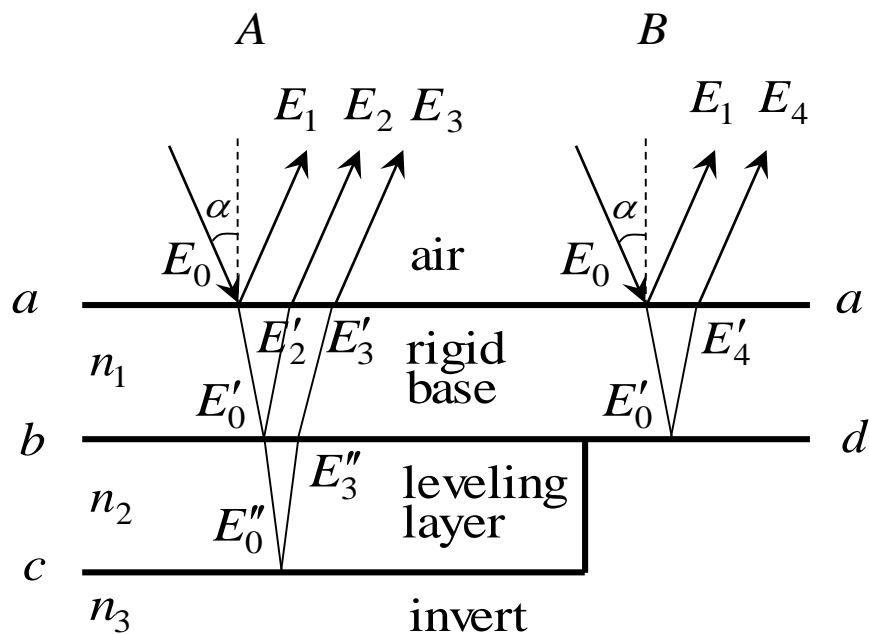


Figure 2.2. Propagation of electromagnetic radiation during examination of two types of the roadway structures of a tunnel

In the tunnel under investigation, two types of carriageway structures are present. In one case, the rigid base is bordered by the leveling layer, under which the invert is placed (Fig. 2.2, position A). Another construction does not contain the leveling layer, or its thickness is negligible (Fig. 2.2, position B).

Consider the case where the antenna unit is placed at a certain height above the surveyed structure and the forward signal is reliably distinguished in the trace. In this case, the equation for the amplitude of the electromagnetic wave reflected from the upper boundary of the rigid base has the form [94]:

$$E_1 = E_0 \frac{n_1 - 1}{n_1 + 1}, \quad (2.1)$$

where  $E_0$  is the amplitude of the electromagnetic wave incident on the upper boundary,  $n_1$  is the absolute refractive index of the rigid base; refractive index of air is taken equal to unity.

When calculating the amplitude of the electromagnetic wave reflected from the upper boundary of the leveling layer “b” (Fig. 2.2), the relations describing the following processes are taken into account. When propagating from the transmitting antenna, an electromagnetic wave can pass from the air into a rigid base through the interface “a” (Fig. 2.2), weaken in its material and be reflected from

the interface “*b*” (Fig. 2.2). The electromagnetic wave reflected in the direction of the receiving antenna undergoes attenuation once again in the material of the rigid base, passes through the interface “*a*” (Fig. 2.2) into the air and consequently the amplitude takes the form:

$$E_2 = E_0 \frac{4n_1}{(n_1 + 1)^2} e^{-2p_1 h_1} \frac{n_1 - n_2}{n_1 + n_2}, \quad (2.2)$$

where  $n_2$  is the refractive index of the leveling layer,  $h_1$  is the thickness of the rigid base,  $p_1$  is the attenuation coefficient of the electromagnetic radiation in the rigid base.

An expression for the amplitude of the wave reflected by the upper boundary of the invert (surface “*c*”, Fig. 2.2), and reaching the receiving antenna, can be obtained in the same manner. In this case, when deriving the expression for the amplitude from equation 2, the process of reflection from the interface “*b*” is excluded (Fig. 2.2). Additionally, the following processes are considered: transmission of electromagnetic radiation through the interface “*b*” (Fig. 2.2), attenuation in the material of the leveling layer, reflection from the interface “*c*” (Fig. 2.2), repeated attenuation in the material of the leveling layer, and exit into the air through the interface “*a*” (Fig.2.2):

$$E_3 = E_0 \frac{4n_1}{(1+n_1)^2} \frac{4n_1 n_2}{(n_1 + n_2)^2} e^{-2p_1 h_1} e^{-2p_2 h_2} \frac{n_2 - n_3}{n_2 + n_3}, \quad (2.3)$$

where  $h_2$  is the thickness of the leveling layer,  $n_3$  is the refraction index of the invert, and  $p_2$  is the coefficient of attenuation of electromagnetic radiation in the leveling layer.

The solution of the system of equations (2.1-2.3) with respect to  $n_1$ ,  $n_2$  and  $n_3$  implies an independent determination of the attenuation coefficients  $p_1$ ,  $p_2$ , and the amplitude  $E_0$ , as well as the measurement of the amplitudes  $E_1$ ,  $E_2$  and  $E_3$ , in radargrams. A rigorous solution of the system of equations (2.1-2.3) implies a self-consistent procedure in the case when the values of  $h_1$  and  $h_2$  are unknown. Realization of a self-consistent procedure implies taking into account in (2.1-2.3) the module of a complex refractive index instead of its real part.

### 2.2.2. Additional equations for the determination of refractive indices

Direct measurement of the amplitude of the electromagnetic wave  $E_0$  incident on the upper boundary may encounter significant difficulties due to the features of the formation and recording of an electromagnetic wave in the near-field region. In addition, in measurements with the movement of the antenna unit along the boundary of the surveyed structure, it is difficult to isolate the value  $E_1$  against the background of the direct transmission signal. These circumstances make it difficult to apply the equations (2.1-2.3) directly to the calculation of the refractive indices. In such cases, it is necessary to use additional information that can be contained in radargrams, and lead to a change in the set of equations for calculating the refractive indices of multilayered structures.

#### 2.2.2.1. GPR images of local objects

In this work, the absolute refractive index of the rigid base ( $n_1$ ) is determined by plotting the hyperbolas reflecting the positions of local objects near their lower boundary by the method employed in the Geoscan32 software package. The method is illustrated in Fig. 2.3, where an antenna block with a linear coordinate  $x$  is displayed moving along the upper boundary of the medium in which a local reflecting object with the coordinates  $x_0, z_0$  is located.

It is evident from Fig. 2.3 that

$$((L + R(x - x_0, z_0))^2 = (x - x_0)^2 + (z_0 + R(0, z_0))^2, \quad (2.4)$$

where  $L$  and  $z_0$  are the shortest distances from the media interface to the reflecting surface of the object, and  $R(x - x_0, z_0)$  is the distance from the center of mass of the reflecting object to its reflecting surface.

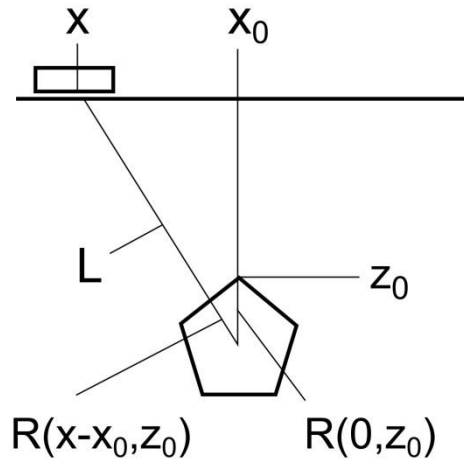


Figure 2.3. Forming a hyperbolic image of a local object

We will take into account that  $L = \frac{ct}{2n}$  and  $z_0 = \frac{ct_0}{2n}$ , where  $c$  is the speed of propagation of electromagnetic radiation in vacuum,  $t$  and  $t_0$  are the propagation time of a pulse of electromagnetic radiation in a medium with a refractive index  $n$  when the antenna unit is placed in positions with linear coordinates  $x$  and  $x_0$ . Then expression (2.4) can be reduced to the form:

$$t = \frac{2n}{c} \sqrt{(x - x_0)^2 + \left( \frac{ct_0}{2n} + R(0, x_0) \right)^2} - R(x - x_0, z_0). \quad (2.5)$$

It can be seen from equation (2.5) that the local objects create a hyperbolic image on the radargram, and that this allows, with a known function  $R(x - x_0, z_0)$ , to restore the value of  $n$ , seeking agreement between theoretical and experimental values of  $t$ .

In this work, cracks in the invert that extend to the lower boundary of the rigid base (Fig. 2.4) and the reinforcement placed at a small depth in the invert (Fig. 2.5) are selected as local objects.

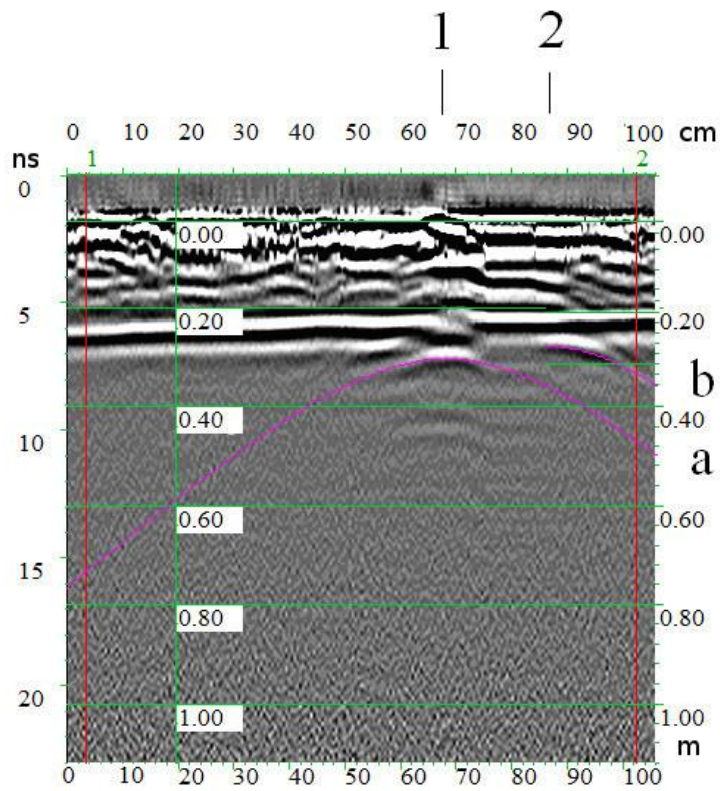


Figure 2.4. GPR image of cracks (1 and 2) in the invert, and their reconstructed hyperbolic images (a and b)

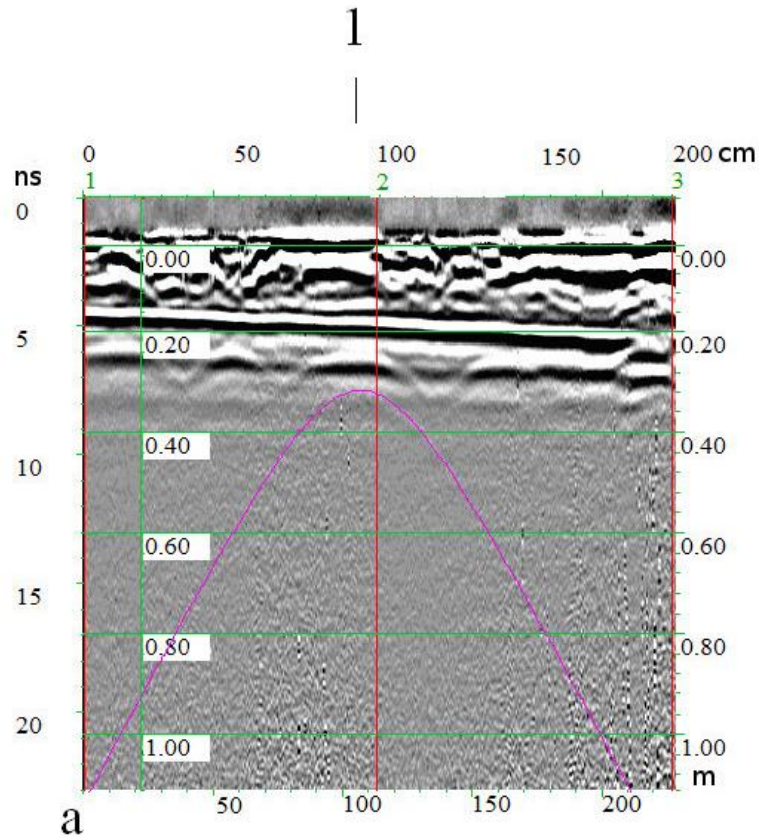


Figure 2.5. GPR image of reinforcement in the invert (1) and its reconstructed hyperbolic image (a)

The curves  $t = t(x)$  are constructed for 10 local objects. The absolute refractive index is assumed to be equal to the average value for all the objects examined and it is found to be  $n_1 = 3.16 \pm 1.5$ . The scatter in the results of individual measurements can be explained by the used mode of binding the radargrams to the trajectory of the antenna unit movement. As mentioned above, in this study, the binding was performed manually, and the scatter in the number of traces between the marks marking the one-meter segments along the path of the antenna unit was about 10%. In addition, the variation in the size of the local objects used can lead to a scatter when determining the refractive index.

The dependence of the hyperbola shape of the GPR feature of a local object of circular cross section on its radius was studied of [31]. Determining the  $n$  values for local objects of arbitrary shape with  $R(x - x_0, z_0)$  dependent on  $x$  via solving equation (2.5) requires the analysis of the amplitudes of reflected waves, and it would be a separate study outside the frame of the study.

In this work, when determining  $n$ , the finite dimensions of the local objects were not taken into account. The relative error in the refractive index and the permittivity introduced by this approximation is evaluated for the case  $R(0, z_0) = R(x - x_0, z_0) = 0.01 m$ , with relative errors  $\delta t = \delta t_0 = 0$ .

For the relative error of the refractive index, one can obtain the following expression using (2.5):

$$\delta n = \frac{\left( \frac{ct_0}{2n} + R(0, z_0) \right) R(0, z_0) \delta R(0, z_0) + \sqrt{\left( x - x_0 \right)^2 + \left( \frac{ct_0}{2n_1} + R(0, z_0) \right)^2} R(x - x_0, z_0) \delta R(x - x_0, z_0)}{\sqrt{\left( x - x_0 \right)^2 + \left( \frac{ct_0}{2n} + R(0, z_0) \right)^2} \left( \sqrt{\left( x - x_0 \right)^2 + \left( \frac{ct_0}{2n} + R(0, z_0) \right)^2} - R(x - x_0, z_0) \right) - \left( \frac{ct_0}{2n} + R(0, z_0) \right) \frac{ct_0}{2n}} \quad (2.6)$$

Assuming  $\delta R(0, z_0) = \delta R(x - x_0, z_0) = \delta R$ ,  $x_0 - x = z_0 = 0.2 m$ , and  $R(0, z_0) = R(x - x_0, z_0) = 0.01 m$ , (2.6) gives  $\delta n = 0.13 \delta R$ . Then the uncertainty of the shape of the reinforcement cross section in the case under consideration can give a maximum contribution to the error in refracting index (at  $\delta R = 1$ ) of up to 15%.

### 2.2.2.2. Contact of the rigid base and the invert

The use of a leveling layer in the construction of automobile tunnels is connected with the need to provide required slope to the rigid base. In this situation, on the curved sections of the road, the areas of contact between the rigid base and the leveling layer can be replaced by the regions of direct contact between the rigid base and the invert (“*d*” in Fig. 2.2).

Examples of this are the road sections near the points *a* and *b* on the radar-gram as shown in Fig. 2.6.

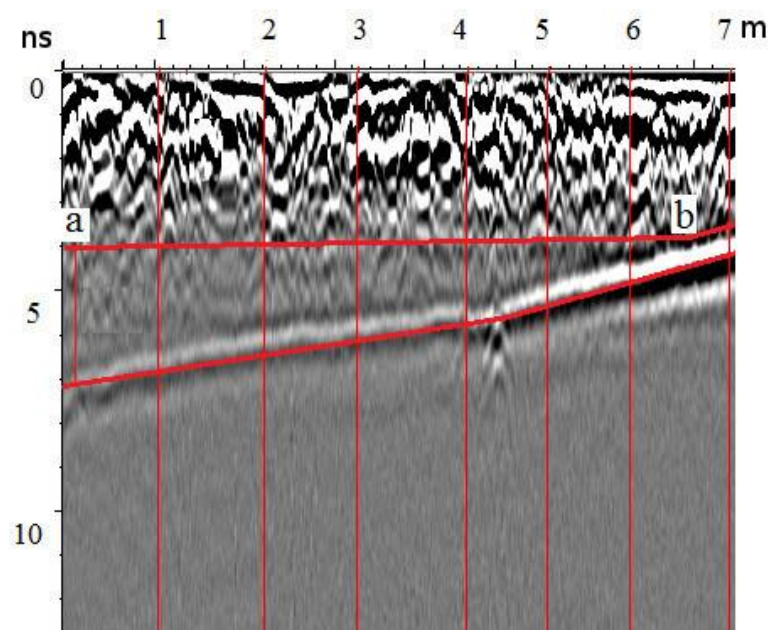


Figure 2.6. GPR image of a leveling layer of variable thickness

In this case, the system of equations (2.1-2.3) can be supplemented by the equation:

$$E_4 = E_0 \frac{4n_1}{(1+n_1)^2} e^{-2p_1 h_1} \frac{n_1 - n_3}{n_1 + n_3}, \quad (2.7)$$

where  $E_4$  is the amplitude of the signal reaching the receiving antenna after reflection from the boundary between the rigid base and the invert.



### 2.2.2.3. Equations for calculating the absolute refractive indices of the leveling layer and the invert

Homogeneity of the dimensions and properties of the rigid base, and the determination of its absolute refractive index according to subsection 2.2.2.1, allow moving the point of comparison of amplitudes from the upper boundary of the structure (“*a*”, Fig.2.2) to the upper boundary of the leveling layer (“*b*”, Fig. 2.2), or the invert (“*d*”, Fig.2.2).

According to the above notation, near these boundaries, the incident radiation has an amplitude  $E'_0$ , the magnitude of which can be obtained from  $E_0$  taking into account the process of passing the electromagnetic wave from the air into the rigid base through the interface “*a*” (Fig. 2.2), and its attenuation in the material of the rigid base. Then the desired amplitudes of radiation can be obtained by excluding from equation (2.2) and (2.7) the processes of attenuation of electromagnetic radiation in the material of the rigid base and the exit into the air through the interface “*a*” (Fig. 2.2); they have the form:

$$E'_2 = E_0 \frac{n_1 - n_2}{n_1 + n_2}, \quad (2.8)$$

$$E'_4 = E_0 \frac{n_1 - n_3}{n_1 + n_3}, \quad (2.9)$$

where, as before,  $n_1$ ,  $n_2$  and  $n_3$  are the absolute refractive indices of the rigid base, the leveling layer, and the invert, respectively.

Similarly, from equation (2.3) we can get the amplitude of the wave reflected by the upper boundary of the invert. We take into account that the radiation reflected by the interface between the leveling layer and the invert passes twice through the interface between the rigid base and the leveling layer, and it weakens while spreading through the leveling layer. We denote the corresponding attenuation coefficient with  $p_2$ .

Then the amplitude at the observation point is determined by the relation:

$$E'_3 = E_0 \frac{4n_1 n_2}{(n_2 + n_1)^2} e^{-2p_2 h_2} \frac{n_2 - n_3}{n_2 + n_3}. \quad (2.10)$$

### 2.3. Numerical procedures for determining the coefficients of attenuation of the electromagnetic field and refractive indices

The technology of the GPR tracking measurements used in this work makes the use of equation (2.1) impossible because of the complexity of measuring  $E_0$  in the near-field region. In this case, the system of equations for the calculation of  $n_2$ ,  $n_3$ , and the amplitude  $E_0$  will include equations (2.8-2.10). The solution of these implies an independent determination of the attenuation coefficients  $p_1$ ,  $p_2$ , as well as the determination of the amplitudes  $E'_1$ ,  $E'_2$  and  $E'_3$  from the radargrams.

In the case of conducting media, the systems of equations (2.1-2.3, 2.7) or (2.8-2.10) should include the modules of the complex refractive indices [94],

which is achieved by replacing  $n$  with  $\sqrt{n^2 + \left(\frac{c}{\omega} p\right)^2}$ , where  $c$  is the speed of light in vacuum,  $\omega$  is the central value of the circular frequency of the GPR pulse. In this case, it is necessary to additionally determine the attenuation coefficients  $p_1$  and  $p_2$ .

Let us consider possible approaches to the determination of the attenuation coefficients.

#### 2.3.1. The use of traces to determine the attenuation coefficients for an example of industrial water

In this section, the possibility of determining the electromagnetic radiation attenuation coefficient via the processing of traces in the case of a 0.2 m thick layer of industrial water is demonstrated. For this purpose, GPR measurements were carried out in laboratory conditions with the antenna unit placed 0.05 m above the water surface. During the examination, as before, the sweep value was chosen to be 24 ns, and during the registration of traces, the averaging was performed over 16 measurements. Registered traces of a total of 100 are averaged and subjected to the Hilbert transform, which converted the values of the traces to the values proportional to the module of the complex amplitude of the electromagnetic field.

Figure 2.7 shows the module of the Hilbert transform amplitude  $H(E)$

against the depth of signal penetration into the water layer.

This relationship is approximated by

$$|H(E)| = Ae^{-2p(r-r_0)}, \quad (2.11)$$

where  $r$  is the current coordinate, and  $r_0$  is the initial point of the approximation. The results of fitting  $|H(E)|$  for  $r_0 = 0.024$  m are shown in Fig. 2.7 by the solid red line. The approximating function (2.11) reflects the attenuation of a plane wave in a medium with an attenuation coefficient  $p$ . At the same time, the attenuation of the experimentally determined module of the complex amplitude against depth can differ from this dependence. In this connection, the numerical values of the constants  $A$  and  $p$  in the approximating function (2.11) depend on the choice of  $r_0$ . Calculated attenuation coefficient  $p$  as function of  $r_0$  is shown in Fig. 2.8. The asymptotic value of the expression is  $p = 10.1 \text{ m}^{-1}$  (Table 2.1).

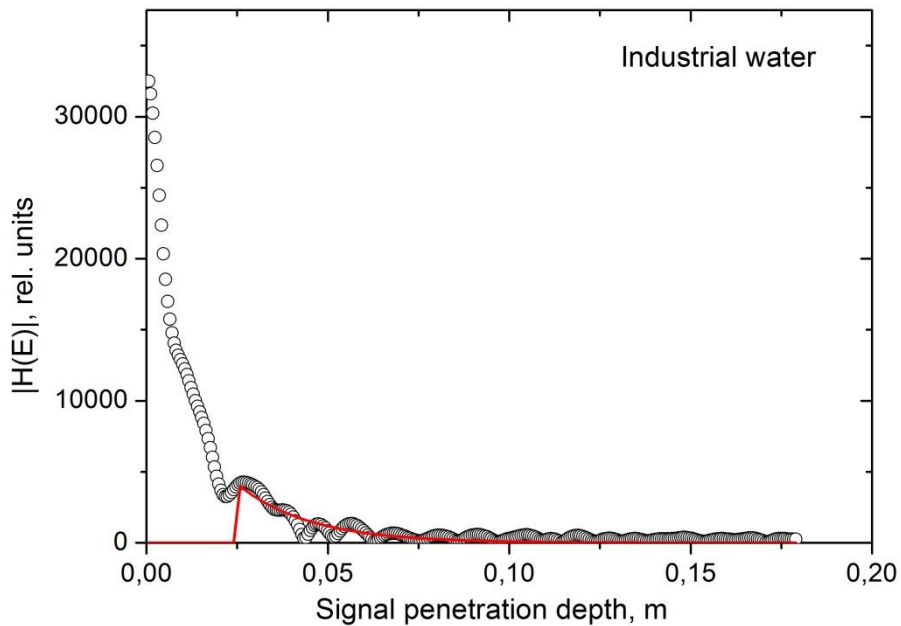


Figure 2.7. Module of the Hilbert transform of the radargram of industrial water. Solid line shows the result of fitting with (2.11) at  $r_0 = 0.024$  m

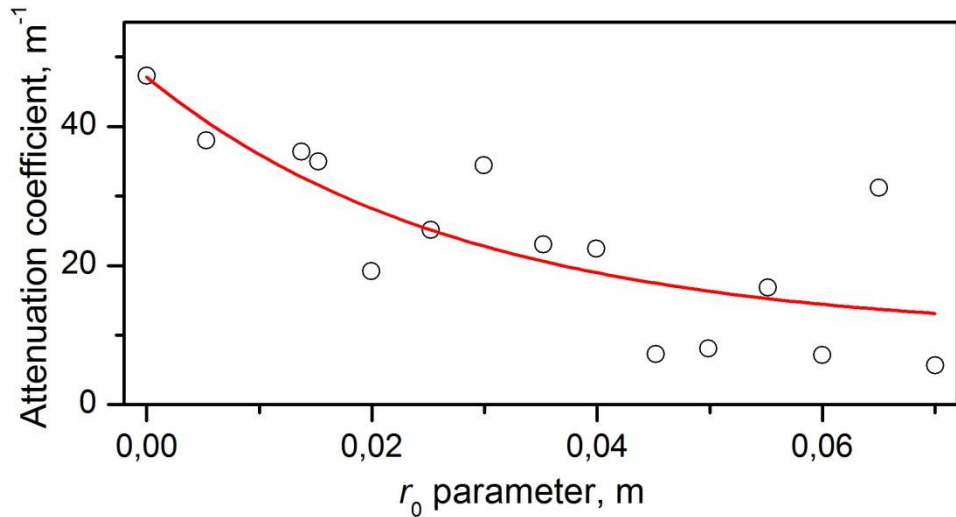


Figure 2.8. Industrial water attenuation coefficient as a function of the distance parameter  $r_0$  in formula (2.11) used for fitting

As seen from Fig. 2.8, calculated attenuation coefficient significantly depends on the choice of the point  $r_0$  near the zero value. This dependence can be related to the effect of a signal reflected from the interface of media. This signal has a certain width due to the features of generation of the electromagnetic radiation pulse.

Fig. 2.9 shows the module of the Hilbert transform of the signal of the “OKO” antenna unit with a center frequency of 1700 MHz. The depth scale is calculated with the formula  $x = \frac{ct}{2n}$  for a medium with an absolute refractive index of  $n=3.16$  close to the one defined in this work for the rigid base of the tunnel.

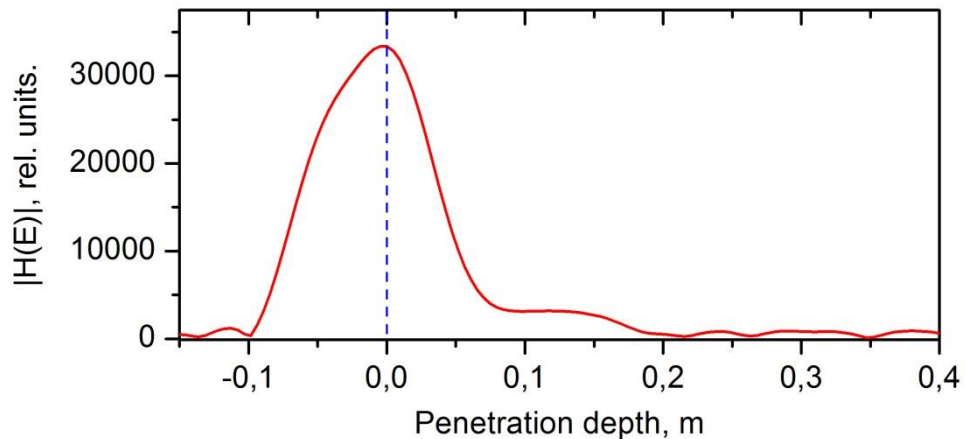


Figure 2.9. Module of the Hilbert transform of direct penetration signal from the antenna unit at a frequency of 1700 MHz.

Suppose that the zero of the depth scale coincides with the boundary between the media. Then one can see from Fig. 2.9 that the signal reflected by the boundary weakens approximately three times at a depth of 0.05 m. It is obvious that at  $r_0 < 0.05$  m the signal recorded by the receiving antenna will consist mainly of the component associated with the reflection from the interface. In this regard, to reduce the error of the numerical procedure for determining the attenuation coefficient in a layer with thickness  $h$ , it is necessary either to use the trace fragments for which the condition  $h \gg r_0 = 0.05\text{m}$  is satisfied, or to reduce the length of the wave train by increasing the center frequency of the GPR pulse.

To estimate the accuracy of the proposed procedure for calculating the electromagnetic waves attenuation coefficient, an independent determination of the attenuation coefficient is made using the amplitudes of the waves reflected by upper and lower boundaries of the water layer. The ratio of equations of the form (2.10) and (2.8) written for a layer of water leads to the following expression for determining the electromagnetic radiation attenuation coefficient  $p$ :

$$p_{H_2O} = \frac{1}{2h} \ln \left( \frac{4n_{H_2O}}{(n+1)^2} \left| \frac{E_1}{E_2} \right| \right), \quad (2.12)$$

where  $n_{H_2O}$  is the absolute refractive index of industrial water,  $h$  is the thickness of the water layer,  $E_1$  and  $E_2$  are the amplitudes of the electromagnetic waves reflected by the upper and lower boundaries of the water layer, respectively. The absolute refractive index of industrial water entering (2.12) is determined from the relation:  $n_{H_2O} = c\Delta\tau / h$ , where  $c$  is the speed of light in vacuum, and  $\Delta\tau$  is the time interval during which the signal travels from the lower boundary of the water layer to the receiving antenna located near its upper boundary. The quantities  $\Delta\tau$ ,  $E_1$  and  $E_2$  required for the calculations, are determined from radargrams. The positioning of upper and lower boundaries of the water layer on the radargram, and the known thickness of the water layer, made it possible to estimate the refractive index of water at a frequency of 1700 MHz,  $n_{H_2O} = 7,3$ , and to calculate the attenuation coefficient  $p_{H_2O} = 8.13\text{m}^{-1}$ .

The values of attenuation coefficients for water obtained with the use of formulas (2.11) and (2.12) are given in Table. 2.1. Comparison of the data in Table 2.1 allows estimating the accuracy of the mathematical procedure for the processing of traces to be about 20%.

**Table 2.1.** Fit parameters in formula (2.11) approximating the modules of Hilbert transforms of radargrams and electromagnetic radiation attenuation coefficients in structural levels of the tunnel

Structural level	$A$ , rel.u.	$r_0$ , m	$p$ , $m^{-1}$
Industrial water, асимптотическое значение eq. (2.11)	37.04		10.1
Industrial water, eq. (2.12)			8.13
Rigid base ( $p_1$ ), eq. (2.11)	7513	0,025	19.28
Leveling layer ( $p_2$ ), eq. (2.11)	141	0.025	7.82
Leveling layer ( $p_2$ ), method of Sect. 3.3	710		6.90
Leveling layer ( $p_2$ ), eq. (2.14)			7.01
Invert ( $p_3$ ), eq. (2.11)	397	0.025	20.79

### 2.3.2. The use of traces to determine the attenuation coefficients of tunnel structural layers

To determine the attenuation coefficients of electromagnetic radiation of the rigid base  $p_1$ , the leveling layer  $p_2$  and the invert  $p_3$ , the radargram shown in Fig. 2.6 treated *via* the method described in Sect. 1 is additionally subjected to the Hilbert transform. The result of the transformation is shown in Fig. 2.10.

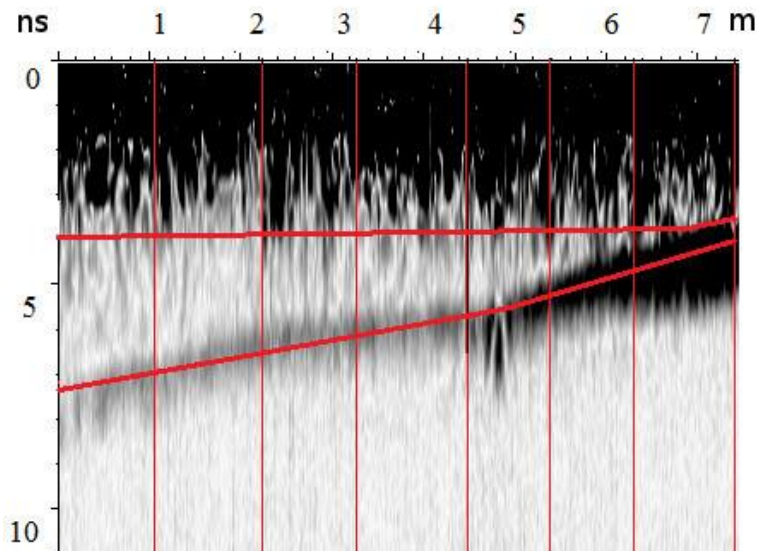


Figure 2.10. GPR image of the module of Hilbert transform of the radargram shown in Fig. 2.6

In the resulting transformed radargram, a section corresponding to the movement of the antenna block by 0.25 m at the beginning of the trajectory of motion is singled out. The traces of this trajectory section subjected to the Hilbert transform, are averaged over the length of the section, after which the in-depth sections are identified that correspond to the rigid base and the leveling layer. Modules of the Hilbert transforms of the radargrams in the region of the rigid base and the leveling layer are shown in Fig. 2.11 and Fig. 2.12.

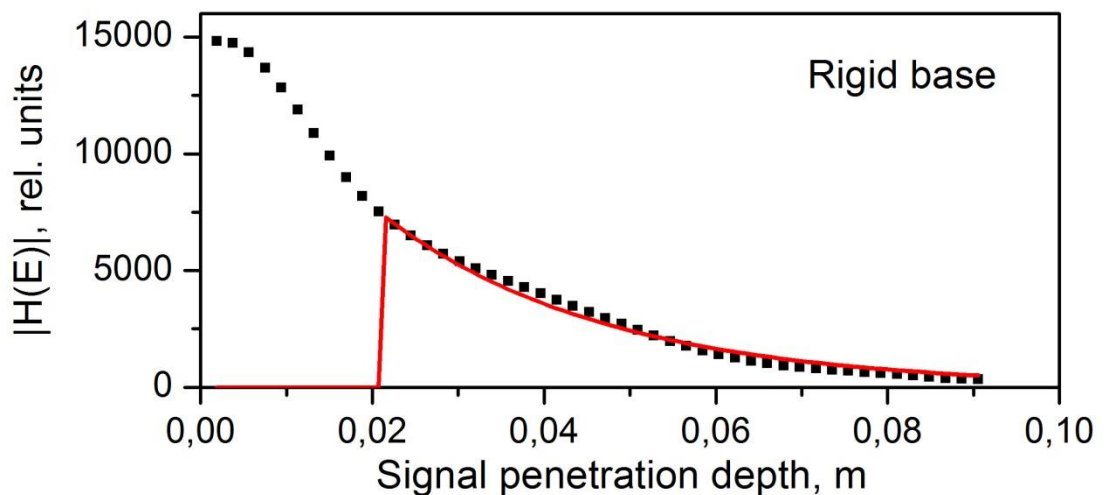


Figure 2.11. Module of the Hilbert transform of radargrams in the region of the rigid base.

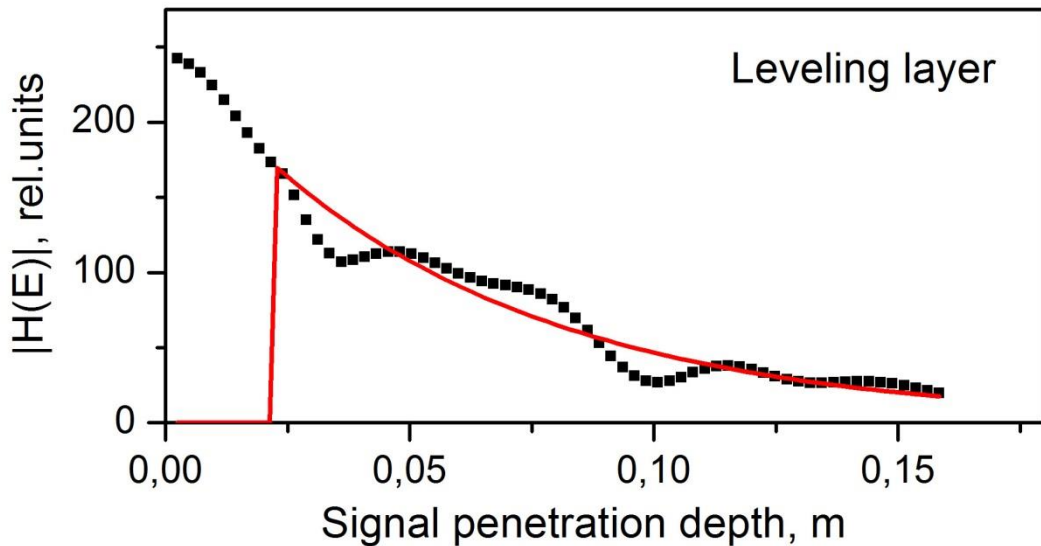


Figure 2.12. Module of the Hilbert transform of radargrams in the region of the leveling layer.

The experimental values of the modules of the transforms in these figures are given by black squares. Solid lines show the results of fitting with (2.11). Optimal values of fit parameters and attenuation coefficients are presented in Table 2.1.

To determine  $p_3$ , in the radargram shown in Fig. 2.10, a section corresponding to the movement of the antenna block by 0.25 m at the end of the trajectory is singled out, where there is a contact of the rigid base and the invert. The traces of this section are averaged, after which an in-depth section corresponding to the invert is selected (Fig. 2.13). Experimental  $|H(E)|$  (solid squares) are fitted with equation (2.11) (solid line). Optimal values of the fit parameters and attenuation coefficient are presented in Table 2.1.



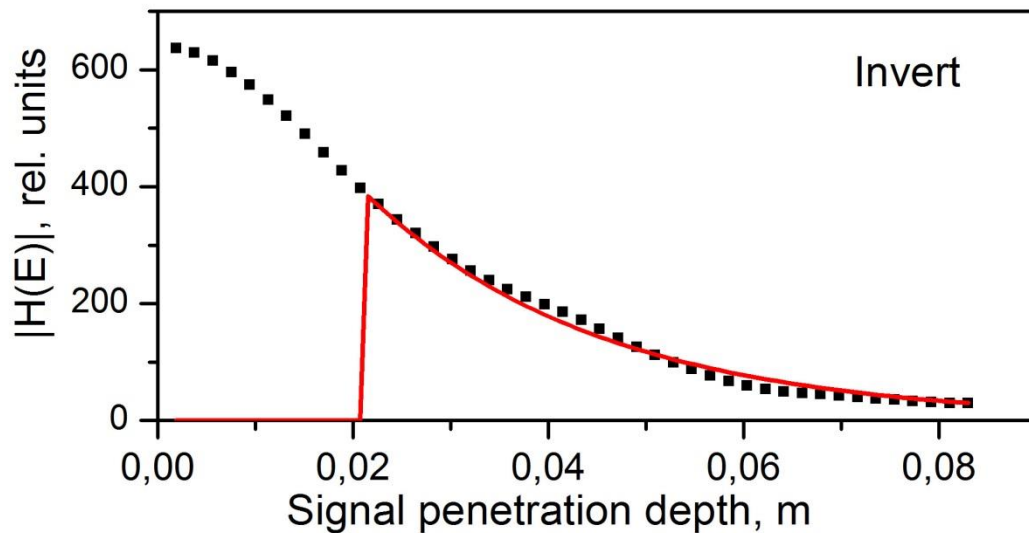


Figure 2.13. Module of the Hilbert transform of radargrams in the region of the invert.

### 2.3.3. Using the amplitude of the signal reflected by the interface of the structural layers of variable thickness to determine the attenuation coefficient of the leveling layer

Variation of the leveling layer thickness in the cross-section of the road surface on the curved sections of the road makes it possible to determine the coefficient of attenuation of electromagnetic radiation by layer material by comparing the intensity of the signal reflected from the boundary with the invert (lower red line in Fig.2.10). In this case, according to (2.3), the amplitude of the signal reaching the receiving antenna after reflection from the boundary depends on the thickness of the leveling layer according to the expression:  $E_3 \sim e^{-2\rho_2 h_2}$ .

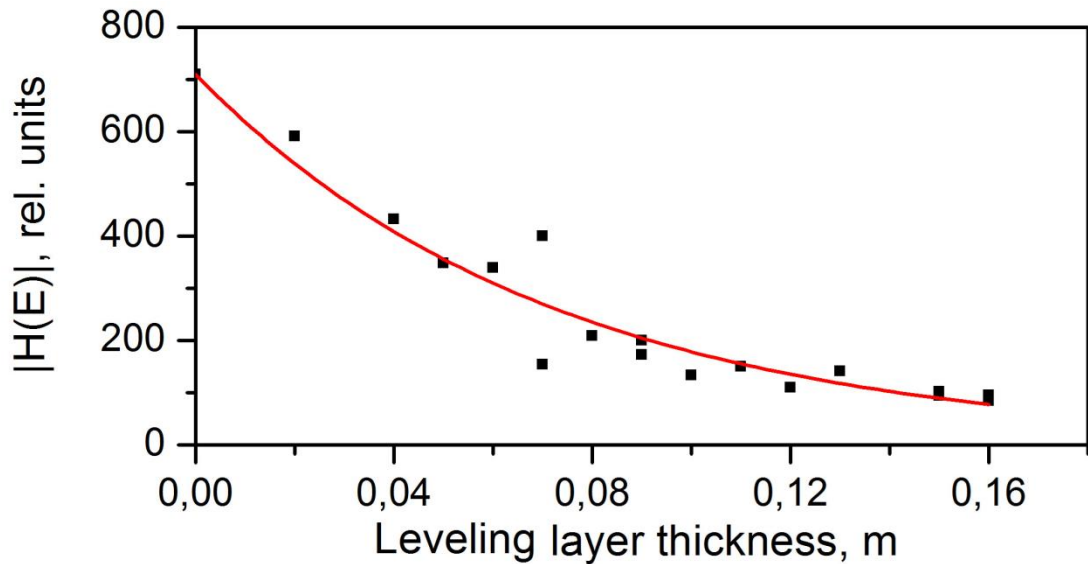


Figure 2.14 Module of the Hilbert transform of the signal reflected from the boundary with the invert as a function of the thickness of the leveling layer.

Figure 2.14 shows the modules of Hilbert transforms of signals reflected from the boundary between the leveling layer and the invert (Fig.2.10) obtained at points spaced 0.5 m apart. The results of fitting of the obtained values with the function (2.11) are given in Table 2.1. Comparison of the attenuation coefficients of the leveling layer given in Table 2.1 makes it possible to estimate the error of the numerical routine to be about 15%.

#### 2.4. Determination of the absolute refractive indices of structural layers

The amplitudes  $E'_2$ ,  $E'_3$  and  $E'_4$  of the reflected waves formed at the interfaces of structural layers (Fig. 2.2) required for the calculation of the refractive indices are given in Table 2.2. For their determination, intervals of the GPR section are identified that do not contain local objects that could distort the wave pattern from the interface between the media. To improve the accuracy of the numerical procedure, averaging was performed over 10 traces of this profile and over three adjacent GPR sections of the same type. Table 2.2 also lists all possible relationships between the refractive indices of the rigid base, the leveling layer and the invert, and the solutions of equations (2.8-2.10) for  $E'_0 > 0$ . It should be noted that the analysis of the phase of electromagnetic radiation reflected from interfaces requires imple-

mentation of numerical procedures for phase analysis; this will be done below. In this section, we consider all possible combinations of the phases of  $E_2'$ ,  $E_3'$ , and  $E_4'$ . The choice of  $E_0' < 0$  in the solution of equations (2.8-2.10) does not give any new physically meaningful values of refractive indices, and reduces to the inversion of phases of  $E_2'$ ,  $E_3'$  and  $E_4'$ .

Table 2.2. Values and relations between the absolute refractive indices of the structural layers calculated by solving the equations (2.8-2.10) with experimental values of the amplitudes  $E_2'$ ,  $E_3'$ ,  $E_4'$ .

	Relation between $n_1, n_2, n_3$	$E_2'$	$E_3'$	$E_4'$	$n_1$	$n_2$	$n_3$	$E_0$
1	$n_1 > n_2 > n_3$	243	95	541	No solution found **			
2	$n_1 > n_3 > n_2$	243	-95	541	No solution found **			
3	$n_1 > n_2 > n_3, n_1 < n_3$	243	95	-541	Solution impossible*			
4	$n_3 > n_1 > n_2$	243	-95	-541	3.16	2.73	4.41	3293
5	$n_2 > n_1 > n_3$	-243	95	541	3.16	3.67	2.27	3293
6	$n_1 < n_2 < n_3, n_1 > n_3$	-243	-95	541	Solution impossible*			
7	$n_2 > n_3 > n_1$	-243	95	-541	No solution found **			
8	$n_1 < n_2 < n_3$	-243	-95	-541	No solution found **			

\*there is a contradiction between the relative values of the refractive indices and the phases of experimental amplitudes of the waves  $E_2'$ ,  $E_3'$ , and  $E_4'$ .

\*\* Refractive indices found have no physical meaning, for example, they become less than unity.

Table 2.3. Solutions of equations (2.8-2.10) for the  $E_0$  wave amplitude and the values of the absolute refractive indices of structural layers absent in Table 2.2.

Relation between $n_1, n_2, n_3$	$E_2'$	$E_3'$	$E_4'$	$n_1$	$n_2$	$n_3$	$E_0$
$n_1 > n_2 > n_3$	243	37	541	3,16	2,72	2,26	3249
$n_1 > n_3 > n_2$	443	-12,5	341	3,16	2,28	2,46	2742
$n_2 > n_3 > n_1$	-443	12.5	-341	3,16	4,38	4,06	2743
$n_1 < n_2 < n_3$	-243	-37	-541	3,16	3,67	4,42	3252

Table 2.3 illustrates the attempts to obtain a solution for the "no solution found" cases in Table. 2.2 by variation of  $E_2'$ ,  $E_3'$  and  $E_4'$  wave amplitudes over wide ranges. It is seen that the deviations of the amplitudes from the experiment we had to use (Table 2.2) significantly exceed possible errors in the experimental measurements (10-20%).

The accuracy of the solutions in Table 2.2 depends on the accuracy with which the values of  $E_2'$ ,  $E_3'$ ,  $E_4'$ , and  $p_2$  and are determined from the radargrams. Figure 2.15 shows the variation in  $n_2$  and  $n_3$  depending on the amplitudes of  $E_2'$ ,  $E_3'$ , and  $E_4'$  for the  $n_3 > n_1 > n_2$  case. It can be seen that the error in determining the amplitudes  $\delta E_i' = 10\%$  can lead to a change in calculated refractive indices by a factor of 2.5. In this regard, to improve the accuracy of the results of the developed numerical procedure, it is necessary to use the GPR equipment, which has high accuracy in determining signal amplitudes (up to  $\delta E_i' = 1\%$ ) due to increasing the stability of the equipment functioning, and reducing the sampling time of the GPR signal.

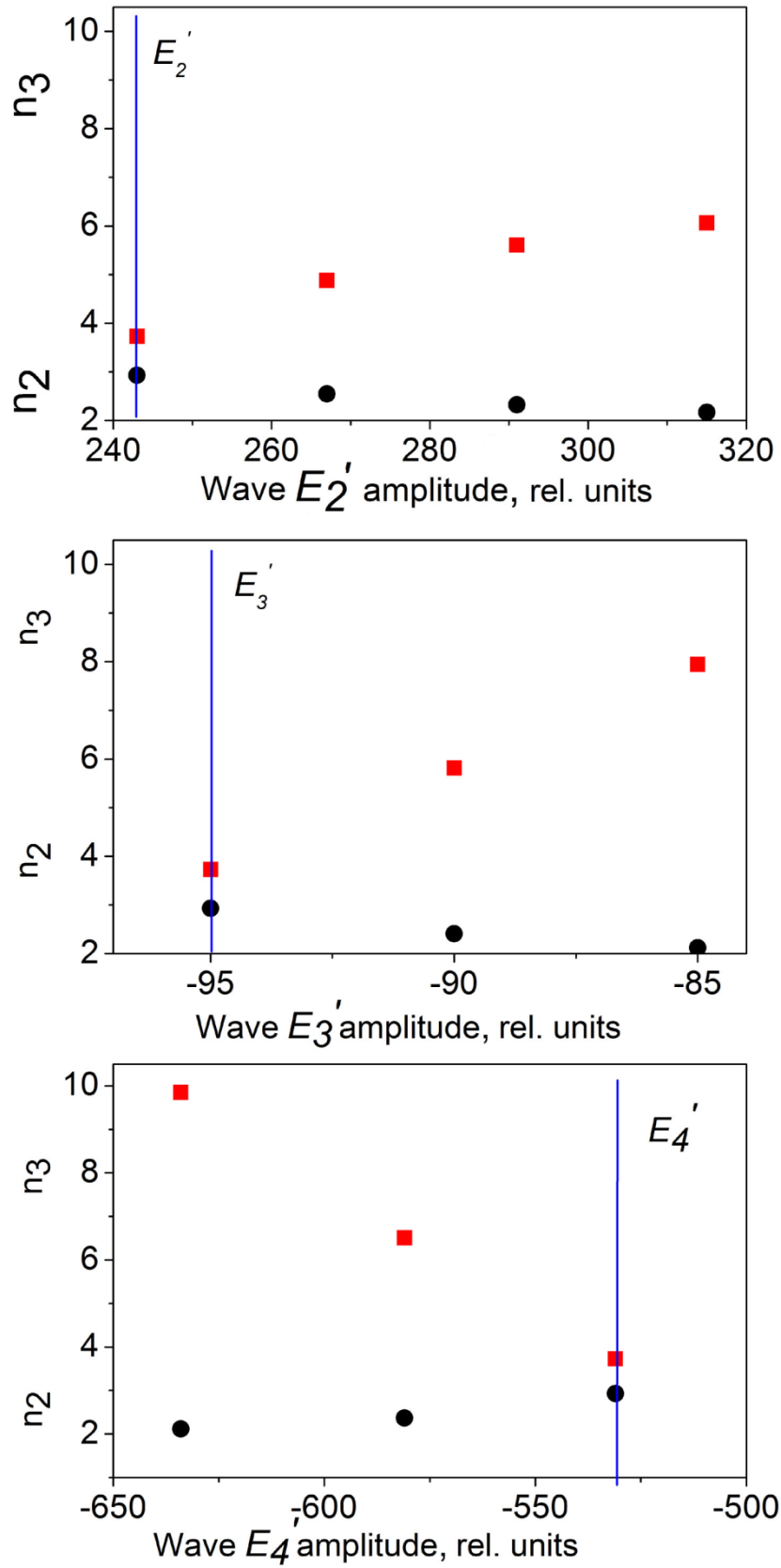


Figure 2.15. Changes in the values of the refractive indices  $n_2$  (circles) and  $n_3$  (squares) depending on the variation of amplitudes  $E_2'$ ,  $E_3'$  and  $E_4'$ . Experimental values are marked with a vertical line.

## 2.5. Selection of refractive indices using phase analysis of radargrams

To select the solutions among the possible options given in Table 2.2, the phases  $\Psi_i(t)$  of the traces  $s_i(t)$  were calculated ( $i$  numbers the traces in the radargram) with

$$\Psi_i(t) = \arctg \frac{\hat{s}_i(t)}{s_i(t)}, \quad (2.13)$$

where  $\hat{s}_i(t)$  is the orthogonal complement of the trace defined by the Hilbert transform:

$$\hat{s}_i(t) = \int_{-\infty}^{\infty} \frac{s_i(\tau)}{\pi(t-\tau)} d\tau.$$

Function  $\hat{s}_i(t)$  satisfies the relation  $\int_{-\infty}^{\infty} s_i(t) \hat{s}_i(t) dt = 0$

Calculated  $\Psi_i(t)$  are shown in Fig.16 together with the traces from the domains of the radargram designated as  $a$ ,  $b$  and  $c$ . It can be seen that near the interfaces of the rigid base and the leveling layer (position  $a$ ), there is no change in the phase of the reflected signal meaning that  $n_1 > n_2$ . At the same time, the phase change is seen at the interface between the leveling layer and the invert (position  $b$ ), as well as at the interface between the rigid base and the invert (position  $c$ ). Inversion of phase at these boundaries means a greater value of the absolute refractive index of the invert  $n_3$  compared to that of the leveling layer,  $n_2$ ; this allows us to choose the solution ( $n_1 > n_2 < n_3$ ,  $n_1 < n_3$ ) as physically justified.

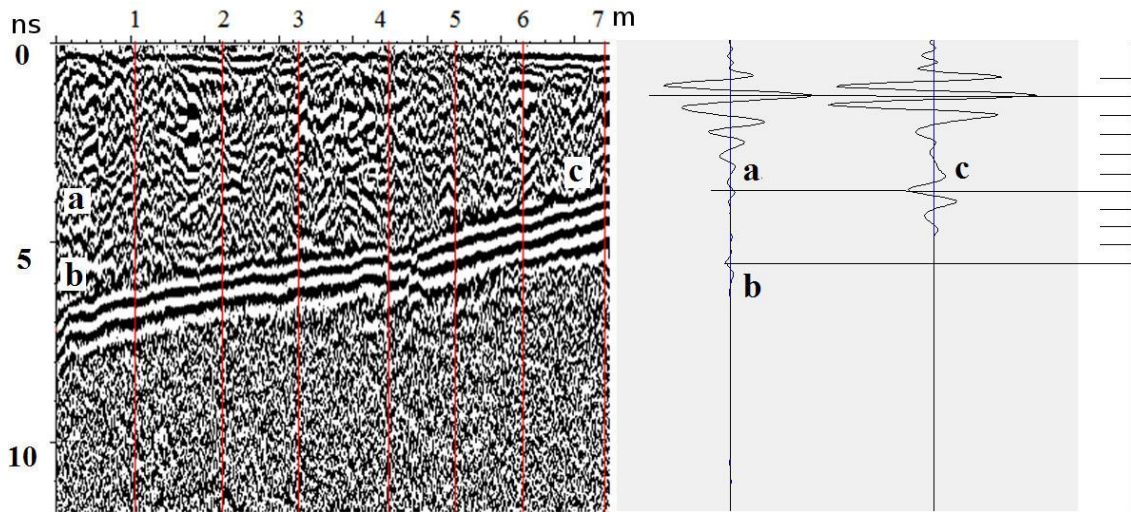


Figure 2.16. The phases of traces in the radargram shown in Fig. 2.6 calculated with (2.13). Horizontal segments on the scale on the right indicate positive values of the trace amplitudes in the absence of media interfaces.

## 2.6. Determination of the attenuation coefficient in the leveling layer by the amplitudes of the signals reflected by its boundaries

Determination of the refractive indices of structural layers by solving the system of equations (2.8-2.10) makes it possible to calculate the leveling layer's attenuation coefficient from the amplitudes of the waves reflected from the interfaces. The ratio of equations (2.10) and (2.8) leads to the following expression for the attenuation coefficient of electromagnetic radiation in the leveling layer:

$$p_2 = \frac{1}{2h_2} \ln \left( \frac{4n_1n_2|n_3-n_2|}{|n_2-n_1|(n_3+n_2)(n_2+n_1)} \left| \frac{E_2'}{E_3'} \right| \right) \quad (2.14)$$

The value of the attenuation coefficient  $p_2$ , calculated with (2.15) for  $h_2 = 0.15$  m is given in Table 2.1.

## 2.7. Results and Discussion

### 2.7.1. Verification of GPR results using alternative methods

GPR studies and the proposed methods for the data processing discussed above made it possible to determine the absolute refractive indices  $n_1$ ,  $n_2$ ,  $n_3$  and the attenuation coefficients  $p_1$ ,  $p_2$ ,  $p_3$  for electromagnetic radiation in the structural layers of the roadway of the automobile tunnel made of concrete of different brands.

The verification of the obtained results was performed as follows. The refractive index  $n_1$  was used to calculate the thickness of the rigid base, which is found to be  $h_1 = 0.19$  m. The thickness of the rigid base made after its disassembly is measured directly and found to be 0.20 - 0.22 m. Comparison of the thicknesses thus obtained gives an estimate of the accuracy of the GPR method for determining the refractive index,  $\delta n_1 = 10\%$ . Comparison of calculated thickness of the leveling layer and the results of its direct measurement leads to a similar estimate of the error of the refractive index  $n_2$ .

To assess the accuracy of the GPR determination of the attenuation coefficient for electromagnetic radiation in the leveling layer, we compare the results of calculations performed by different methods and given in Table 2.1. It is clear that those results are similar; the average value is  $p_2 = 7.24 \text{ m}^{-1}$  with an error less than 5%.

At the same time, solving the system of equations (2.8-2.10) provides the significantly different values of the refractive indices of the rigid base and the invert made of concrete of the same B25-type (Table 2.2). This can be explained by the overmoisture of the invert, which was confirmed by the excavation work of the rigid base and the leveling layer (Fig. 2.17).

To determine possible moisture of the concrete of the invert we confine ourselves to the approximation of independent media. In this approximation, the optical density of water-saturated concrete is a sum of the optical densities of the concrete frame, and the pore water.

Suppose that the volume of the invert  $V$  contains the volume of water  $V_{H_2O}$ , then:

$$n_3 = n_1 + wn_{H_2O}, \quad (2.15)$$

where the volumetric moisture of concrete is determined by the relation:

$$w = V_{H_2O}/V.$$



Relation (2.15) allows one to estimate the volumetric moisture to be  $w=14\%$ . In (2.15), the refractive indices from Table 2.2 and the refractive index of industrial water determined in this work were used.

A similar estimate of the volumetric moisture can be made based on the attenuation coefficient of electromagnetic radiation in the rigid base, the invert and water:

$$p_3 = p_1 + wp_{H_2O}. \quad (2.16)$$

The attenuation coefficients necessary for the calculations with (2.16) are obtained by averaging the values given in Table 2.1. Relation (2.16) allows estimating the volumetric moisture to be  $w=17\%$ ; it compares with the value obtained from (2.15) with an accuracy of 18%.

The proximity of the obtained moisture values can serve as an indirect evidence of reliability for the proposed methods for processing GPR data in obtaining the numerical values of  $n_3$ ,  $p_1$ , and  $p_3$ .

### 2.7.2. Contrast of construction layers

According to the tunnel construction project, a B25-type concrete was used to form the rigid base and the invert, and the leveling layer is made of a B15-type concrete. The concretes used can have significant variations both in the composition of the ingredients and in their electrical properties. It is therefore advisable to check the validity of the relation  $n_1 > n_2$  in laboratory conditions, for example by the method [55]. In addition, the approximate relationship between the refractive indices of these layers can be estimated at the frequencies of the GPR measurements by the relation:

$$\frac{n_{B25}}{n_{B15}} = \frac{n_c m_c + n_s m_s + n_{cs} m_{cs}}{n_c m_c + n_s m_s + n_{cs} m_{cs}}, \quad (2.17)$$

where  $n_c$ ,  $n_s$ ,  $n_{cs}$  and  $m_c$ ,  $m_s$ ,  $m_{cs}$  are refractive indices and mass concentrations of cement, sand and crushed stone, respectively, the stroke indicates the components of the B15-type concrete.

To estimate the ratio of refractive indices, the values of the refractive indices of materials are used from "Recommendations for quality control of road construction works using the GPR method" published on the basis of the instruction of the Federal Road Agency dated 10.06.2016 No. 1025-p, and from the study of [95]. The values of mass concentrations are taken from the standard "GOST 27006-86 Concrete. Rules for the selection of composition". The values of refractive indices and mass concentrations used in the calculation may well vary depending on the frequencies of GPR surveys, materials used, and required density of concrete mixes. In this regard, the evaluation of the refractive indices ratio with (2.17) should be considered rather approximate. The calculation showed that the grade B15 concrete can have a refractive index 10% less than the B25 concrete, which is consistent with the ratio of 1.10 obtained with formula (2.16) using the data given in Table 2.2.

The proximity of the electrical characteristics of concretes grades B15 and B25 allows explaining the low contrast of the interface between the rigid base and the leveling layer equation (2.8). It can be seen from Fig. 2.6 that the interface between these structural layers is formed from fragments of the GPR irregularity patterns in a rigid base.

At the same time, the interface between the leveling layer and the invert is represented by a contrast line in the GPR section shown in Fig. 2.6; this can be explained by a noticeable difference in the refractive indices (eq. 2.10) caused by water saturation of the invert.



Figure 2.17. Water in the area of local dismantling of the rigid base and leveling layer

## 2.8. Conclusions

Timely and successful implementation of anti-deformation and repair works on extended transport infrastructure objects depends largely on the analysis of the state of the construction layers. In this work, we propose a method for determining the electrical characteristics and moisture content of road construction layers based on the use of the GPR technologies.

The method does not require additional integration with other geophysical or destructive methods. It is used in this work to calculate the refractive indices and attenuation coefficients for electromagnetic radiation in the concrete layers of the carriageway of the automobile tunnel. The use of modern GPR equipment and the proposed numerical procedures made it possible to determine the values of electrophysical quantities with an accuracy of 10–15%. The results obtained were used to clarify the dimensional parameters of the layers and to determine the volumetric moisture of the concrete of the invert which are necessary when planning reconstruction activities.

The possibility of determining the electrophysical quantities without using any additional information makes the proposed method promising for the use in the software systems for automatic processing of GPR information when monitoring

extended sections of roads and railways. Electrophysical quantities and moistures determined during surveying allow estimating the rate of degradation of structural layers' materials which is necessary for timely repairs.

Further development of the method, along with the development of the self-consistent procedures for the solution of equations (2.1-2.3, 2.7) or (2.8-2.10), may be associated with the refinement of physical assumptions, namely, with the rejection of the approximation of normal incidence, with additional consideration of the spectral features of the incident radiation, and dispersion dependences of electrophysical quantities.

The practical use prospect of the developed monitoring method depends significantly on the accuracy of obtaining and processing the GPR data, which, in turn, is associated with the technical capabilities of the GPR equipment and surveying techniques.

## **Chapter 3. Resonance method for determining the electrophysical properties of soils and materials.**

### **3.1. Objectives of the study.**

The presence of water in the structural layers of engineering structures, roadbed layers of roads and railways can adversely affect the stability of the structures. In this regard, it is important to quantitatively characterize the soil moisture both at individual points of the structure [95] and along its extended sections [53].

Traditionally, the density and humidity of soils are determined by destructive methods, for example, by drilling and sampling. These methods are characterized by high accuracy of measurements, however, they are relatively expensive and time consuming; they also require stopping the traffic on the surveyed site during the measurements. To overcome these difficulties, it is increasingly recommended to use non-destructive geophysical methods [95,96].

An important place among geophysical methods is occupied by the GPR method, which allows obtaining continuous information about the state of soil layers, both in the mode of detailed diagnostics, and as part of specialized diagnostic mobile tools (railway cars, mortises, and automobiles). For its effective use in solving the problems of quantitative diagnostics of infrastructure facilities, the procedure of integration of the GPR methods and the methods of direct measurements of electrophysical properties of soils and materials seems promising.

*In this regard, this chapter solves the problem of developing a technique for resonant measurements of the dielectric constant and specific conductivity of soil-forming minerals at different humidity at a frequency of 1400 MHz.*

For solving the problem, the following studies have been performed.

- 1) Designing a cavity resonator for measuring the properties of materials extracted from the core.
- 2) Determination of the dependence of the resonant frequency on the dielectric constant of samples with known values of basic electrophysical parameters.
- 3) Creating a computer model of the cavity resonator, in accordance with the prototype, using the software CST Studio Suite.

4) Determination of the resonance frequency of electromagnetic waves that have passed through the reference samples with known dielectric constant values.

*The second problem of the research is connected with the creation and use of a number of methods, including GPR and resonance measurements, for determining the electrophysical properties of soil media and materials at different values of moisture.*

To solve it, the following studies were performed.

1) Integrated study of dielectric properties of soil-forming minerals with different moisture using the cavity resonator method, and simultaneous GPR measurements at a frequency of 1.4 GHz.

2) Determination of the real part of dielectric constant and the conductivity of soil-forming minerals by the developed set of methods.

### **3.2. Soils model**

The principal components of the soil are soil-forming minerals, air, water in various aggregative states, aqueous solutions of salts, organic and inorganic impurities. The diversity of the pore space structure and different nature of surfaces of the soil particles lead to specific features of their interaction with water vapor and water. The mechanism of absorption and retention of moisture depends on the size and shape of their pore space, as well as on the surface area, and surface hydrophilicity. Water in grounds, rocks and soils can be in a free or a bound state. Free water is water under the action of gravity in non-capillary-sized macropores and rock cracks, as well as water held in pores and cracks by capillary forces. In contrast, the bound water is retained in soils due to chemical and physicochemical forces acting from the surface of the particles and changing its properties in comparison to the free water [97].

### 3.3. Analytical models of dielectric constant in soils

#### 3.3.1. Water in soils

Natural dispersed structures, including rocks and soils, are complex polydisperse formations with a diverse structure of the pore space and different nature of the surface of the particles forming them. In this regard, the soils have specific features when interacting with water vapor and liquid water (Fig. 3.1). The absorption and retention of moisture depends on the size and the shape of their pore space, as well as on the area of their surface, and its hydrophilicity.

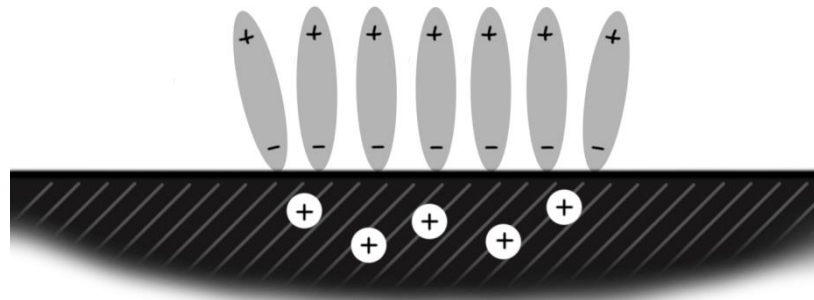


Figure 3.1. Orientation of water molecules dipoles on the adsorption centers of the mineral surface

According to the classification often used in soil science and geology [96-99], the soil moisture is divided into free and bound, and the latter is subdivided into tightly bound and loosely bound (weakly bound).

I. **Tightly bound water** is divided into:

- 1) chemically bound, *i. e.* being the part of minerals in the form of ions in molecules of the mineral, or in the form of molecules in the crystal lattice of the mineral;
- 2) adsorbed - physically absorbed from solutions by soil particles;
- 3) hygroscopic - absorbed by soil particles from the air.

Tightly bound water is not capable of moving in the soil without its heating or compaction.

II. **Loosely bound water** is water that envelops soil particles with a film of different thickness and it moves along the film as a liquid from areas with greater film thickness to areas with smaller thickness.

III. **Free water** is divided into:

1) gravitational water - its movement in the pores under the action of gravity is not hampered by capillary and electromolecular forces; water in separately localized pores larger than 1 mm also belong to this kind;

2) capillary water held in pores and cracks by capillary forces.

It is believed that all water, except chemically bound, can be removed from the soil by heating it to a temperature of 105–110 ° C.

According to an alternative classification, there are the following types of water in soil:

I. **Bound water**. It is retained in the soil due to chemical and physicochemical forces acting from the surface of the particles and changing its properties in comparison with free water (Fig. 3.2). It is subdivided into two types:

1. Water of the lattice (constitutional, crystallization-bound). This water is part of minerals in the form of ions in the molecule of the mineral, or in the form of molecules in the crystal lattice of the mineral.

2. Adsorption water (monomolecular and polymolecular adsorption). Adsorption-bound water has different energy types:

a) of higher binding energy (40–120 kJ/mol) – the water of monomolecular adsorption;

b) of lower binding energy (<40 kJ / mol) – the water of polymolecular adsorption



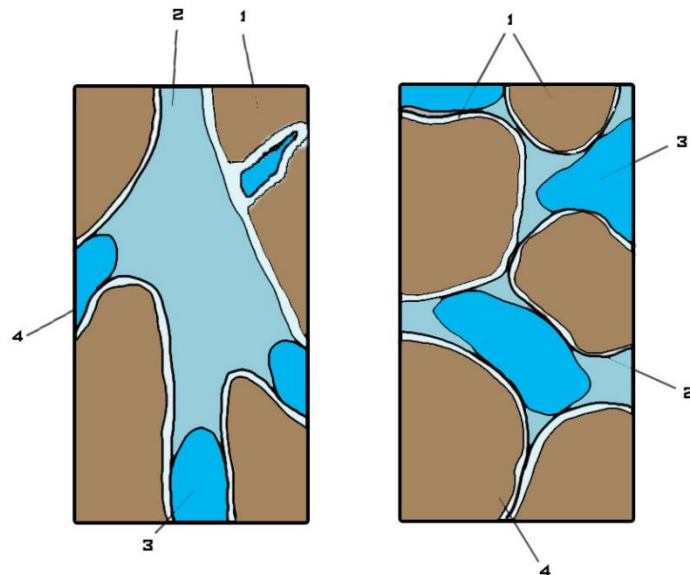


Figure 3.2. Bound water in the soil: 1 - soil particles; 2 - capillary water; 3 - air; 4 - adsorption water

**II. Water of transitional type** (from bound to free) is determined on the basis of insignificant action of surface forces on it; its properties and mobility are close to those of free water, but at the same time it is held near the surface of a particles of the soil grounds due to weak “physical-mechanical” bonds (Fig. 3.2). It is subdivided into two moisture types.

1. "Osmotically" absorbed water - absorbed due to selective diffusion of water in the direction of the surface of the particles ("surface osmosis"). The layer of “osmotically” absorbed water experiences some influence of surface forces, which can affect its structural features. In this case, in the water layer of up to  $10^{-6}$  cm, not only the ordered arrangement of its molecules is possible, but also the formation of a transition (“melted”) layer of moisture with a “disordered” arrangement of molecules in it. In the case of high salinity of the solution interacting with the rock, “osmotic” water is not formed.

2. Capillary water (capillary condensation and absorption) is water in the capillary-sized pores ( $<1$  mm), absorbed by capillary pressure and held by the capillary forces of the meniscus at the inter-phase boundary: water - air - solid surface.

III. **Free water** (closed in large pores and flowing). Water in a liquid state ("gravitational"), which is exclusively under the action of gravity in non-capillary-sized macropores and rock cracks (> 1 mm), and water in closed macropores.

All of these types of water are found in soils of different composition, and the greater the specific surface area of the solid component (the surface area of particles in 1 g of soil) and the lower the soil moisture, the greater is the role played by bound water.

The variety of water types in the soil is characterized by several parameters. The main parameter is the weight moisture of the soil, which is determined as the ratio of the mass difference of a soil sample before and after drying at 105–110 ° C to the absolutely dry state to the mass of absolutely dry soil sample; is expressed in fractions or in percent. Along with the weight moisture, there exists the parameter of volumetric moisture, which is the volume of water in a unit volume of soil.

### 3.3.2. Analytical dielectric permittivity models related to the porosity parameter

To create a model that describes the distribution of the dielectric constant in a real environment (soil, clay, sand), we use the porosity parameter ( $\phi$ ). The porosity of the soil is the ratio of volume occupied by the soil voids, to the total volume of the soil with natural moisture. Using the relationship of the refractive index and dielectric constant

$$n = \sqrt{\epsilon_r} \quad (3.1)$$

one can express the refractive index in the approximation of non-interacting phases that make up the soil:

$$\sqrt{\epsilon_r} = n = (1 - \phi)\sqrt{\epsilon_{r,g}} + \phi S_w \sqrt{\epsilon_w} + \phi(1 - S_w)\sqrt{\epsilon_{r,a}} \quad (3.2)$$

where  $\phi$  is the soil porosity,  $S_w$  is the degree of humidity,  $\epsilon_{r,g}$ ,  $\epsilon_{r,w}$ ,  $\epsilon_{r,a}$  are the real parts of the dielectric constant of soil, water and air, respectively. The degree of moisture can be determined with  $W = \frac{m_{water}}{m_{soil}}$  by the relation:

$$W = \frac{\phi \times S_w \times V_{box} \times \rho_w}{m_{soil}}, \quad (3.3)$$

where  $V_{box}$  is the volume of the cubic form in which the sample is placed,  $\rho_w$  is the density of water,  $m_{soil}$  is the mass of the sample.

### 3.3.3. Models of effective dielectric constant

Consider soil samples as diverse systems of microparticles. If any macroscopic parts of this system exceed characteristic dimensions of its components, and the distances between them are large, then the so-called effective model can be used to describe its properties. In this model, the soil is considered as a homogeneous medium (matrix) having its macroscopic characteristics, and inclusions (Fig.3.3) [100-101].

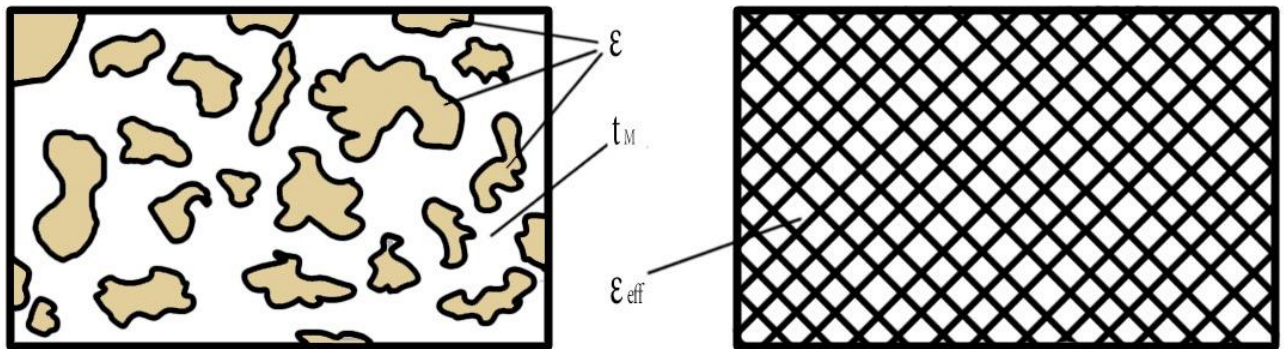


Figure 3.3. Schematic representation of the real heterosystem (left) and its effective model (right).

Consider the matrix of a medium with a dielectric constant  $\epsilon$  having isolated inclusions (for convenience, we assume that all the inclusions are spherical) with a dielectric constant  $\epsilon_1$ . We assume that all inclusions have the same macroscopic properties and their volume fraction  $f_1$  is much smaller than that of the matrix. Due to the rarity of inclusions, it is assumed that in an electric field, the resulting polarization in the sphere will not affect the polarization of the matrix as a whole. In this case, each selected sphere is placed in a uniform electric field and surrounded by a medium with dielectric constant  $\epsilon$ . Then the polarization inside this sphere is calculated as:

$$\vec{P} = 3\epsilon_0 \frac{\epsilon_{eff} - \epsilon}{\epsilon_{eff} - 2\epsilon} \quad (3.4)$$

On the other hand, this polarization is the sum of polarizations of all the inclusions:

$$\vec{P} = \frac{1}{V} \sum_k 3\varepsilon_0 \frac{\varepsilon_1 - \varepsilon}{\varepsilon_1 + 2\varepsilon} \langle \vec{E} \rangle \Delta V_k = 3f_1 \frac{\varepsilon_1 - \varepsilon}{\varepsilon_1 + 2\varepsilon} \langle \vec{E} \rangle, \quad (3.5)$$

where  $f_1 = \frac{1}{V} \sum_k \Delta V_k$  is the volume fraction of inclusions and  $k$  numbers the inclusions.

From the equality of the right-hand sides of equations (3.4) and (3.5) follows the expression for the effective dielectric constant:

$$\frac{\varepsilon_{eff} - \varepsilon}{\varepsilon_{eff} + 2\varepsilon} = f_1 \frac{\varepsilon_1 - \varepsilon}{\varepsilon_1 + 2\varepsilon}$$

or

$$\varepsilon_{eff} = \varepsilon \frac{\varepsilon_1(1 + 2f_1) + 2\varepsilon(1 - f_1)}{(1 - f_1)\varepsilon_1 + (2 + f_1)\varepsilon}, \quad (3.6)$$

At  $f_1 \rightarrow 0$ , (3.6) is reduced to  $\varepsilon_{eff} = \varepsilon$ .

The models described make it possible to calculate the dielectric constant of various media for small and large volume contents of inclusions.

### **3.4. Designing a cavity resonator for measuring the properties of materials taken from the core.**

Depending on the size of the sample, various types of resonators and measurement methods are used. Since in this work the sample taken from the core is a cylinder with a diameter of  $d_0 = 19.7$  mm and a height of  $l = 8.04$  mm, the cavity resonator designed should be a limited segment of a circular waveguide with transverse dimensions close to the dimensions of the sample under study.

For the correct measurement of the properties of materials, a cavity resonator with the oscillation of  $H_{01p}$  type for samples in the form of a disk was used. The operating frequency range in which the resonator should operate was determined from the frequency range at which diagnostics of the structural layers of the

transport infrastructure is carried out; it ranges from 0.4 GHz to 1.7 GHz. The most common in practice are quarter-wave resonators, in which

$$\lambda = \frac{4L}{2n-1} \text{ или } L = \frac{\lambda}{4}(2n-1), \quad (3.7)$$

where  $\lambda$  is the wavelength of the electromagnetic signal,  $L$  is the length of the resonator,  $n = 1, 2, 3 \dots$

Accordingly, choosing the working resonant frequency  $f_p = 1.4$  GHz and using the expression  $\lambda = c/f_p$ , we determine the cavity length  $L = 53.57$  mm for  $n = 1$ . For  $n = 2$ , the length of the resonator is  $L = 160.71$  mm, for  $n = 3$ ,  $L = 268.85$  mm. When using the expression (3.7), we take the cross-sections of the resonator having outer and inner diameters  $D$  and  $d$ , but these are limited by the condition of the absence of higher types of waves:

$$\frac{\pi}{2}(D+d) < \lambda_0 \quad (3.8)$$

The values of the diameters, in addition to the condition (3.8), determine the losses in the walls of the resonator and, therefore, affect the magnitude of the intrinsic quality factor  $Q_0$ .

The size of the internal diameter  $d$  is determined by the size of the sample. The value of the external diameter  $D$  of the resonator is selected based on the condition (3.8). In this study, the internal diameter of the resonator should be  $d \geq 20$  mm, and corresponding external diameter,  $D > 30$  mm (3.8).

The drawing of the resonator and the specification of its structural materials are presented in Fig. 3.4.

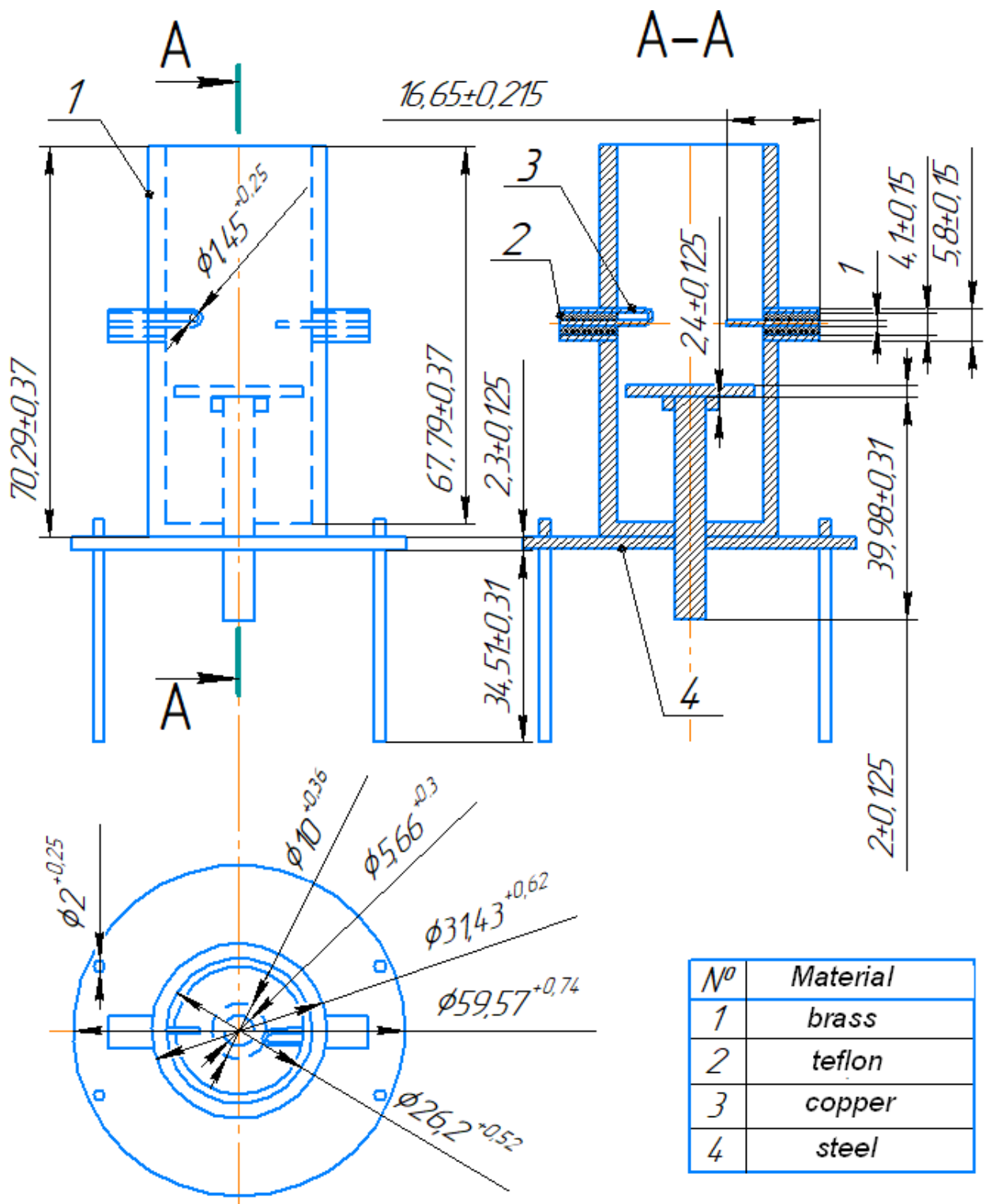


Figure. 3.4. Drawing of the resonator and specification of its structural materials

### 3.4.1. Creating a computer model of a cavity resonator, in accordance with the prototype, in the software CST Studio Suite.

Theoretical study of the resonance properties of soils was carried out on the basis of computer simulation of the propagation of an electromagnetic field in a microwave resonator with samples of various materials [102]. The computer model of the cavity resonator was developed in the CST STUDIO SUITE environment. For each component of the model (Figure 3.5), geometric dimensions and electrical properties were specified in accordance with the dimensions and properties of the prototype (Figure 3.4).

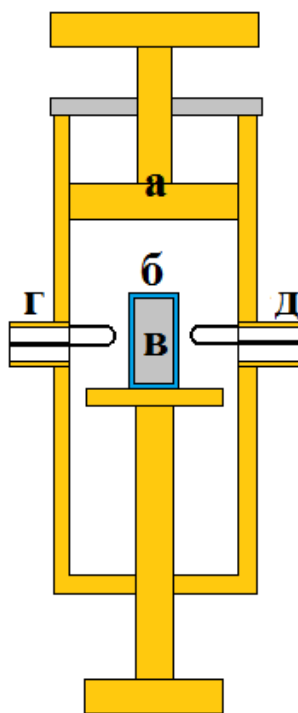


Figure 3.5. Schematic representation of a resonator with a sample. а- resonator, б- plastic cup, в- sample, г- port 1, д- port 2

In the calculation, a finite elements integration method was used, implemented using the “Eigenmode Solver” software block with the division of space into discrete cells of hexahedral form. With its help, the natural frequencies and respective distributions of electromagnetic fields of systems with different electro-physical parameters are determined (Figures 3.6 - 3.10).

In the created model, after simulating the case with a sample with  $\epsilon = 1$ , the field has the maximum value of the vector  $E = 2.72 \cdot 10^8$  V/m (Fig. 3.6).

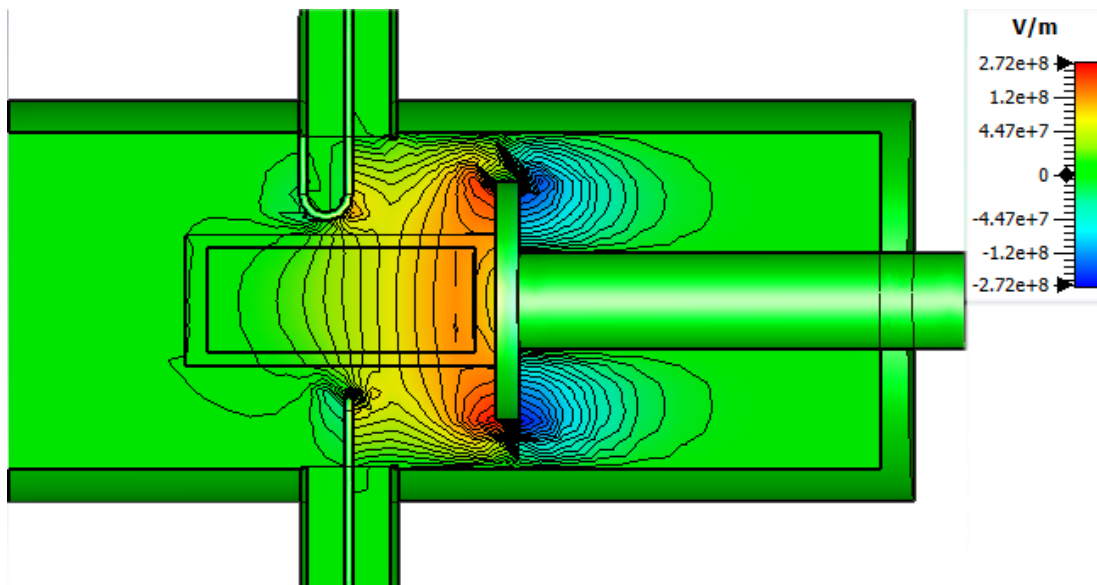


Figure 3.6. Penetration of the field. Sample  $\epsilon = 1$

With the increase in the dielectric constant of the sample, the field is pushed out of its volume (Figures 3.7 - 3.9). As the dielectric constant in the sample increases, the electric field is pushed out of the sample more and more strongly, and, at  $\epsilon > 30$ , it practically does not pass through it.

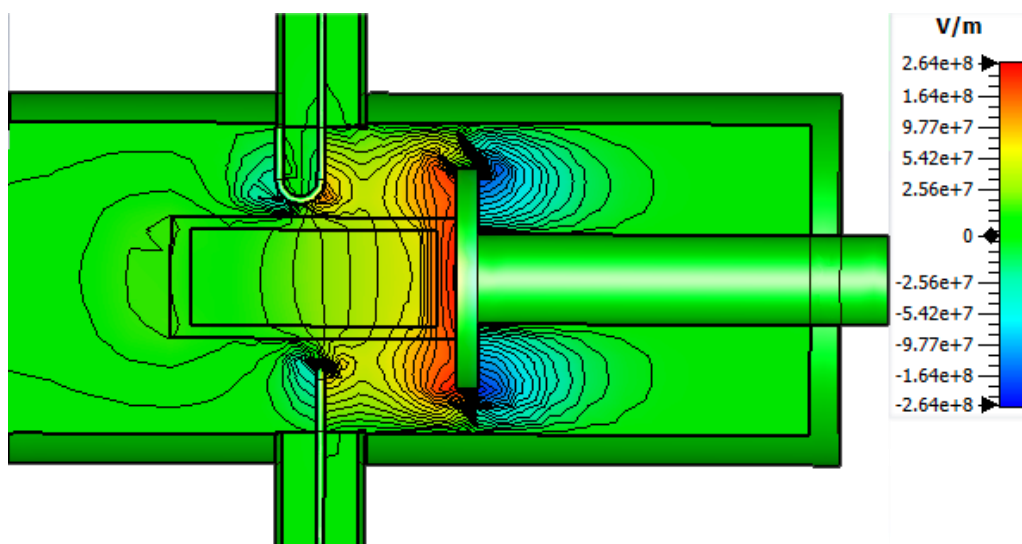


Figure 3.7. Penetration of the field. Sample  $\epsilon = 10$ ,  $\sigma = 5.5E-06$ .



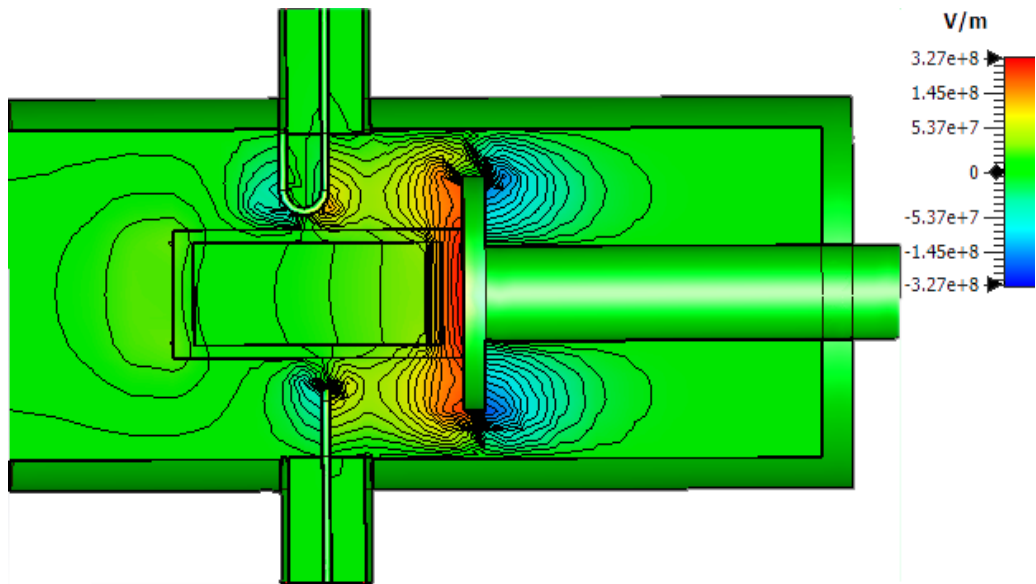


Figure 3.8. Penetration of the field. Sample  $\varepsilon = 30$ ,  $\sigma = 5.5E-06$ .

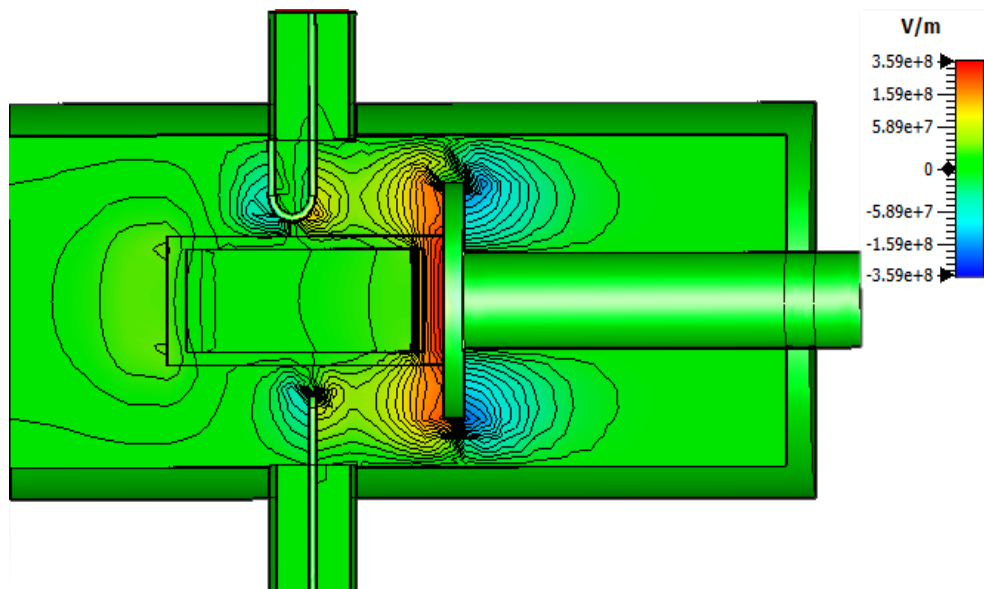


Figure 3.9. Penetration of the field. Sample  $\varepsilon = 50$ ,  $\sigma = 5.5E-06$ .

Thus, the design of the resonator has limitations on the range of the measured dielectric constant of the samples, which can be estimated by  $\varepsilon > 30$ .

### 3.5. Software and hardware device for experimental studies of the electrophysical properties of samples.

The necessary measurement tools for experimental studies of the electrophysical properties of samples (see Fig. 3.10) include the P2M-04 transmitter and reflection

modulus meter, operating in the frequency range 10 MHz – 4 GHz (a), a brass resonator containing the sample container (б) made of plastic with a dielectric constant of 2.98, as well as a computer with a specialized software (B).

The R2M-04 device includes hardware and software parts. The hardware part performs a number of basic functions that determine the measurement modes. The software part provides the implementation of the user-selected measurement mode, control of measurements, and display of measurement results.

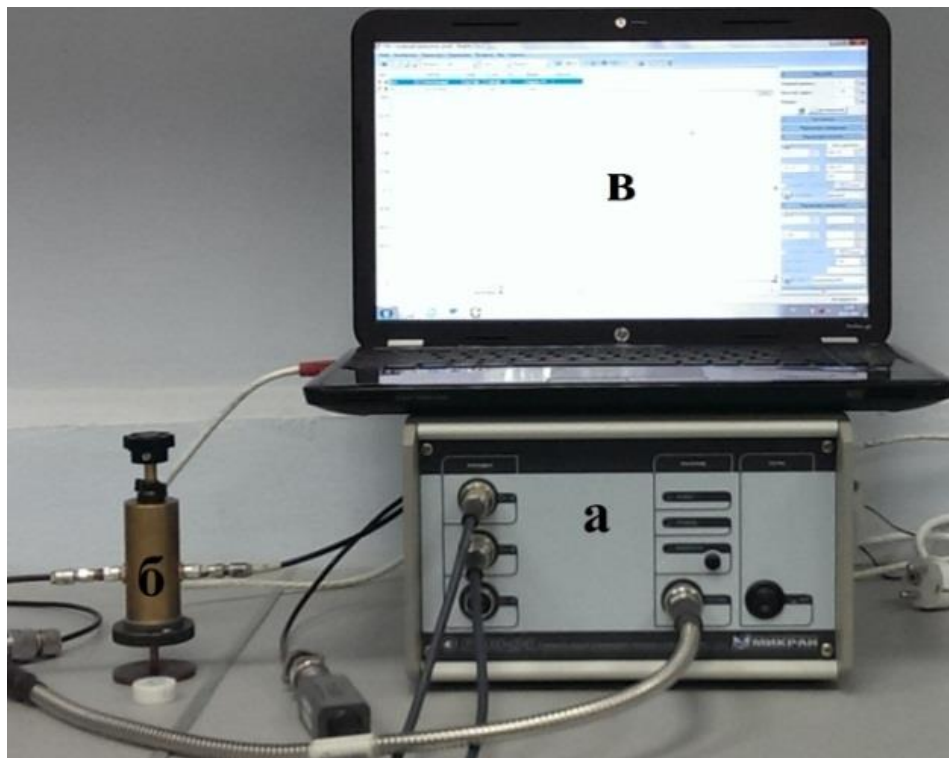


Figure 3.10. Setup for resonant measurements

Complex dielectric constant determination is based on the comparison of the results of direct measurements of signal's frequency and quality factor, and the results of their computer simulations at given dielectric constant and conductivity.

### 3.5.1. Determination of the resonance frequency of electromagnetic waves transmitted through reference samples with known dielectric constant values.

When plotting the calibration curve, materials with guaranteed dielectric permeabilities were used: Fluoroplast with  $\varepsilon = 2.08$ , PCT-3 with  $\varepsilon = 3$ , Polystyrene with  $\varepsilon = 2.6$ , FLAN 2.8 with  $\varepsilon = 2.8$ , glass fiber laminate with  $\varepsilon = 6$  and FLAN 10 with  $\varepsilon = 10$ . These materials were used to make discs with the diameter  $d_0=19$  mm and the thickness of  $l = 2$  mm.

The results are presented in Figure 3.11. It can be seen that the accuracy of the computer model and the numerical procedure can be estimated at 0.5%.

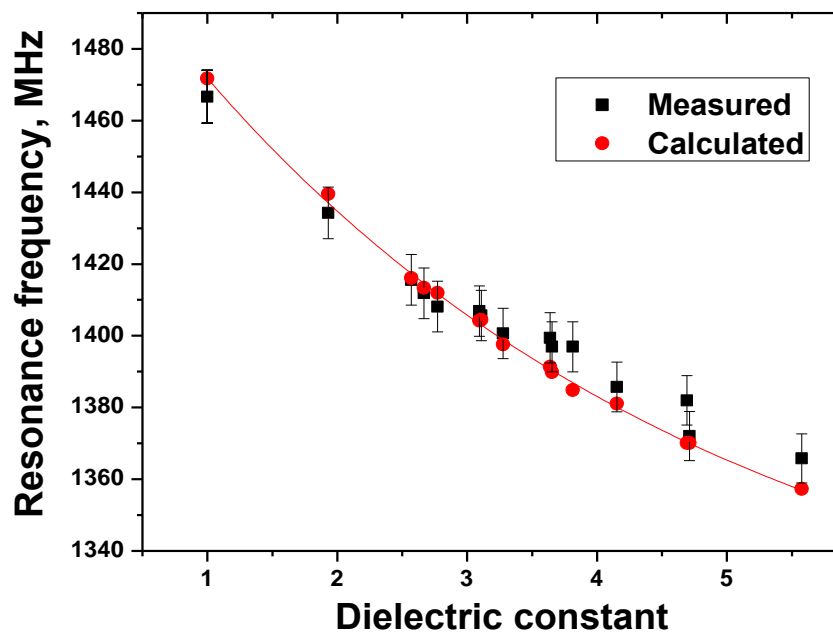


Figure 3.11. Dependence of resonance frequency on dielectric constant. The errors of experimental measurements of 0.5% are shown.

### 3.6. An integrated study of the dielectric properties of soils of different moistures by volume resonator method and simultaneous GPR measurements at frequencies of 1.4 GHz.

Calibration of the GPR method by resonant measurements is based on determining the values of the real part of the dielectric constant  $\varepsilon^*$  and conductivity  $\sigma^*$  by the resonant method and simultaneous GPR measurements of soil properties. Here and

below, the sign (\*) indicates that the parameters belong to the physical state of the soil at which the GPR data were calibrated by resonance measurements.

Combination of these physical quantities allows us to calculate the attenuation coefficient determined by the processes of absorption and scattering of electromagnetic radiation ( $p_e^*$ ), and the refractive index ( $n^*$ ), with the expressions [94]:

$$p = \frac{\omega}{c} \sqrt{\frac{1}{2} \left\{ -\varepsilon + \sqrt{\varepsilon^2 + \frac{\mu_0^2 c^4 \sigma^2}{\omega^2}} \right\}} \quad (3.9)$$

$$n^2 = \frac{1}{2} \left\{ \varepsilon + \sqrt{\varepsilon^2 + \frac{\mu_0^2 c^4 \sigma^2}{\omega^2}} \right\}, \quad (3.10)$$

where  $\omega$  is the most probable value of the cyclic frequency,  $c$  is the speed of light in vacuum, and  $\mu_0$  is the magnetic permeability of vacuum. Since the radiation of the GPR pulse is not monochromatic, the most probable circular frequency was used in the calculations by formulas (3.9–3.10). For the radiation of the AB-1700 antenna of the “OKO” series GPR used in this work, it is determined to be  $\omega = 2\pi f = 8.79 \cdot 10^9 \text{ s}^{-1}$ .

Algebraic transformations of expressions (3.9-3.10) allow us to associate the absorption coefficient and specific conductivity by the relation:

$$\sigma = \frac{2pn}{\mu_0 c} \quad (3.11)$$

For a given soil condition, from the results of the GPR measurements, we determine the intensity of the reflected signal  $E^*$ , the position of the interface between the soil layers, and the attenuation coefficient of electromagnetic radiation  $p^*$ .

Electromagnetic radiation propagating in medium undergoes angular divergence, the value of which depends on the antenna design and the properties of the medium, as shown in Figure 3.12. We define the attenuation coefficient associated with the spatial divergence of electromagnetic radiation in the sample by

$$\Delta p = p^* - p_e^*. \quad (3.12)$$

The basis for determining the value of the complex dielectric constant of the sample is a comparison of the results of direct measurements of signal's frequency and quality factor with the results of their computer simulation with specified dielectric permeability and conductivity. When the container with the soil is placed in the cavity of the resonator, and with the increase of soil's moisture, the dielectric losses increase. To take them into account in a computer model, in addition to the real part of the dielectric constant, additional parameters of the sample are introduced: conductivity ( $\sigma$ ) or dielectric loss tangent ( $\tan\delta$ ).

In this work, calibration of the results of georadar survey of sand placed in a volume of cubic shape with a side of 0.5 m was performed. The antenna unit was placed above the surface of the sand at a height of 0.15 m. The sand humidity was  $W = \frac{m_{H_2O}}{m_{SiO_2}} 100\% = 0.51\%$ . Conductivity is determined by the formulas:  $\sigma^* = \sigma - \sigma_{cm}$ ,  $\sigma = \varepsilon\varepsilon_0\Delta\omega$ , where  $\sigma$  is the specific conductivity of the sample placed in the container,  $\sigma_{cm} = 0.92 \cdot 10^{-3}$  S/M is the specific conductivity of the container without sand,  $\Delta\omega$  is the width of the resonance curve at half height.

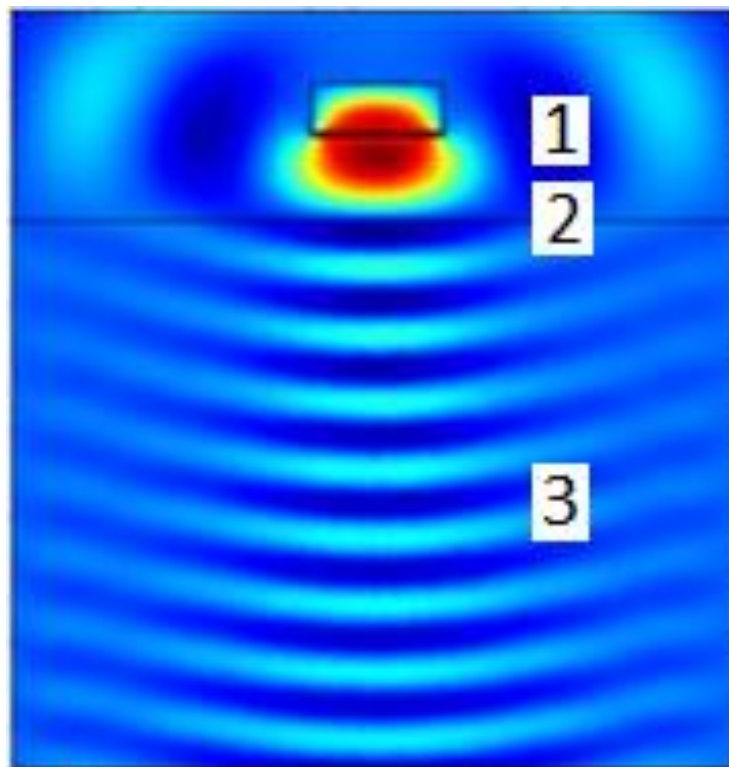


Figure 3.12. Antenna unit (1) and angular divergence (3) of electromagnetic radiation in a medium bounded by a surface (2)

The calculation results are shown in table 3.1. The value of the attenuation of electromagnetic radiation in the sample is determined from the results of the GPR study. For this, the traces ( $F = F(r)$ ) are subjected to a Hilbert transform ( $G = G(F(r))$ ), and then the result obtained is approximated by the relation  $G(F(r)) = G(F(0)) * e^{-p(r-r_0)}$  (Figure 3.13) under condition  $G(F(r)) \rightarrow 0, r \rightarrow h$ , where  $h$  is the doubled layer thickness, and  $r_0$  is the beginning of the approximation (the point of the trace where the signal reflected on the surface can be considered small).

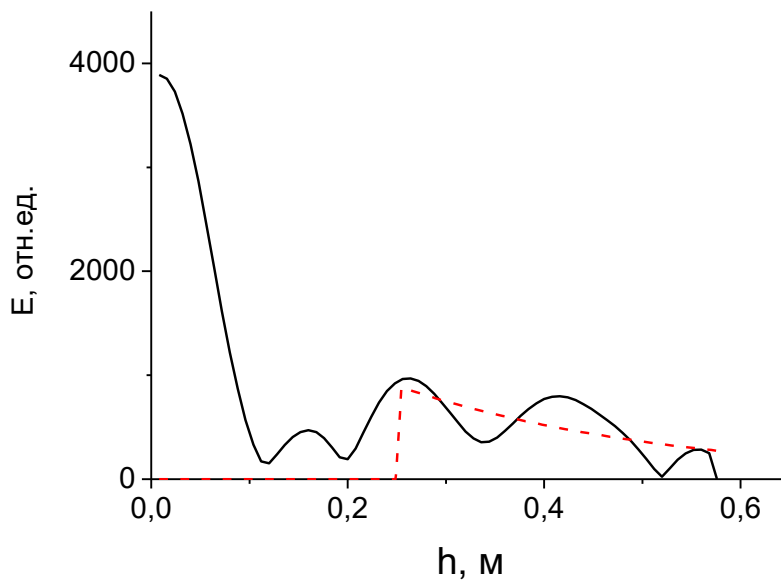


Figure 3.13. Approximation of the trace segment when calculating the attenuation coefficient

Table 3.1. Physical parameters of the sample at the calibration point ( $W = 0.51\%$ ) of the GPR method.

	$\varepsilon^*$	$\sigma^* \cdot 10^3 \text{ S/m}$	$p^* e, \text{ m}^{-1}$	$p, \text{ m}^{-1}$	$\Delta p^*, \text{ m}^{-1}$	$n^*$
Method	resonance	resonance	Eq. (3.9,3.11)	GPR	Eq. (3.12)	Eq. (3.10)
	3.30	3.71	0,38	3.63	3.25	1.82

### 3.7. Determination of the real part of dielectric constant and the conductivity of soil-forming minerals using GPR calibrated method.

Determination of electrophysical properties of soils after a change in their state, which may be caused by the change of moisture, is carried out using the calibrated GPR method.

Implementation of the method is related to determining the intensity of the reflected signal  $E_0$ , the position of the corresponding interface  $\Delta m$  and the attenuation coefficient of electromagnetic radiation.

The calculation of the dielectric constant of the soil in a new physical state is performed using the expressions:

$$n = n^* \left( \frac{\Delta m}{\Delta m^*} \right) \quad (3.14)$$

Calculated refractive indices for sand of different moisture are given in Table 3.2. The table also shows attenuation coefficients determined by analogy with section 3.7.

$$p + \Delta p^* \rightarrow p. \quad (3.15)$$

Table 3.2. Electrophysical parameters of sand with different moistures calculated using calibrated GPR data.

$W, \%$	$\Delta m$	$n$	$p + \Delta p^*$	$p$	$\sigma, S/M$	$\varepsilon$	$\sigma, S/M$	$\varepsilon$
Method	radargram	Eq. (3.14)	GPR	Eq. (3.15)	Eq. (3.11)	Eq. (3.10)	resonance	resonance
0,51	104	1,82*	3,63	0,38	0,0037	3,31	0,0037	3,30
1,78	126	2,21	4,18	0,93	0,0109	4,88	0,0056	3,46
2,196	139	2,43	4,01	0,76	0,0098	5,90	0,0097	4,54
4,84	157	2,75	4,08	0,83	0,0121	7,56	0,0163	6,63
7,73	184	3,22	4,34	1,09	0,0186	10,37	0,0232	8,57
10,01	204	3,57	4,99	1,74	0,0330	12,74	0,0265	10,56
14,42	252	4,37	6,20	2,95	0,0684	19,09	0,0553	17,14
16,05	255	4,46	6,33	3,08	0,0729	19,88	0,0593	18,35

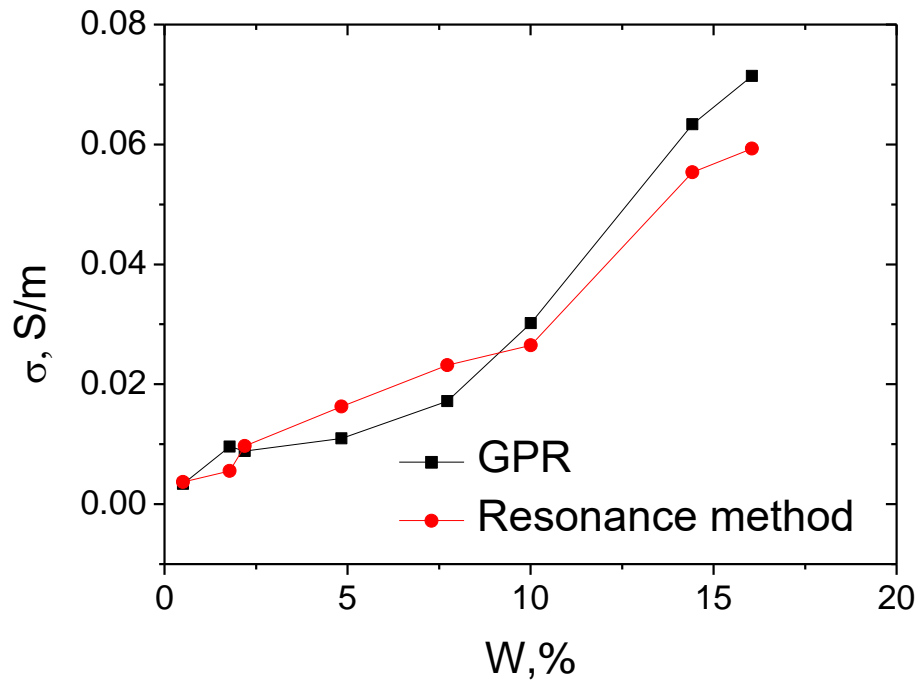


Figure 3.14. Specific conductivity of sand of different moisture

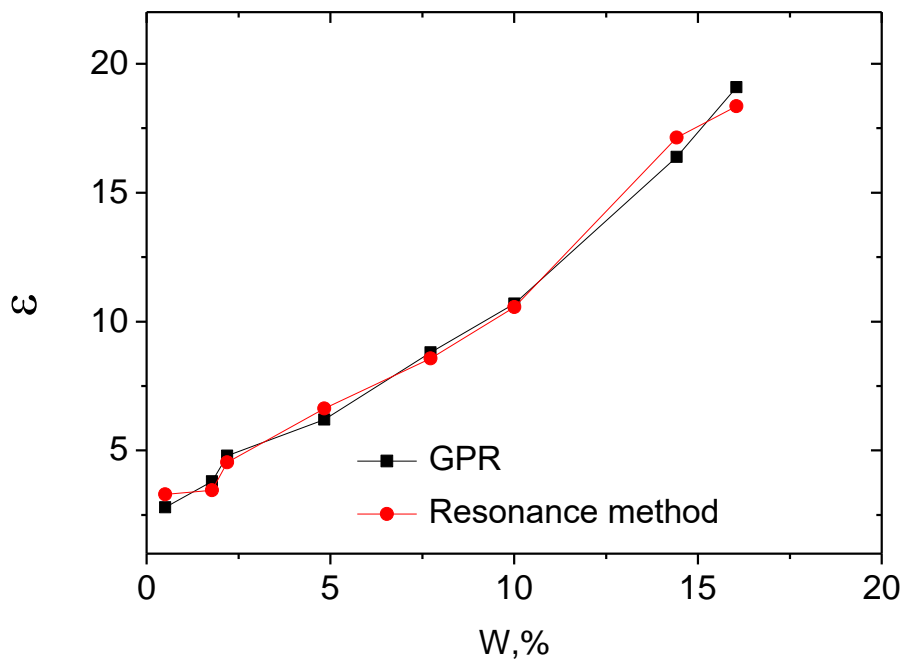


Figure 3.15. Dielectric permeability of sand of different humidity



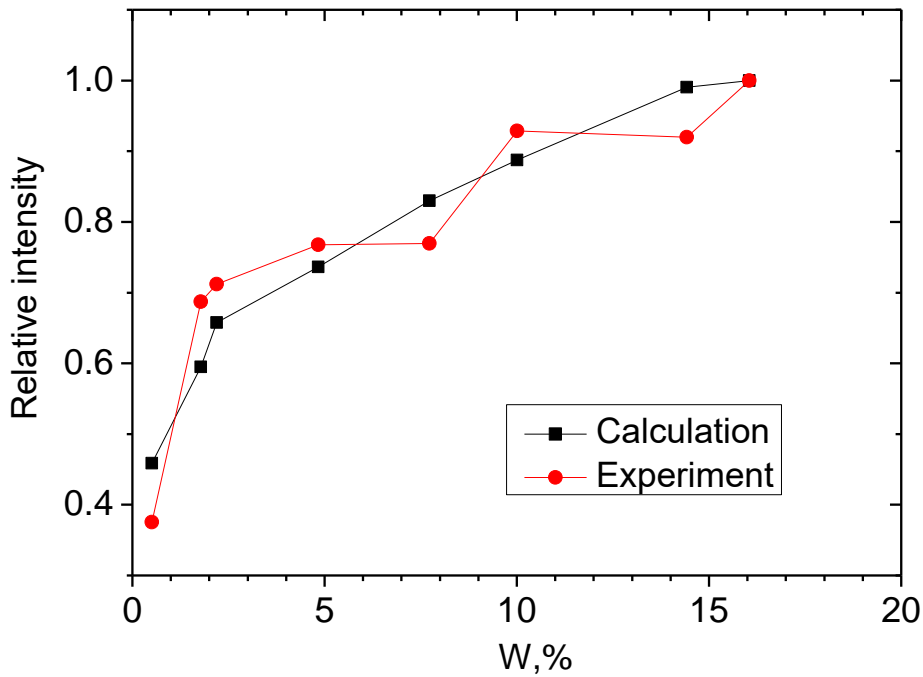


Figure 3.16. Relative intensity of the signal reflected from the upper boundary

The accuracy of electrophysical parameters obtained by the calibrated GPR method is determined in relation to the results of resonance measurements. The values of errors are illustrated in Figures 3.14 and 3.15. Estimates showed that the average values of relative errors are 10–15%.

Thus, the deviation of the results of determining the dielectric constant and specific conductivity of samples by the GPR method calibrated at one moisture point does not exceed 10-15% of the measurement results by the resonant method.

Another way to determine the accuracy of the obtained values of dielectric constant and specific conductivity of sand of different moisture can be a comparison of theoretical (3.16) and experimental (3.17) values of relative intensity of the signal reflected by the upper surface of the layer (Khakiev et al., 2014):

$$A = \sqrt{\frac{(n-1)^2 + \chi^2}{(n+1)^2 + \chi^2}}, \quad (3.16)$$

$$A = \frac{E}{E_0} \quad (3.17)$$

In the (3.16) the following notation is used:

$$\chi = \frac{c}{\omega} p$$

The data shown in Figure 3.16 allows us to estimate the relative deviation of the calculated and experimental values of relative intensities with a value of 0.10 - 0.15%.

Combined use of formulas (3.16) and (3.17) made it possible to determine the electric field strength of the incident wave on the sample surface during the GPR surveys of this work:  $E_0 = 15000 \pm 10\%$ . The possibility to estimate the electric field strength of an incident wave at different distances from the emitter can be used in evaluating the efficiency of designing antenna units.

### **3.8. Determination of sample moisture using calibrated GPR data**

The solution of the problem of determining the correlation between the complex dielectric constant and the moisture content of soil samples has been addressed in [103], where this correlation dependence is approximated to a high degree of accuracy  $\delta < 10\%$  by a third-order polynomial  $\varepsilon = A + BW + CW^2 + DW^3$ , where the parameters  $A$ ,  $B$ ,  $C$  and  $D$  depend on the composition of the sample, but at the same time their ratio being 1: 9: 60: 30.

It can be seen that the main contribution to the approximation of the dielectric constant is comes from the quadratic term. This suggests that the dependence of the refractive index on moisture and is close to linear. The dependence of the refractive index on moisture for sand obtained in this work is shown in Figure 3.17. It is obvious that the tangent of the slope of the straight line will depend on the composition of the samples, therefore the calibration of the GPR data should be carried out at two points.

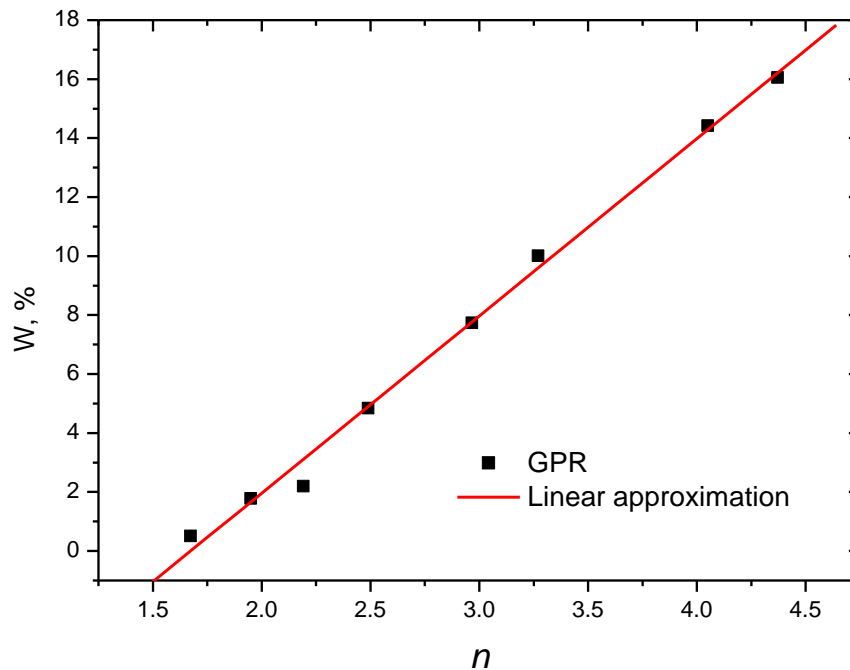


Figure 3.17. Moisture of sand samples against the refractive index

### 3.9. Conclusions

In this work, a method has been developed for determining the complex dielectric constant and soil moisture by the resonant method, the results of which are used for calibrating the GPR measurements.

To this end:

- a numerical model of a cavity resonator was developed in the software product CST Studio Suite;
- the cavity resonator for measuring the properties of materials taken from the core is designed;
- the dependences of the resonance frequency on the dielectric constant of samples with known values of the basic electrophysical parameters are determined;
- the resonance frequencies of electromagnetic waves transmitted through reference samples with known dielectric constants are measured.

Methods for determining the complex dielectric constant and moisture by the GPR method calibrated by laboratory measurements of these values, have been

proposed and laboratory tested. The assessment of the accuracy of determining the electrophysical properties of soils allowed formulating requirements for improving the resolution of the equipment used and its capabilities. As a result, recommendations can be developed to optimize the operation of railways, to make plans for repair and rehabilitation works that are adequate to infrastructure objects current state, to also monitor seasonal and weather changes in reflectivity which can provide a criterion for evaluating the effectiveness of drainage systems. In addition, the data obtained can help interpret observed disorders of railways and provide necessary information on the nature and volume of repair work needed.

The developed method allows, in a shorter time, to diagnose the state of extended objects, since it combines the advantages of the high-speed GPR method with a limited number of calibration measurements of the dielectric constant and moisture by laboratory methods.

The use of GPR methods for monitoring extended sections of railways using mobile diagnostic tools leads to the need to process and interpret a large amount of information. As a result, recommendations can be developed for optimizing the operating conditions of railways; repair and rehabilitation works can be planned that are adequate objects current state.

In particular, the control of seasonal and weather changes of reflectivity can give a criterion for evaluating the effectiveness of functioning of drainage systems.

#### **Chapter 4. The effect of soil salinity on the depth of GPR surveys.**

As noted in the previous chapter, non-destructive geophysical methods are used to overcome technological difficulties associated with the monitoring of soils and structural layers of artificial structures with destructive methods. An important place among these methods is occupied by the GPR method which allows obtaining continuous information on the state of local and extended objects. For its effective use in solving problems of quantitative diagnostics when planning experiments, it is necessary to take into account the depth limitations that are directly related to the conductivity of soils and materials. This physical characteristic, in turn, is determined by the moisture and mineralization of soils and materials. High depth of GPR research in sands, ice and rocks is known, as well as low depth in low-ohm clays.

*In this regard, in this chapter, the effect of humidity and salinity on the conductivity of some soil-forming minerals is studied using the method of resonance measurements.*

The reliability of transport and civil engineering structures is significantly dependent on the accuracy of determination of plasticity and other mechanical properties of cohesive soil materials. Currently, when designing the construction of artificial structures, these measurements are carried out using standard methods set forth in international and national regulatory documents. At the same time, it is known that the accuracy of plasticity determination is not always acceptable, and the problem of its enhancement using infrared spectroscopy methods is discussed in the literature [104,105].

*In this chapter, the studies have been performed to establish the correlation between the plastic and electrophysical properties of soil-forming materials determined in the microwave range of electromagnetic waves.*

## 4.1. Materials used

### 4.1.1. Cohesionless materials

For this research, career sand was used; its physical characteristics were obtained during the tests in the laboratory “Testing and monitoring in civil and transport construction”, accreditation certificate RA.RU.21PS69 issued February 18, 2016. The physical characteristics of the soil and the test methods used are presented in Tables 4.1-4.4 and in Fig. 4.1.

Table 4.1. Physical characteristics of soil.

№	Characteristic	units	Measured value	Regulatory documents establishing the rules and test methods (measurements)
1	2	3	4	5
1	Size Module $M_K$	-	1.77	GOST 8735-88
2	True density, $\rho$	$\text{g/cm}^3$	2.60	GOST 8735-88
3	Bulk density, $\rho_H$	$\text{g/cm}^3$	1.30	GOST 8735-88
4	Clay content in lumps, $\Gamma_l$	%	0.00	GOST 8735-88
5	Content of dust and clay particles, $\Pi$	%	0.40	GOST 8735-88
6	Maximal density $\rho_{dmax}$	$\text{g/cm}^3$	1.75	GOST 22733-2016
7	Optimum moisture, $W_{onm}$	%	12.0	GOST 22733-2016

Table 4.2. Results of determination of particle size (grain) composition in accordance with GOST 12536-2014.

Residue	Sieve size, mm							
	10	5	2	1	0.5	0.25	0.1	<0.1
Particular, %	0.0	0.0	6.5	3.1	6.3	58.3	24.9	0.9
Total, %	0.0	0.0	6.5	9.6	15.9	74.2	99.1	100.0

Table 4.3. Results of determination of particle size (grain) composition in accordance with GOST 8735-88.

Residue	Sieve size, mm					
	2.5	1.25	0.63	0.31	0.16	<0.16
Particular, %	6.3	2.0	3.2	45.0	38.0	5.5
Total, %	6.3	8.3	11.5	56.5	94.5	100.0

Table 4.4. Results of determining the maximum density and optimum soil moisture.

Compaction No	Moisture, %	Density, $\text{g/cm}^3$	Density of dry sand,	Optimum moisture, %	Maximum density of dry sand

			g/cm <sup>3</sup>		, g/cm <sup>3</sup>
1	7.0	1.64	1.53	12.0	1.75
2	8.7	1.65	1.52		
3	9.8	1.69	1.54		
4	11.0	1.79	1.61		
5	12.0	1.96	1.75		
6	13.3	1.82	1.61		

According to laboratory tests, the soil, in accordance with GOST 25100-2011, is classified as follows:

- class: dispersed;
- subclass: cohesionless;
- a variety of particle size distribution: medium size sand.

Figure 4.1 shows the results of determining the optimal moisture required to achieve the maximum density of sand; measurements are performed by implementation of the technique set out in GOST 22733-2016. The value of the optimum moisture is found to be 12%.

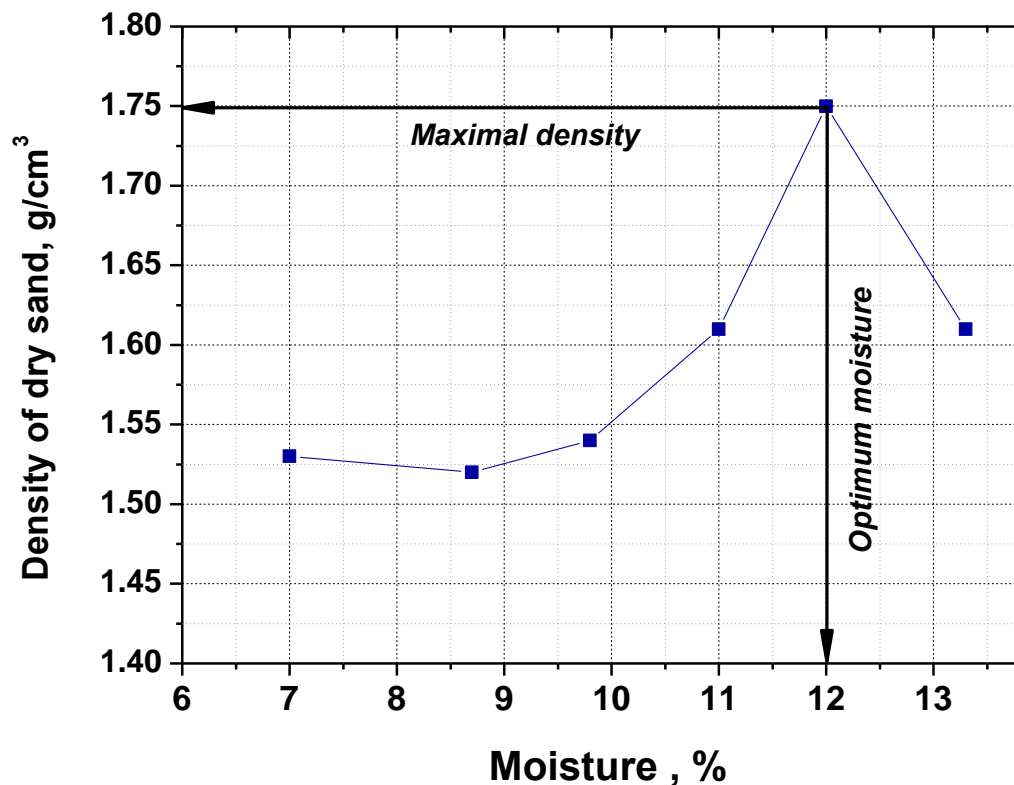


Figure 4.1. Results of determining the maximum density and optimum moisture of sand. Standard compaction curve

#### 4.1.2. Cohesive materials

According to structural and mineralogical characteristics, clay minerals can be divided into three most common groups [106]:

1. The group of montmorillonite;
2. The group of kaolinite;
3. A mixed group of illite and hydromica.

They are the main rock-forming clay minerals, which are complex multi-component systems, including associations of layered and layered-band silicates, amorphous organic and inorganic substances, and other minerals of rocks, the most common of which include: quartz, calcite, dolomite, field spars, phosphates, gypsum, etc.

The generally accepted formula of montmorillonite is  $Al_2 \cdot nSiO_2 \cdot mH_2O$ . The crystal structure of montmorillonite is a three-layer packet in which an aluminate, an octahedral layer, is located between two layers of silicon-oxygen tetrahe-



dra. The delimitation of packets occurs on hydroxyl ions, therefore, the packets are easily moved apart upon penetration of water. Isomorphic substitutions can occur in both tetrahedral and octahedral layers. These minerals have a layered-type structure. The main features of the structure of montmorillonite were identified in the works of Pauling and Marshall, and then repeatedly clarified. Both surfaces of the package consist of oxygen atoms; the interaction between the oxygen surfaces is due to the weak van der Waals forces.

Bentonites are part of layered-band aluminosilicates with an increasing structure, due to their high sorption properties. Bentonites containing more than 70% of montmorillonite are true bentonites, all others belong to bentonite-like clays. In turn, the true bentonites are divided by the presence of the main exchange cation into [107]:

1. alkaline (sodium, calcium and magnesium);
2. alkaline earth (calcium - magnesium).

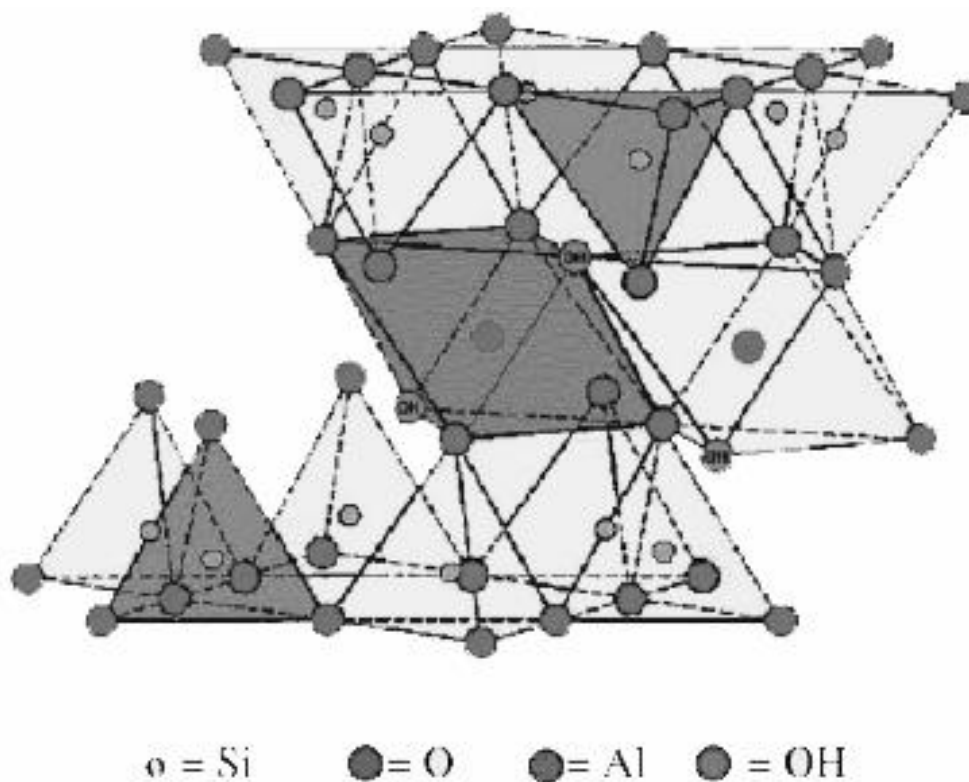


Fig. 4.2. Montmorillonite lattice structure

The basis of the kaolinite crystal structure is a double layer consisting of silicates and aluminates with small internal isomorphous substitutions. Free hydroxyl groups are in the nodes of the crystal structure. In the two-layer packet, the tetrahedral positions are occupied by  $\text{Si}^{4+}$  ions, and the octahedral positions by  $\text{Al}^{3+}$  ions.

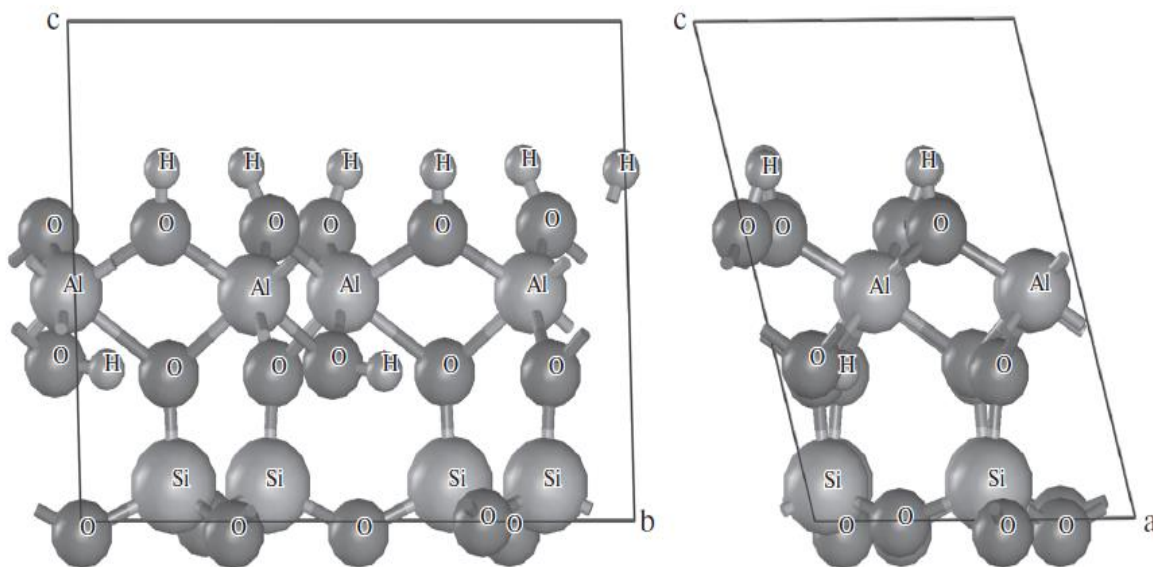


Fig. 4.3 - Kaolinite unit cell

Clay minerals, due to their unique properties, are the subject of constant scientific interest. For example, the ability of bentonites to swell in a non-polar medium was studied in [108], and the adsorption of surface-active substances was measured. It is concluded that the location of adsorbed organic cations in the inter-layer space and the ability of modified bentonites to swell depend on the cation exchange capacity.

The adsorption properties of bentonites and materials based on them were studied in [109-111], and the swelling kinetics of Zyryanov bentonite was studied in [112].

## 4.2. Electrophysical properties of sand

### 4.2.1. Electrophysical properties of wet sand

In this section, the electrophysical properties of sand are studied depending on its moisture in the moisture range including the optimum value. As the upper limit of the range, a value of 16% is chosen since the further addition of water leads to its release in natural conditions.

Samples for measurements were prepared from pre-washed with distilled water and dried according to GOST 22733-2016 sand by adding distilled water. When performing measurements, a constant mass of 4.269 g was used at any humidity. The samples were placed in a container with a volume of 2833.85 mm<sup>3</sup>, made of the ABS plastic (acryl butadiene styrene - solid, impact-resistant, thermo-plastic industrial resin based on a copolymer of acrylonitrile with butadiene and styrene), which was previously used to calibrate the resonator.

Measured dielectric constant and conductivity determined according to Chapter 3, are shown in Figures 4.4 and 4.5.

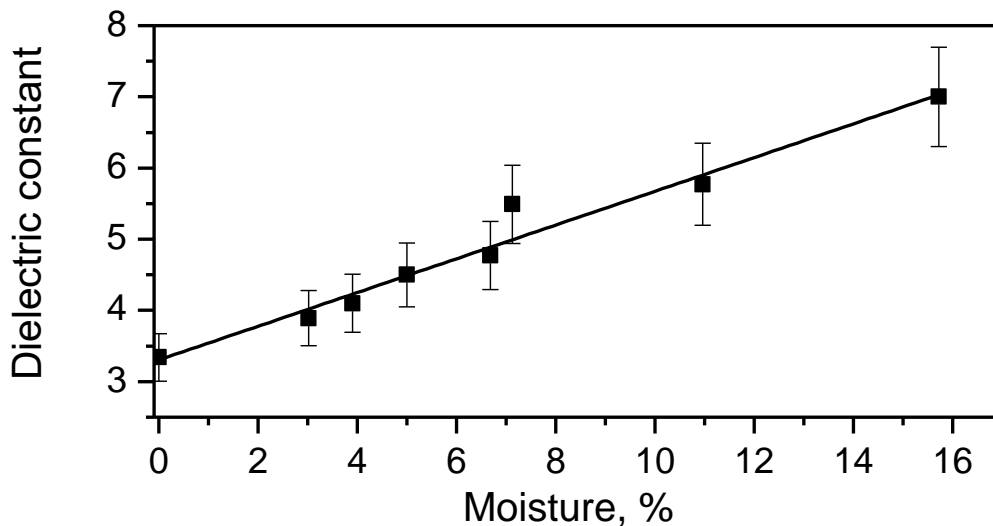


Figure 4.4. Dielectric constant of sand as a function of moisture

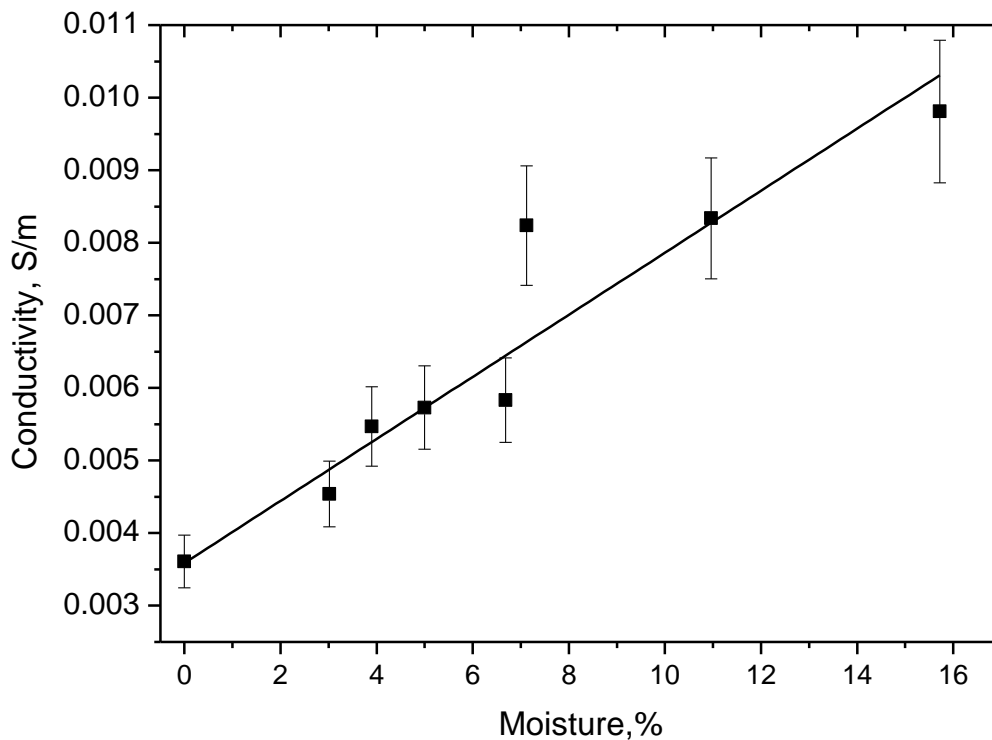


Figure 4.5. Conductivity of sand as a function of moisture

In these figures, the vertical segments indicate the errors that make up 10% of the experimentally determined values of these quantities. The measurement results are used to perform a linear approximation which, as follows from the figures, has accuracy better than the specified error.

#### 4.2.2. Electrophysical properties of wet saline sand

In this section, the effect of salt impurities on the electrophysical properties of sand is studied. Measurements are performed for a sand with moisture content of 5%. At this value of moisture, the dielectric constant of sand was 4.50, and the specific conductivity, 0.00574 S/m. The salts used in the experiment, as well as some features of the preparation of samples for measurements, are listed in Table 4.5.

Table 4.5 - Masses of salts used in the preparation of samples.

Salt concentration	0.075%	0.100%	0.115%	0.2%	0.25%	0.3%
--------------------	--------	--------	--------	------	-------	------

in the sand at a moisture of 5%							
Mass, g	NaCl, KCl, BaCl <sub>2</sub>	0.225	0.300	0.450	0.600	0.750	0.900
	H <sub>2</sub> O	14.775	14.700	14.550	14.400	14.250	14.100

Measured dielectric constants and specific conductivities are shown in Table 4.6. The results of experimental data processing, according to the methodology of Chapter 3, are given in Table 4.5 and in Figures 4.6 and 4.7. The figures also show vertical segments reflecting corresponding to a relative error of 10%, and the results of a linear approximation of the experimental data.

Table 4.6 - Specific conductivity of salts.

<b>NaCl</b>				
C %	Dielectric constant	Conductivity	Peak width	Resonance frequency
0	4.44	0.00435	17.62	1374.2
0.075	4.39	0.00867	35.53	1375.26
0.100	4.42	0.00962	39.17	1374.74
0.115	4.47	0.01524	61.31	1373.7
0.200	4.64	0.01695	65.74	1371.1
0.250	4.50	0.0159	62.38	1374.48
0.30	4.69	0.0202	77.49	1370.06
<b>KCl</b>				
C %	Dielectric constant	Conductivity	Peak width	Resonance frequency
0	4.44	0.00435	17.62	1374.2
0.071	4.31	0.01025	42.78	1377.08
0.095	4.82	0.01257	46.93	1369.02
0.143	4.56	0.00941	37.14	1371.88
0.190	4.19	0.01128	48.42	1379.68
0.240	4.81	0.01699	63.57	1369.28
0.286	4.47	0.01306	52.58	1373.44
<b>BaCl<sub>2</sub></b>				
C %	Dielectric constant	Conductivity	Peak width	Resonance frequency
0	4.44	0.00435	17.62	1374.2
0.071	4.62	0.0077	30	1371.88

0.095	4.29	0.00715	30	1378.12
0.143	4.44	0.00836	33.87	1375.52
0.190	4.55	0.00961	38.02	1373.44
0.240	4.5	0.01018	40.69	1373.44
0.286	4.84	0.01383	51.4	1367.46

It is seen from Fig. 4.6 that the dielectric constant values of the samples depend little on the impurity of the salts in the indicated concentration range, and the linear approximation procedure is performed with an accuracy significantly better than 10%.

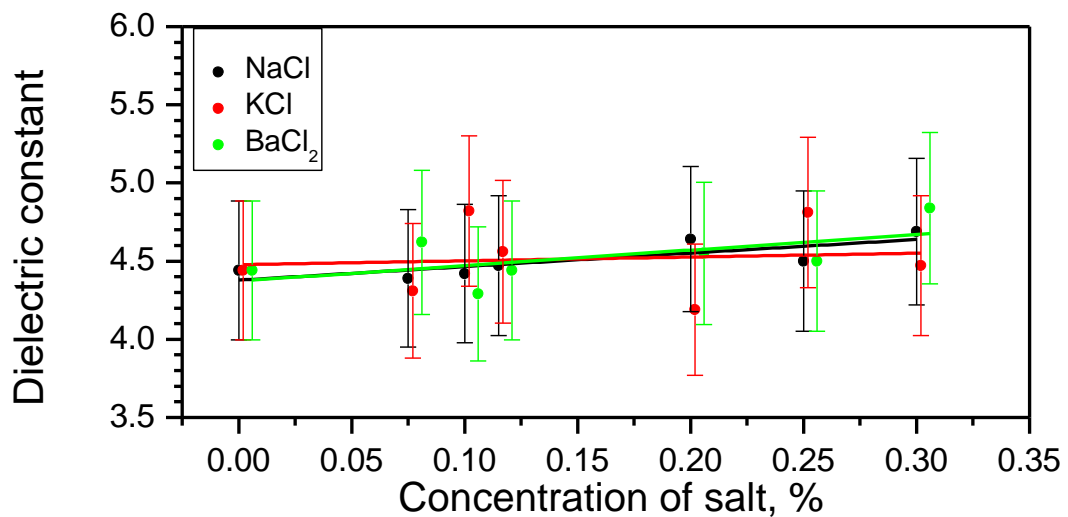


Figure 4.6. Measured dielectric constant of sand at moisture of 5% as a function of the salt concentration

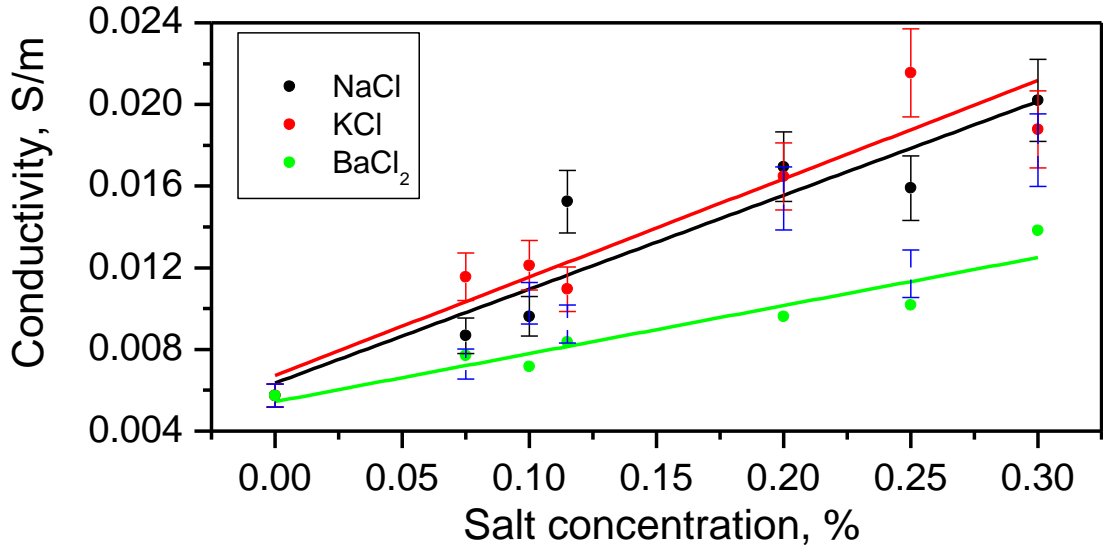


Figure 4.7. Measured conductivity of sand at moisture of 5% as a function of the salt concentration.

To interpret the results obtained, we take into account that the conductivity associated with the mobility of ions formed during the dissociation of salts in aqueous solutions is determined by the relation:

$$\sigma = \alpha en(v_k + v_a),$$

where  $\alpha$  is the degree of dissociation,  $e = 1,602 \cdot 10^{-19}$  C is the elementary charge,  $n$  is the number of salt molecules in the solution,  $v_k$  is cations mobility,  $v_a$  - anions mobility.

Calculate the concentration of salt molecules by the expression:

$$n = mN_A/(\mu V),$$

where  $m$  is the salt mass,  $N_A$  is the Avogadro number,  $\mu$  is the molar mass, and  $V$  is the sample volume.

Suppose that the degree of dissociation is close to unity for all the salts used. We calculate the conductivity of salts under the assumption that the mobility of ions does not depend on the frequency of the electromagnetic field. The calculation results are given in table 4.7.

Table 4.7. Specific conductivities of salts.

Salt	Specific conductivity	
	Calculated	Measured
NaCl	1	1
KCl	0,99	1,05
BaCl <sub>2</sub>	0,66	0,62

From a comparison of the data given in table 4.7, one can conclude that the results of measurements and calculations in the approximations described differ by less than 10%.

#### 4.2.3. Electrophysical properties of wet saline sand at low temperatures

In this section, electrophysical properties of the sand sample in different states at low temperature are studied. The following reference samples were used: dry sand (exposure at a temperature of 105° for 3 hours), sand at a moisture of 5%, and sand at a moisture of 5% with a salt concentration of NaCl of 0.268%. The samples for studying the effects of low temperatures were obtained by exposure of reference samples for 24 hours at a temperature of -5 °C. Table 4.8 shows the obtained values of dielectric constant and conductivity.

Table 4.8. Dielectric constants and conductivities of samples with different moisture and salinity at different temperatures.

Sample state	Dielectric constant	Conductivity, S/m
W=0%, t=25 <sup>0</sup>	3.34	0.00361
W=0%, t=-5 <sup>0</sup>	3.36	0.00315
W=5%, t=25 <sup>0</sup>	4.80	0.00570
W=5%, t=-5 <sup>0</sup>	4.51	0.00373
W=5%, C <sub>NaCl</sub> =0.268%, t=25 <sup>0</sup>	4.71	0.02081
W=5%, C <sub>NaCl</sub> =0.268%, t=-5 <sup>0</sup>	4.13	0.00711

Comparison of the data given in table 4.8 allows us to make the following conclusions:



- an increase in sample moisture leads to an increase in dielectric constant and conductivity;
- the introduction of NaCl in the sample of sand with a moisture of 5% leads to an increase in the specific conductivity of up to 3 times while the value of the dielectric constant does not change;
- the change in conductivity with the introduction of salt ions allows one to create a method for determining the salinity of construction materials;
- binding of ions by freezing free water leads to a decrease in the specific conductivity while the dielectric constant varies only within the measurement error interval.

### **4.3. Some properties of the samples used**

In this work, the objects of study were:

- Bentonite Dusch (Figure 4.8.a) The Dash-Salakhninsky deposit (Azerbaijan Republic, Gazakh river, Dash-Salakhny village); it belongs to the calcium-magnesium type. The active surface reaches 700–800 m<sup>2</sup>/g and the cation exchange capacity is 80–150 mmol/100g [28].
- Bentonite Kutch (Figure 4.8.b) of the Kutch deposit (Gujarat state, India) of the alkaline type with the main exchange cation Na<sup>+</sup> and Ca<sup>++</sup>. Cation exchange capacity is 90.54 mmol/100g
- Bentonite Zir (figure 4.8.c) of the Zyryanovskoye field (st. Zyryanovka, Kurgan region); it belongs to the calcium-magnesium group has low binding capacity, active surface of 700-800 m<sup>2</sup>/g, and a cation exchange capacity of 80-150 mmol/100g. The compressive strength in the wet state is up to 0.1 MPa [113].
- Kaolinite of dry enrichment from "Zhuravlinny Log" field (Figure 4.4.g), fraction <5 microns. The chemical formula is Al<sub>4</sub>(OH)<sub>8</sub>[Si<sub>4</sub>O<sub>10</sub>] [114].



Fig. 4.8. Samples of bentonite clays and kaolinite

The chemical composition of the bentonite clays used in the thesis is taken from [115] and [116] and is given in Table 4.9. The results of measurements of moisture at the plastic and liquid limits are given in table 4.10.

Table 4.9. Chemical composition of bentonite clays (in %)

Chemical compound	Field		
	Kutch [115]	Zyryanskoye [116]	«Dash-Salakhinskoye» [116]
SiO <sub>2</sub>	45.16	57.37	58.60
Al <sub>2</sub> O <sub>3</sub>	15.84	19.40	13.40
Fe <sub>2</sub> O <sub>3</sub>	7.66	5.97	4.70
FeO		0.94	0.18
TiO <sub>2</sub>	0.87	0.15	0.39
CaO	2.63	1.81	2.05
MgO	3.82	3.01	2.30
P <sub>2</sub> O <sub>5</sub>		0.040	0.11
SO <sub>3</sub>		0.10	0.25
K <sub>2</sub> O	0.41	1.03	0.39
Na <sub>2</sub> O	4.04	0.78	2.30
Other	19.57	9.4	15.33
Total	100	100	100

Table 4.10 Moisture of the materials used at plastic and liquid limits

Clay	Moisture at plastic limit $W_p$ , %	Moisture at liquid limit $W_L$ , %
Bentonite "Dusch"	39.41	163.24
Bentonite "Kutch"	47.69	335.72
Bentonite "Zir"	35.92	158.38
Kaolinite "KZhV"	27.4	46.1

The results presented in Table 4.8 show that sodium is the predominant cation in the Kutch bentonite, which makes it possible to attribute it to the alkaline type (the predominance of sodium, calcium and magnesium ions). The larger size of Na ions explains the high liquid level (according to data from [115], 459%). Similarly, the bentonites "Dusch" and "Zir" can be attributed to the alkaline earth bentonites with a predominance of calcium and magnesium ions.

#### **4.3.1. Electrophysical properties of bentonite "Dusch"**

##### **4.3.1.1. Determination of the accuracy of the measurements of electrophysical quantities**

To assess the accuracy of measurements in the used range of bentonite moistures, two series of experiments performed to measure the dielectric constant and specific conductivity of bentonite "Dusch" at various moistures of samples. In preparation for measurements in each series, the samples of a given humidity were prepared anew by mixing bentonite with a specified amount of distilled water. Then the samples were kept in hermetic laboratory glassware for at least a day in order to undergo consolidation processes. The measurement results are presented in Figures 4.9 and 4.10.

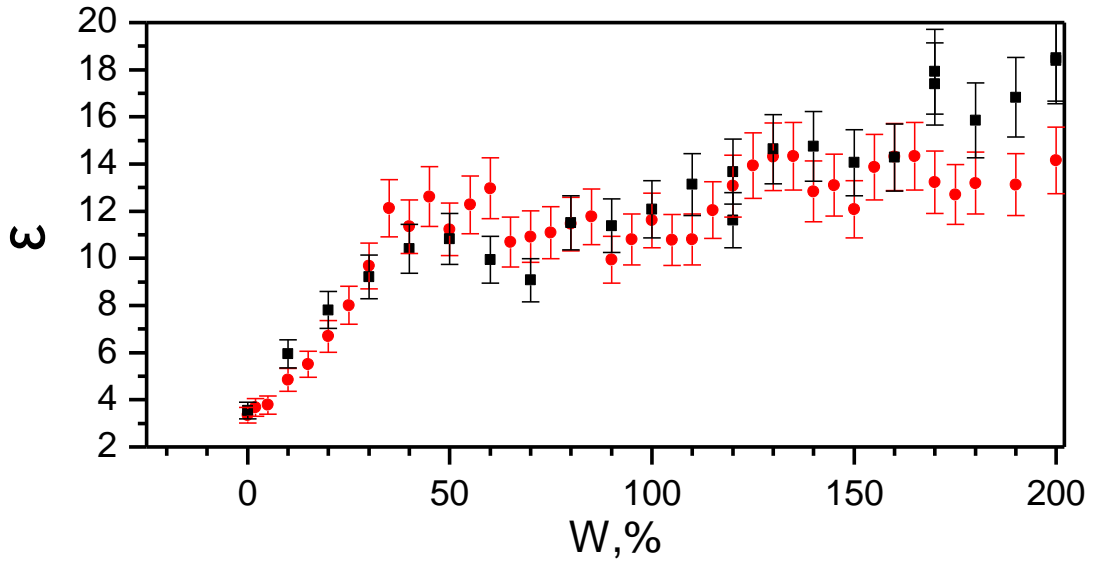


Fig. 4.9. The results of two series of experiments on measuring the dielectric constant are shown in red and black. Vertical bars indicate errors of 10%.

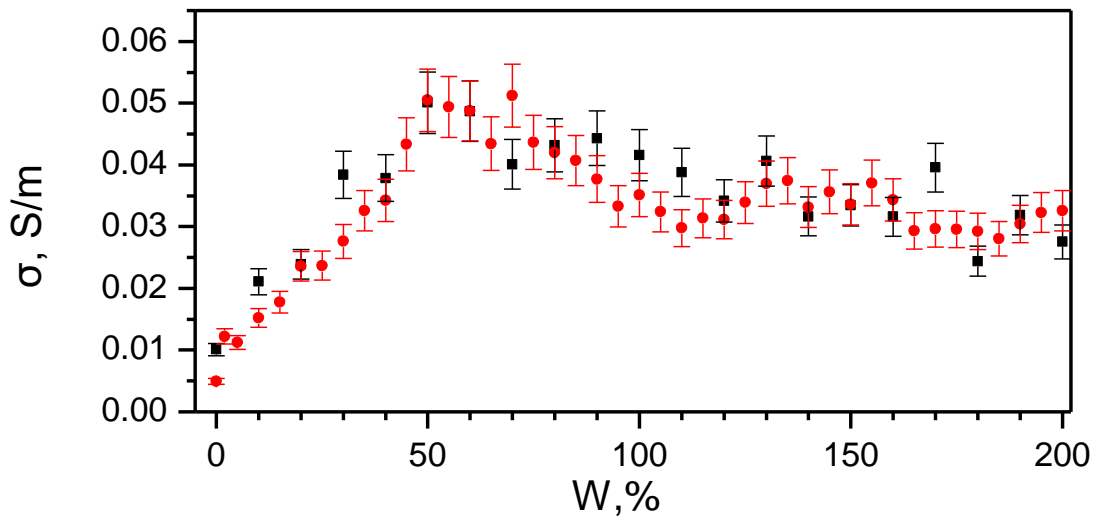


Fig. 4.10. The results of two series of experiments on measuring the specific conductivity are shown in red and black. Vertical bars indicate errors of 10%.

It can be seen from the figures that the scatter in measured values is about 10%. Not more than 10% of experimental points fall out of this error range.

### 4.3.1.2. The effect of salinity on the electrical properties of the bentonite of type "Dusch"

To study the electrical properties and assess the effect of additional salinity of bentonite "Dusch" on the results of measurements of dielectric constant and conductivity, the samples of different moisture were used. When preparing samples of a given moisture, bentonite was mixed with a specified amount of NaCl salt solution of a certain concentration. Before measurements, the samples were kept in hermetic laboratory glassware for at least one day in order to undergo possible consolidation processes. The measurement results are presented in Figures 4.11 and 4.12.

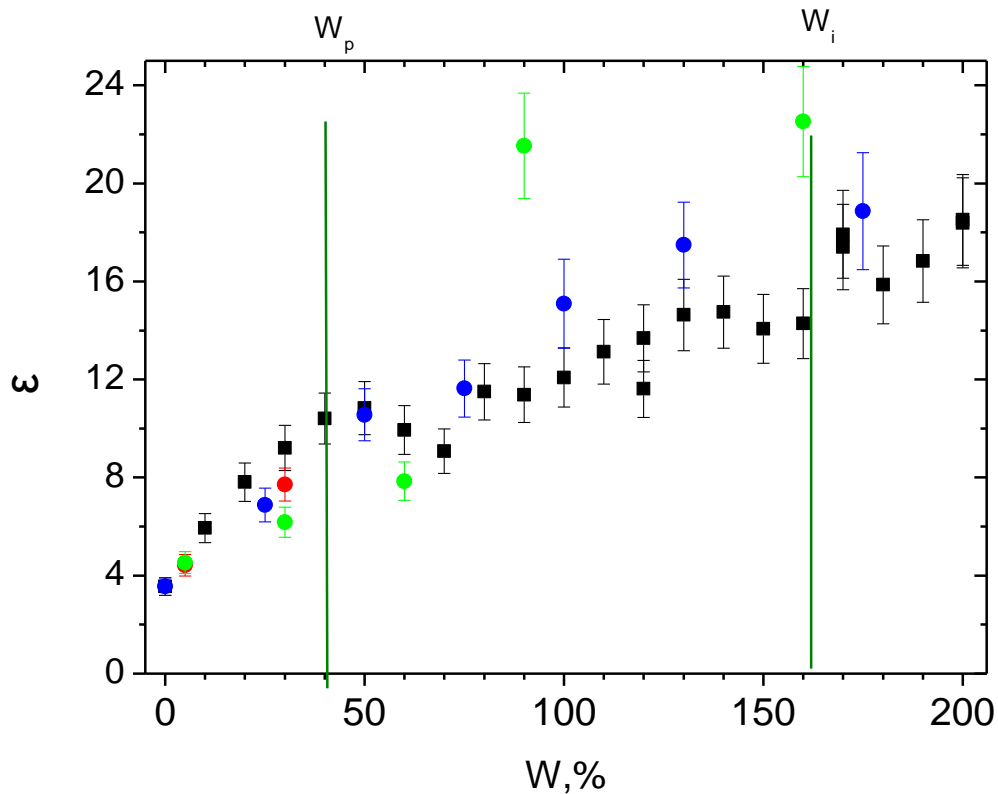


Fig. 4.11. Dielectric constant measured at different concentrations of NaCl additionally introduced into the sample. In the figure, the following notations are used: ● - non-saline sample, ● - 1% solution, ● - 2% solution, ● - 10% solution. Vertical bars indicate the errors of 10%. Vertical lines mark the moisture at the plastic limit ( $W_p$ ) and liquid limit ( $W_l$ ).

Measurement of the electrophysical properties of samples with a 10% concentration of NaCl was possible only at moistures less than 50%. A further increase in moisture leads to the pushing the field out of the sample, which complicates the interpretation of the experimental results. It can be seen from Figure 4.11 that with the introduction of salt ions into the sample, the dielectric constant increases with increasing concentration.

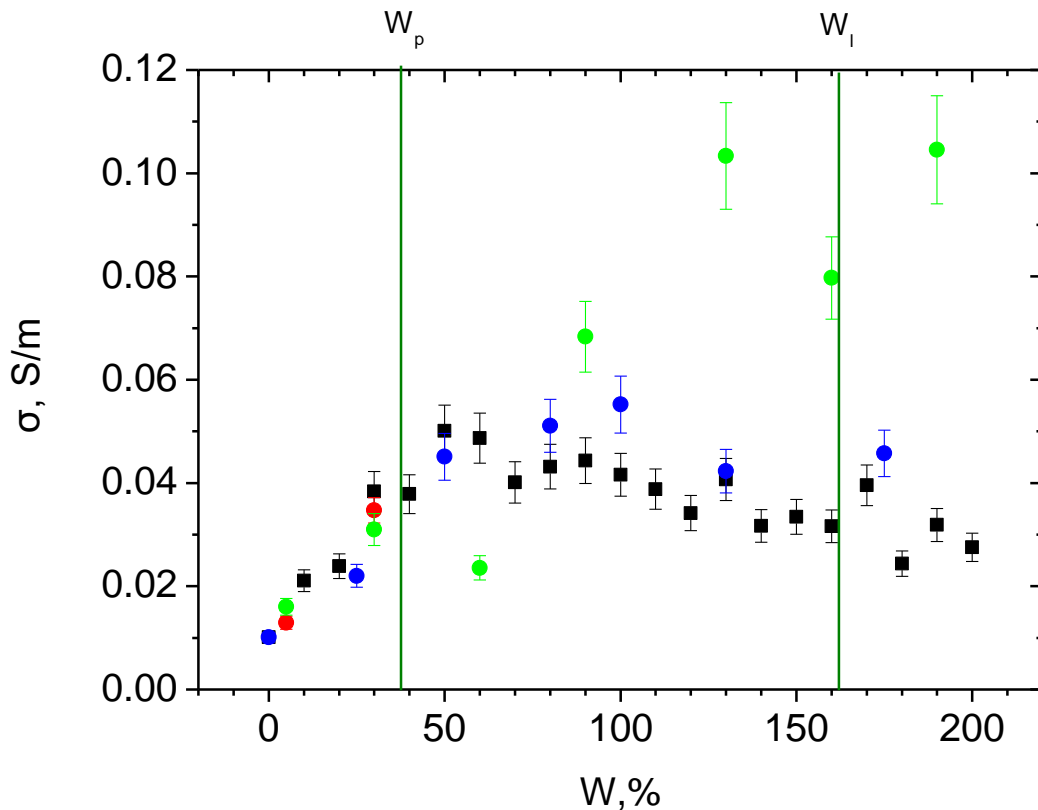


Fig. 4.12. Specific conductivities measured at different concentrations of NaCl additionally introduced into the sample. In the figure, the following notations are used: ● - non-saline sample, ● - 1% solution, ● - 2% solution, ● - 10% solution. Vertical bars indicate errors of 10%. Vertical lines mark the moisture at the plastic limit ( $W_p$ ) and liquid limit ( $W_l$ ).

Figures 4.13 and 4.14 show the dependences of the dielectric constant and specific conductivity on salinity at a fixed sample moisture of 100%.

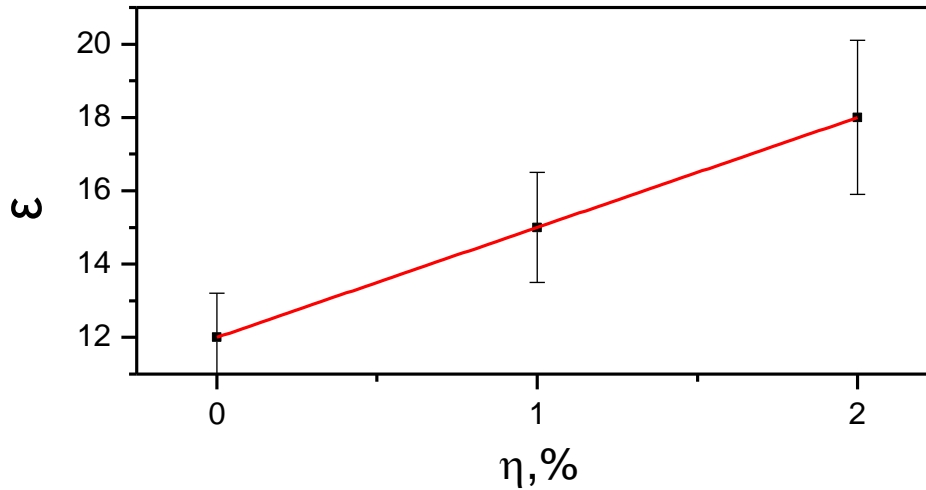


Fig. 4.13. Dielectric constant measured at different concentrations of NaCl additionally introduced into the sample. Vertical segments reflect measurement errors of 10%. The approximating line is shown in red color.

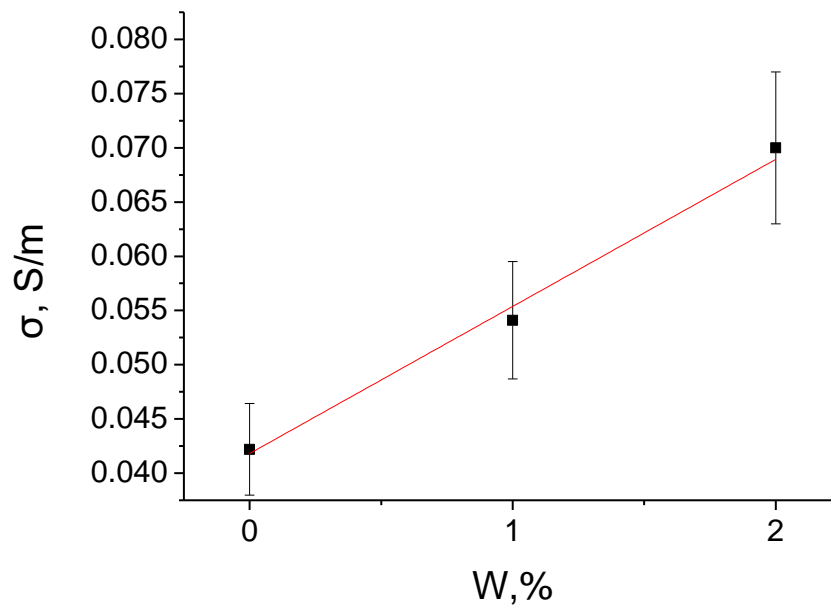


Fig. 4.14. Specific conductivities measured at different concentrations of NaCl additionally added to the sample. Vertical bars reflect measurement errors of 10%. The approximating line is shown in red color.

To determine the degree of the approximation polynomial, we apply the expression from [94], reflecting the change in the dielectric constant when conduction is present:

$$\varepsilon \rightarrow \frac{1}{2} \left\{ \varepsilon + \sqrt{\varepsilon^2 + \frac{\mu_0^2 c^4 \sigma^2}{\omega^2}} \right\} = \frac{\varepsilon}{2} \left\{ 1 + \sqrt{1 + \frac{\mu_0^2 c^4 \sigma^2}{\varepsilon^2 \omega^2}} \right\} \quad (4.1)$$

Denoting  $\alpha = \frac{\mu_0^2 c^4 \sigma^2}{\varepsilon^2 \omega^2}$ , a numerical evaluation of this expression is

Обозначим  $\alpha = \frac{\mu_0^2 c^4 \sigma^2}{\varepsilon^2 \omega^2}$  и выполним численную оценку этого выражения:

$$\alpha = \frac{\mu_0^2 c^4 \sigma^2}{\varepsilon^2 \omega^2} = \left( \frac{4\pi \cdot 10^{-7} \cdot 9 \cdot 10^{16}}{2\pi \cdot 10^9} * \frac{\sigma}{\varepsilon} \right)^2 < 0.1$$

The smallness of  $\alpha$  allows to bring the expression (4.1) to the form:

$$\varepsilon \rightarrow \varepsilon + \frac{\mu_0^2 c^4 \sigma^2}{2\varepsilon \omega^2} \quad (4.2)$$

Suppose that the conductivity depends linearly on the concentration of ions in the solution (Fig. 4.14). Since the second term in expression (4.2) contains in the denominator the dielectric constant which is also dependent on the concentration of ions, and the square of the conductivity in the numerator, it can be approximated by a polynomial, the degree of which can vary in the range from one to two. In this paper, a first-degree polynomial is used to approximate the experimental values.

Figures 4.11 and 4.12 demonstrate that

- for samples prepared using 1% and 2% NaCl solution, there is a tendency to increase of the measured electrophysical parameters.
- the use of a 10% solution of NaCl at moistures lower than 50% does not lead to a noticeable change in the electrophysical values; this may indicate a slight dependence of conductivity on salinity at low humidity of the samples.

#### 4.3.1.3. Electrical and mechanical properties correlation

In figures 4.11 and 4.12, the vertical lines show the moistures values at the plastic and liquid limits of the “Dusch” bentonite, given in table 4.10. It is known that with an increase in the moisture content of the sample from values close to zero, the formation of the H<sub>2</sub>O layers on the surface of clay particles begins. At these values of moisture, a monotonic increase in the dielectric constant and conductivity is observed.



The formation of surface-bound water is completed when the moisture is that of the plastic limit when dry friction between clay particles gives way to the friction associated with the interaction of water layers on the surfaces of the particles. As seen from Figs. 4.11 and 4.12, Near this moisture values, special points (local maxima) are observed on the plots of the dielectric constant and specific conductivity against moisture. Starting from this moisture, the dielectric constant increases with moisture is not so rapidly; this it may be due to:

- the peculiarities of the measurement technique, in particular with the displacement of the field from the volume occupied by water;
- with the swelling of the sample and reducing the influence of the properties of bentonite on the properties of the sample as a whole.

In this range of moisture variation, the specific conductivity decreases due to the replacement of clay particles with water molecules at a constant sample mass.

The transition to a liquid state is characterized by a further pushing the field from the volume of the conductor, which leads to an apparent decrease in the dielectric constant and specific conductivity of the sample.

#### 4.3.1.4. Correlation of electrical properties and temperature

To determine the effect of temperature on the electrophysical parameters of bentonite “Dusch”, an independent series of measurements was performed, the results of which are shown in table 4.11.

Таблица 4.11. Результаты измерения диэлектрической проницаемости и удельной проводимости при разных влажностях и температурах.

Sample state	Dielectric constant $\epsilon$	Specific conductivity $\sigma$
W=0%, t=25 <sup>0</sup>	4.13	0.01159
W=50%, t=25 <sup>0</sup>	8.15	0.03981
W=50%, t=-5 <sup>0</sup>	4.28	0.01097

The results obtained at room temperature differ from those obtained earlier and used in the plots of Figures 4.9–4.12 by about 10%. The results given in Table 4.11 show that when the sample humidity exceeds the plastic limit, and the temperature drops down to under zero degrees Celsius, then ice is formed; this results in a decrease in the dielectric constant. At the same time, the ions mobility decreases, which is reflected in a decrease in the specific conductivity to values characteristic of dry bentonite.

#### 4.3.2. Electrophysical properties of the “Kutch” bentonite

To study the electrical properties and assess the effect of additional salinity of the Kutch type bentonite on its dielectric constant and conductivity, the samples of different moistures were used that were obtained according to the technology described in Sections 4.3.1.1 and 4.3.1.2. The measurement results are presented in Figures 4.15 and 4.16.

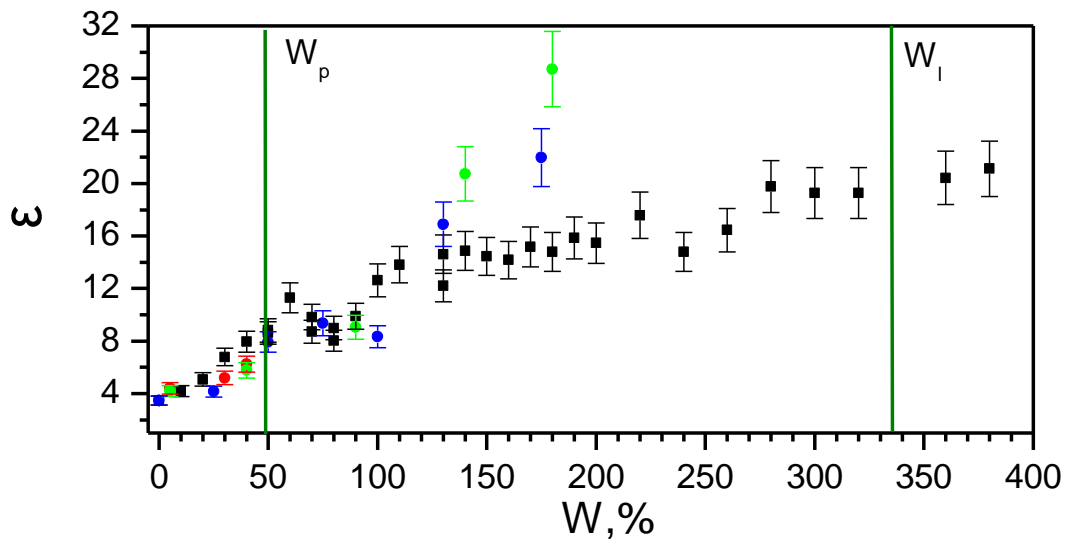


Fig. 4.15. Dielectric constant measured at different concentrations of NaCl additionally introduced into the sample. In the figure, the following notations are used: ● - non-saline sample, ● - 1% solution, ● - 2% solution, ● - 10% solution. Vertical bars indicate errors of 10%. Vertical lines mark the moistures at the plastic limit ( $W_p$ ) and liquid limit ( $W_l$ ).

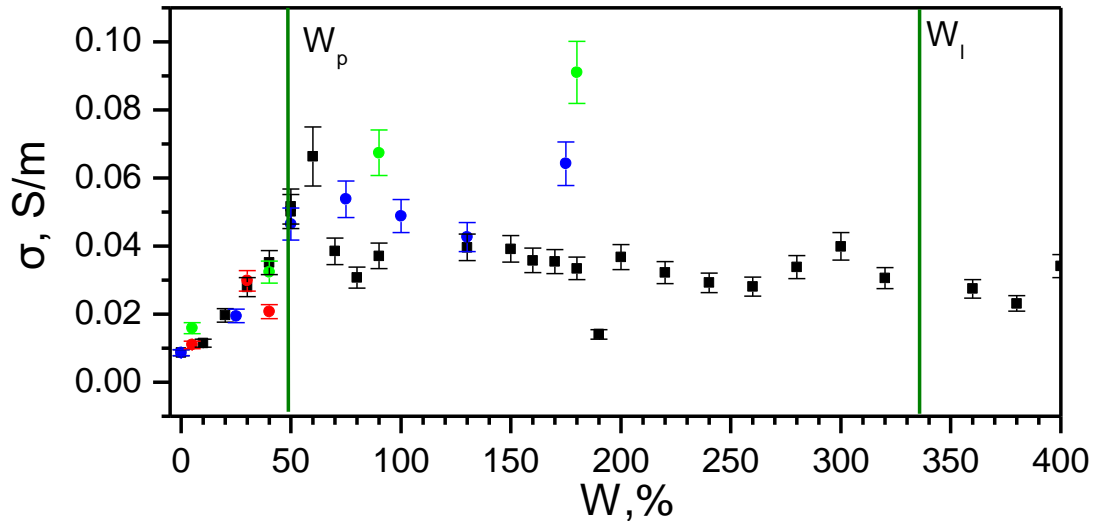


Fig. 4.16. Specific conductivities measured at different concentrations of NaCl additionally introduced into the sample. In the figure, the following notations are used: ● - non-saline sample, ● - 1% solution, ● - 2% solution, ● - 10% solution. Vertical bars indicate errors of 10%. Vertical lines mark the moistures at the plastic limit ( $W_p$ ) and liquid limit ( $W_l$ ).

The measurements of the electrophysical properties of samples with a NaCl concentration of 10% were only possible at samples moisture less than 50% since a further increase in moisture at such salinity leads to the pushing the field out of the sample, which makes it difficult to interpret the results of the experiment.

At salinities of 1 and 2%, the behavior of the electrophysical quantities against moisture qualitatively coincides with their behavior in the “Dusch” bentonite.

In figures 4.15 and 4.16, the vertical lines show the moisture values at the plastic and liquid limits of the Kutch bentonite given in Table 4.10. As in the case of Dusch bentonite, the moisture at the plastic limit is characterized by a value less than 50%. At this moisture, local maxima of the dielectric constant (Figure 4.15) and conductivity (Figure 4.16) are formed.

The liquid limit moisture value of the “Kutch” bentonite turned out to be almost two times higher (335.7%) than that of the bentonite “Duch” (163.2). In the

vicinity of this moisture value (300%) special points are seen in the dielectric constant and conductivity graphs.

### **4.3.3. Electrophysical properties of bentonite "Zir"**

To assess the effect of additional salinity of the "Kutch" bentonite on dielectric constant and conductivity, we used the samples of various moistures, prepared according to the technology described in sections 4.3.1.1 and 4.3.1.2.

The measurement results are presented in Figures 4.17 and 4.18.

The measurement of electrophysical properties of samples with a NaCl concentration of 10% was performed only at moistures less than 60% since a further increase in moisture at such salinity leads to the pushing the field out of the sample, which makes it difficult to interpret the results of the experiment.

At salinities of 1 and 2%, the behavior of the electrophysical quantities against humidity qualitatively coincides with their behavior in the bentonite "Duch" and "Kutch".

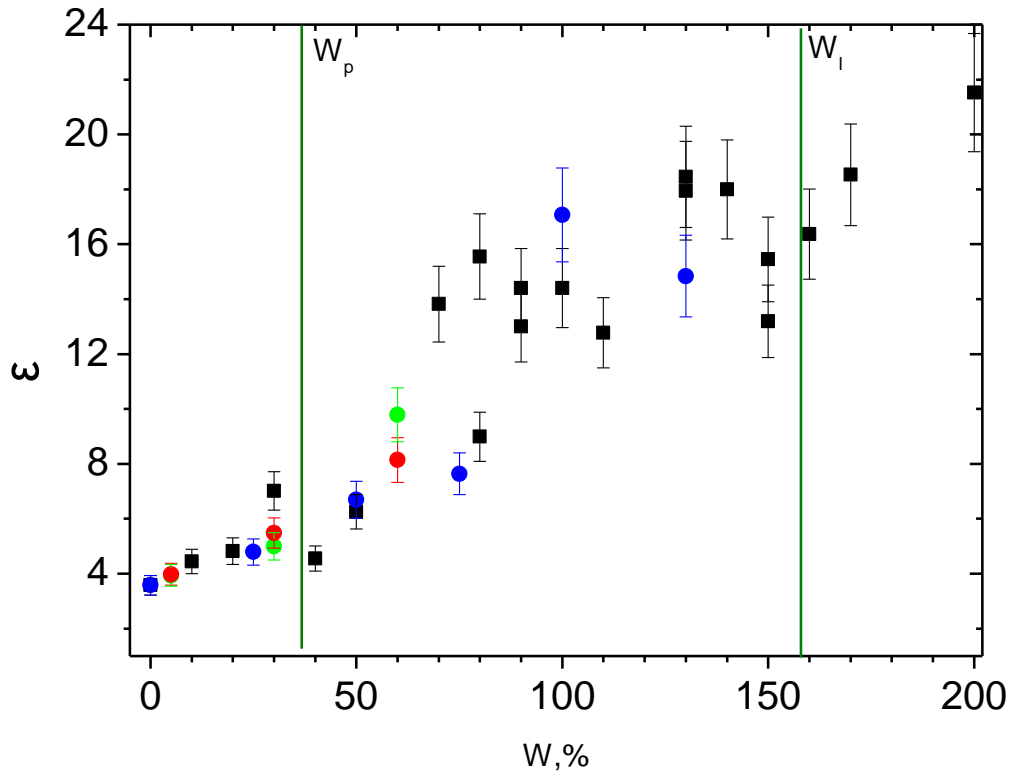


Fig. 4.17. Dielectric constant measured at different concentrations of NaCl additionally introduced into the sample. In the figure, the following notations are used: ● - non-saline sample, ● - 1% solution, ● - 2% solution, ● - 10% solution. Vertical bars indicate errors of 10%. Vertical lines mark the moistures at the plastic limit ( $W_p$ ) and liquid limit ( $W_l$ ).

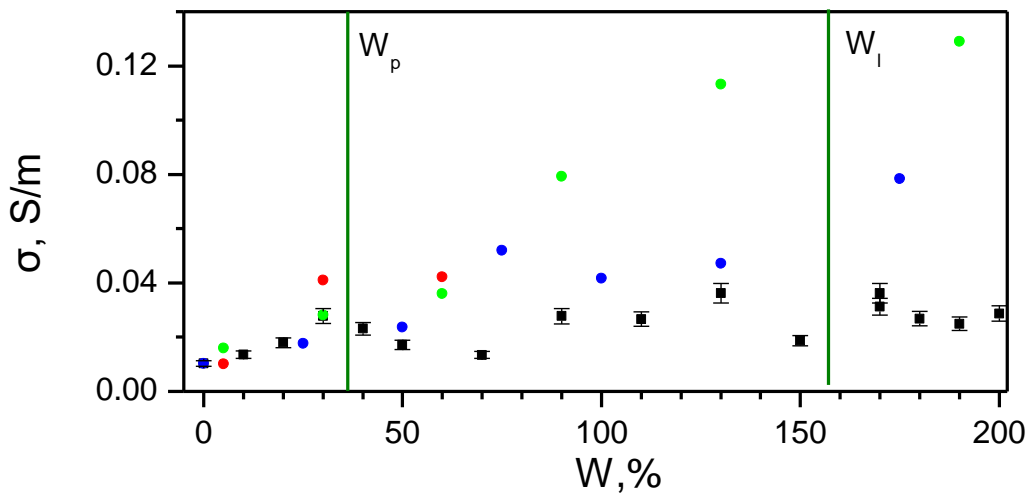


Fig. 4.18. Specific conductivities measured at different concentrations of NaCl additionally introduced into the sample. In the figure, the following notations are used: ● - non-saline sample, ● - 1% solution, ● - 2% solution, ● - 10% solution. Vertical bars indicate errors of 10%. Vertical lines mark the moistures at the plastic limit ( $W_p$ ) and liquid limit ( $W_l$ ).

In Figures 4.17 and 4.18, the vertical lines show the moisture values at the plastic and liquid limits of the «Zir» bentonite given in Table 4.10. As in the case of the “Dusch” bentonite, the moisture at the plastic limit is characterized by a value less than 50%. At this moisture, local maxima of the dielectric constant (Figure 4.17) and conductivity (Figure 4.18) are formed.

The liquid limit moisture value of the “Kutch” bentonite (158.4) differ little from that of the bentonite “Duch” (163.2). In the vicinity of this moisture value special points are seen in the dielectric constant and conductivity graphs.

#### 4.4. Comparison of electrophysical properties of bentonites

For a quantitative comparison of the electrophysical properties of bentonites, their dielectric constant and conductivity are shown in Figures 4.19 and 4.20 along with lines marking the moisture values at the plastic ( $W_p$ ) and liquid ( $W_l$ ) limits.

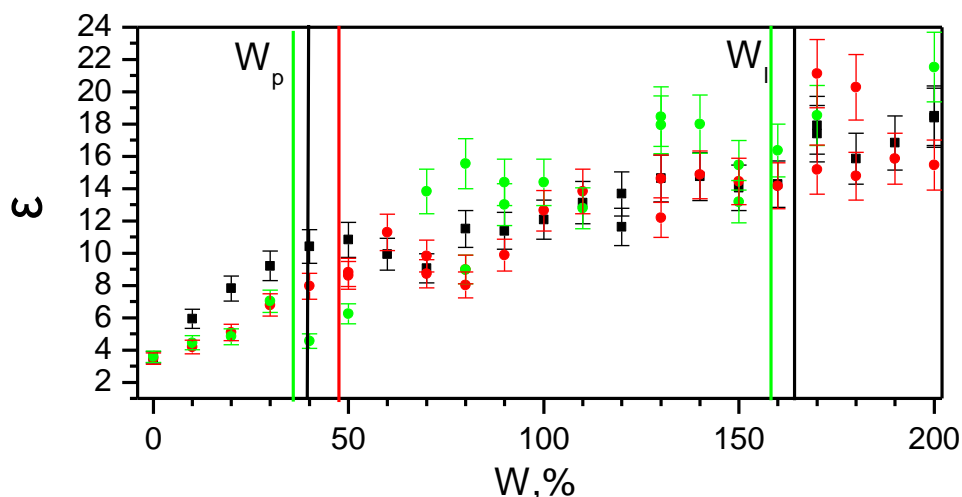


Fig. 4.19. Dielectric constant of bentonites (● - Duch; ● - Kutch; ● - Zir). Vertical bars indicate errors of 10%. Vertical lines mark the moistures at plastic limits ( $W_p$ ) and liquid limits ( $W_l$ ).

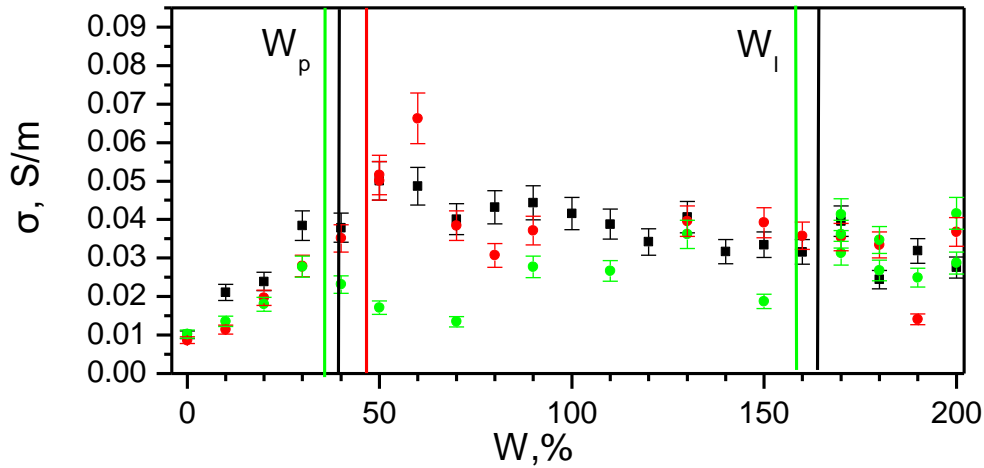


Fig. 4.20. Specific conductivity of bentonites (● - Duch; ● - Kutch; ● - Zir). Vertical bars indicate errors of 10%. Vertical lines mark the moistures at plastic limits ( $W_p$ ) and liquid limits ( $W_l$ ).

Comparison of the above data allows to note that:

- at the moisture regions near the plastic limits, the position of special points (local maxima) on the plots of dielectric constant and conductivity at  $W = 50\%$ ,  $60\%$  and  $30\%$ , correlates with respective values from Table 4.10 (39.4%, 47.7%, and 39.4%);
- the scatter of the experimental dielectric constant and specific conductivity for bentonites that differ in the composition of exchange ions, with the exception of a few points, is about 20%.

#### 4.5. Electrophysical properties of kaolinite "KZHV"

The kaolin concentrate Zhuravliniy Log is characterized by the presence of the main rock-forming mineral kaolinite (89–92%), quartz (5–7%), microcline up to 4%, as well as the presence of an irregular smectite phase. The composition contains kaolinite, illite, quartz and microcline. Montmorillonite (smectite), as an independent mineral phase, has not been found.

To study the electrophysical properties and to assess the effect of additional salinity of the "KZhV" type kaolinite on dielectric constant and conductivity, the

samples of different moisture were used, obtained according to the technology described in sections 4.3.1.1 and 4.3.1.2.

The measurements results are presented in Figures 4.21 and 4.22.

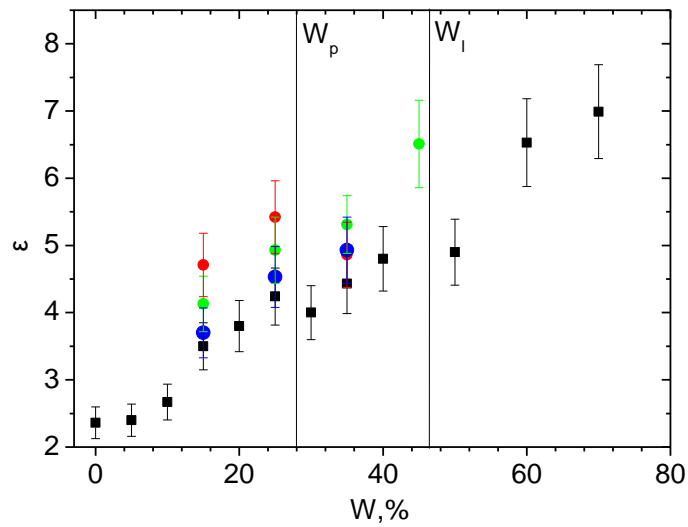


Fig. 4.21. Dielectric constant measured at different concentrations of NaCl additionally introduced into the sample. In the figure, the following notations are used: ● - non-saline sample, ● - 1% solution, ● - 2% solution, ● - 10% solution. Vertical bars indicate errors of 10%. Vertical lines mark the moistures at the plastic limit ( $W_p$ ) and liquid limit ( $W_l$ ).

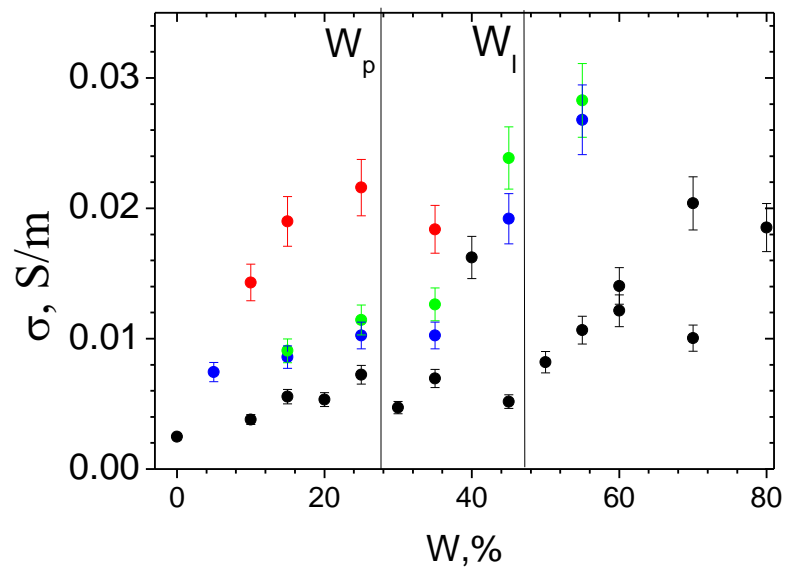




Fig. 4.22. Specific conductivities measured at different concentrations of NaCl additionally introduced into the sample. In the figure, the following notations are used: ● - non-saline sample, ● - 1% solution, ● - 2% solution, ● - 10% solution. Vertical bars indicate errors of 10%. Vertical lines mark the moistures at the plastic limit ( $W_p$ ) and liquid limit ( $W_l$ ).

Measurement of the electrophysical properties of samples with a NaCl concentration of 10% was performed only at moistures less than 35%, since a further increase in moisture at such salinity leads to the pushing the field out of the sample, which complicates the interpretation of the experimental results.

At salinities of 1% and 2%, the variation of electrophysical quantities of the “KZhV” kaolinite with moisture qualitatively coincides with their behavior in bentonites. The most noticeable difference is the increase in electrophysical parameters at humidities above the plastic limit.

#### **4.6. Comparison of the electrophysical properties of bentonites, kaolinite, and sand**

Figures 4.23 and 4.24 show the dielectric constant and specific conductivity of the bentonites used in this work and additionally salted with a 2% NaCl solution.

Figure 4.23 shows that the introduction of additional ions in the considered range of humidity:

- do not lead to a difference in dielectric permeabilities within the error intervals with the exception of the  $W = 90\%$  point;
- it does not allow distinguishing the predominant mineral (montmorillonite or kaolinite) in samples.

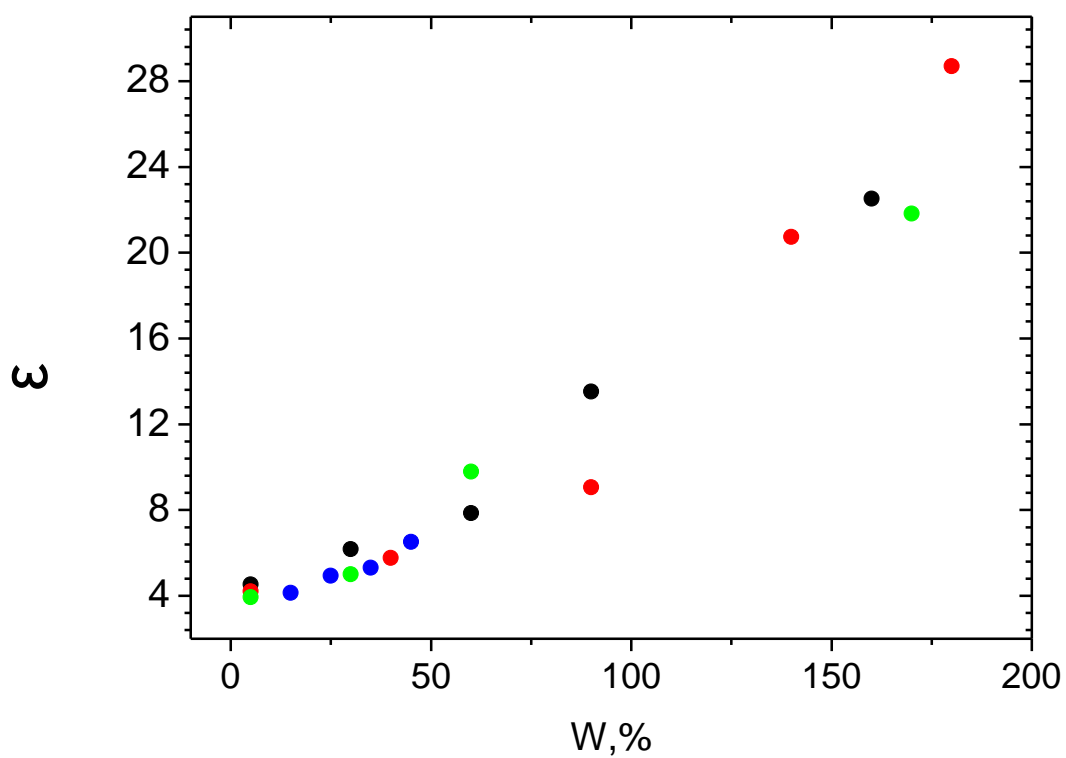


Fig. 4.23. Dielectric constant of samples with a 2% concentration of salt NaCl additionally introduced into the sample. In the figure, the following notations are used: (bentonites: ● - Dusch; ● - Kutch; ● - Zir, and ● - KZhV kaolinite).

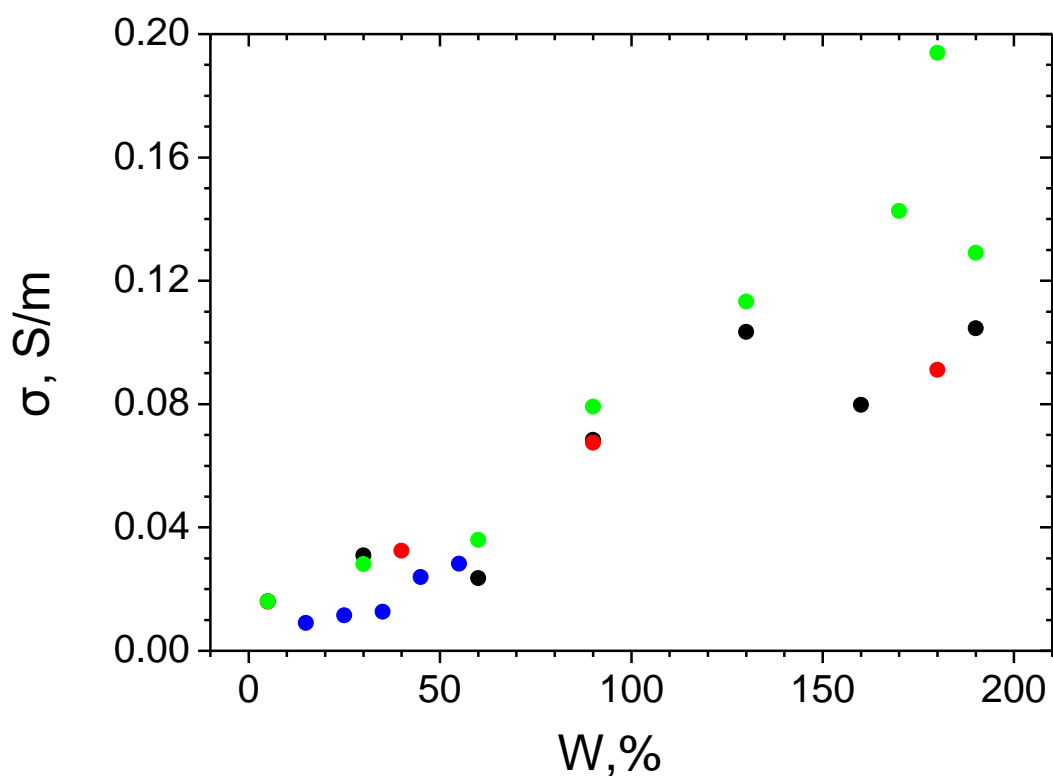


Fig. 4.24. Specific conductivity of samples with a 2% concentration of salt NaCl additionally introduced into the sample. In the figure, the following notations are used: (bentonites: ● - Dusch; ● - Kutch; ● - Zir, and ● - KZhV kaolinite).

Figure 4.24 shows that the introduction of additional ions in the moisture range up to 50%, the specific conductivities of bentonites are approximately twice as large as those of kaolinite.

In Figures 4.25 and 4.26 dielectric constants and specific conductivities of the “Dusch” bentonite, “KZhV” kaolinite, and sand are compared.

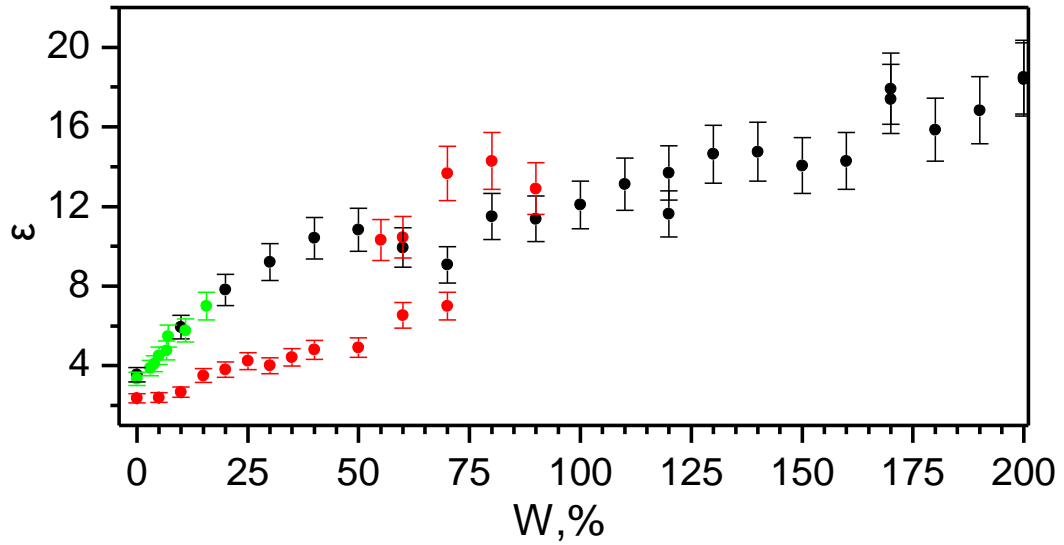


Fig. 4.25. Dielectric constant of minerals. The following notations are used in the figure: (● - Dusch; ● - KZhV; ● - sand). Vertical bars indicate errors of 10%.

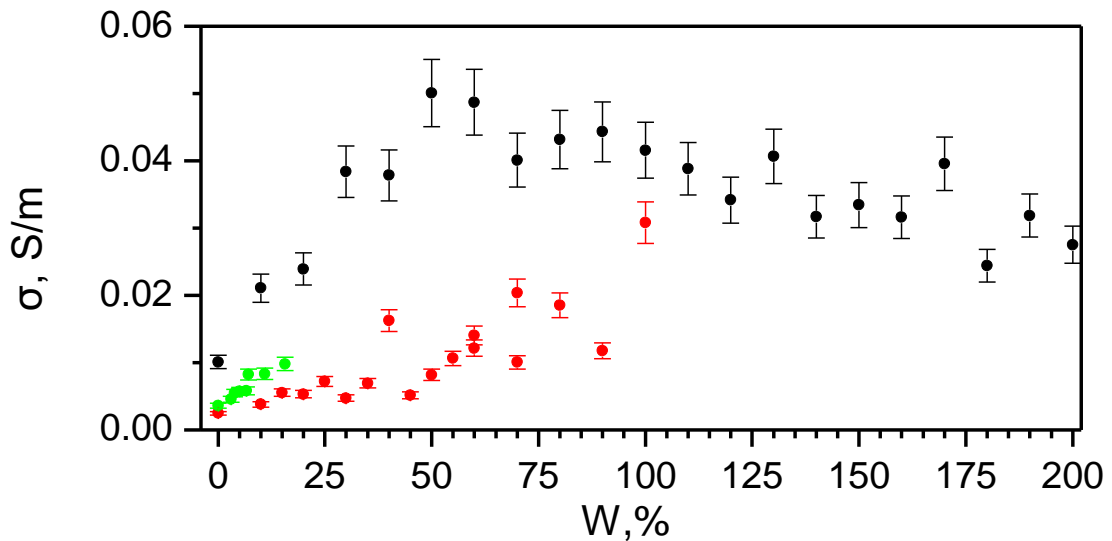


Fig. 4.26. Specific conductivity of minerals. The following notations are used in the figure: (● - Dusch; ● - KZhV; ● - sand). Vertical bars indicate errors of 10%.

Figure 4.25 shows that at moistures under 15%, the dielectric constant of sand and bentonite differs slightly, and it is approximately two times greater than that of kaolinite. This relationship between the dielectric constant of bentonite and

kaolinite can be seen up to moisture close to the liquid limit (46.1%) above which free water begins to form in the sample of kaolinite; now it determines the dielectric constant of the sample. At a moisture of about 75%, the dielectric constant of the kaolinite sample is close to that of bentonite at a moisture content beyond its liquid point (163.2%).

This circumstance should be taken into account when interpreting the GPR data.

It can be seen from Figure 4.26 that at moistures under 15%, specific conductivity of bentonite differs from that of sand approximately two times, and from that of kaolinite, four times. A further increase in moisture content up to the liquid limit of kaolinite leads to an increase in the difference in specific conductivities of clays based on montmorillonite and kaolinite. This circumstance explains the limited applicability of the GPR method in low-resistance clays that are in a natural state of humidity. A further increase in the moisture content of bentonite leads to a decrease in the value of specific conductivity, which may be due to a decrease in the density of ions in the sample, the number of which is determined by the composition of bentonite.

#### **4.7. Conclusions**

1. At moistures under 15%, the dielectric constant and specific conductivity of the sand studied in the work allows linear approximation.
2. The introduction of additional ions of salts of NaCl, KCl and BaCl<sub>2</sub> to the sand at a salt concentrations under 0.3%, does not lead to the changes in dielectric constant within the accuracy of 10%. The variation in conductivity obeys a linear law.
3. The introduction of ions into NaCl in the sample of sand with a moisture content of 5% leads to an increase in the specific conductivity up to 3 times while maintaining the value of the dielectric constant.
4. The change in conductivity with the introduction of salt ions allows creating a method for determining the salinity of construction materials;

5. The binding of ions by freezing free water leads to a decrease in the specific conductivity while the dielectric constant do nit vary within the measurements error.
6. For samples of the "Dusch" type bentonite prepared using 1% and 2% NaCl solution, there is a tendency to increase in dielectric constant and conductivity
7. The use of a 10% NaCl solution for the manufacturing the "Dusch" bentonite samples with moisture under 50% does not lead to a noticeable change in the electrophysical values; this indicates a slight dependence of conductivity on salinity at low samples moisture.
8. The formation of surface-bound water is completed in cohesive soils at moisture at the plastic limit. In the vicinity of this moisture, special points are observed on the plots of dielectric constant and specific conductivity against moisture.
9. At the moistures of plastic limits of bentonites (Dusch, Kutch, Zir) the positions of the specific points (local maxima) on the graphs of dielectric constant and conductivity at moistures of 50%, 60% and 30% correlate with the plastic limit values  $W_p$  equal to 39 , 4, 47.7% and 39.4%.
10. The scatter of experimental results for the dielectric constant and specific conductivity for bentonites, differing in the composition of exchange ions, except for a few points, is about 20%.
11. At moisture under 15%, the dielectric constants of sand and bentonite differ slightly and are approximately twice as large as that of kaolinite. This relationship between the dielectric constant of bentonite and kaolinite can be seen up to a moisture close to the liquid limit (46.1%), when free water begins to be formed in the sample of kaolinite. This circumstance should be taken into account when interpreting GPR data.
12. At moistures under 15%, the specific conductivity of bentonite differs from that of sand by about two times, and from that of kaolinite, by four times. A further increase in moisture content up to the kaolinite liquid limit leads to an increase in the difference in the specific conductivities of clays based on montmorillonite and kaolinite. This circumstance explains the limited applica-

bility of the GPR method in low-resistance clays that are in a natural state of humidity.

## **General conclusions**

The methods for determining the electrophysical properties of ground materials considered in **Chapter 1** significantly expand the capabilities of the method for diagnosing structural layers of artificial structures, which will allow the transformation of an indicative GPR method into a method for geophysical measurement. In this context, in this study, the problem of the development of the GPR method for determining the electrophysical properties of soils on the basis of integration with optical and resonant methods has been solved.

Successful and timely implementation of anti-deformation and repair activities on extended transport infrastructure depends largely on the speed of analysis of moisture content and degradation of structural layers. In **Chapter 2**, in the framework of classical electrodynamics, a method has been developed for determining the absolute refractive indices of structural layers and corresponding attenuation coefficients in the microwave range of 1200–1700 MHz, based on the quantitative processing of GPR data. The developed method of processing the GPR data is based on the use of amplitudes of reflected waves; it makes it possible to determine dielectric constants and electrical conductivities of structural layers with an error of not more than 10-15%. This makes it promising for the use in software systems for the automatic processing of GPR information when monitoring the state of extended sections of roads and railways.

Traditionally, the density and moisture of soils are determined by destructive methods, for example, by drilling and sampling. These methods are characterized by high accuracy of measurements, however, they are relatively expensive and time consuming, they also require a stopping of the traffic on the surveyed site for the duration of the measurements. To overcome these difficulties, it is increasingly recommended to use a non-destructive GPR method, which allows one to obtain continuous information about the state of soil layers, both in the detailed diagnostics mode and as part of specialized diagnostic mobile tools (railway cars, matrices and automobiles). For its effective use in solving problems of quantitative diagnos-



tics of infrastructure facilities, the procedure of integration of GPR methods and the methods of direct measurements of electrophysical properties of soils and materials seems promising. In this regard, **Chapter 3** solves the problem of developing a technique for resonant measurements of the dielectric constant and specific conductivity of soil-forming minerals at different moistures at a frequency of 1400 MHz. As a result, Methods for determining the complex dielectric constant and moisture by the GPR method, calibrated by laboratory measurements, are proposed and assessed. The developed approach allows rapid diagnosing the state of extended objects, since it combines the advantages of the high-speed GPR method with a limited number of calibration measurements.

In order to effectively apply the GPR method for solving problems of quantitative diagnostics, when planning experiments, it is necessary to take into account depth limitations that are directly related to the specific conductivity of soils and materials. This physical characteristics, in turn, are determined by the moisture and mineralization of soils and materials. High-depth of GPR research in sands, ice and rocks are possible, whereas only low depth GPR studies in low-resistivity clays are feasible. In this regard, in **Chapter 4**, the effect of moisture and salinity on the conductivity of some soil-forming minerals is studied using the method of resonance measurements. The dependences of the dielectric constant and specific conductivity on the moisture have been investigated in a number of bentonites with different composition of exchangeable ions. A correlation between these electrophysical quantities and the plasticity of bentonites is established

## References

1. ASCE CI/ASCE38-02. American Society of Civil Engineer Standard Guideline for the Collection and Depiction of Existing Subsurface Utility Data. – URL: <http://www.asce.org/templates/publications-book-detail.aspx?id=8162>.
2. ASTM D6432-11. Standard Guide for Using the Surface Ground Penetrating Radar Method for Subsurface Investigation. – URL: <https://www.astm.org/Standards/D6432.htm>
3. ICE PAS 128: 2014. British Standard: Specification for Underground Utility Detection, Verification and Location Institute of Civil Engineer. – URL: <https://www.ice.org.uk/eventarchive/publically-available-specification-128-launch>.
4. CEI-883. Regulations for Performing Preliminary Surveys with Ground-probing Radar for Before Laying Underground Utilities and Infrastructures. – URL: <http://yadda.icm.edu.pl/yadda/element/bwmeta1.element.baztech-b014ca2a-3a66-496b-a536-31fe1f74eab5>.
5. Euro GPR guideline. Policy on Utility Detection. URL: <http://www.eurogpr.org/vn2/index.php/introduction-to-gpr/guidelines> (дата обращения 08.08.2018).
6. Ground penetrating radar applications, principles, procedures. Mississauga / A. P. Annan. – Canada: Sensors and Software, 2004. – P. 278.
7. Subsurface radar issues. Collective monograph / A.Yu. Grinev; by ed. A.Yu. Grineva. - M., 2005. - 34 p.
8. Introduction to GPR / M.L. Vladov, A.V. Starovoytov. - M.: Publishing House of MSU, 2004. - 153 p.
9. Davis J., Annan A. Ground-penetrating radar for high resolution mapping of soil and rock stratigraphy: geophysical prospecting // Geophysical Prospecting – 1989. – Vol. 37. – P. 531–51.
10. Daniels D.J. Ground Penetrating Radar. – London: The Institution of Electrical Engineers, 2004. – 726 p.
11. Conyers L.B., Goodman D. Ground-penetrating Radar. – Walnut: Alta Mira Press, 1997. – 232 p.

12. Jol H.M. Ground penetrating radar theory and applications. – Oxford: Elsevier; 2009. – 544 p.
13. Benedetto A., Pajewski L. Civil engineering applications of ground penetrating radar. – London: Springer, 2015. – 371 p.
14. Slob E., Sato M., Olhoeft G. Surface and borehole ground-penetrating-radar developments // *Geophysics* – 2010. – Vol. 75, No.5. P. 75A103-75A120.
15. *Antennas and Screening* / E. C. Utsi, Ed.: E. C. Utsi. – Butterworth-Heinemann, 2017. – P. 93–104.
16. Congedo F., Monti G., Tarricone L. Modified bowtie antenna for GPR applications // *Proceedings of the XIII International Conference on Ground Penetrating Radar / Lecce: IEEE, 2010. – P. 1–5.*
17. Turk A. S., Nazli H. Hyper-wide band tem horn array design for multi band ground-penetrating impulse radar // *Microwave and Optical Technology Letters* – 2008. – Vol. 50, No.1. – P. 76 - 8.
18. Yavna V. A., Khakiev Z. B., Bilalov A. V., Morozov V. A. Broadband directional antennas for monitoring the state of the ballast section of a railway track // *Abstracts of the reports of the second international scientific-practical conference “Engineering Geophysics - 2006 ”/ M., 2006. - P.82-83.*
19. Rial F. I., Pereira M., Lorenzo H., Arias P., Novo A. Resolution of GPR bowtie antennas: An experimental approach // *Journal of Applied Geophysics* – 2009. – Vol. 67, No.4, P. 367-373.
20. Xu X., Miller E. L., Rappaport C. M., Sower G. D. Statistical method to detect subsurface objects using array ground-penetrating radar data // *IEEE Transactions on Geoscience and Remote Sensing* – 2002. – Vol. 40, No.4. P. 963-976.
21. Kikuchi K., Mikada H., Takekawa J. Improved imaging capability of phased array antenna in Ground Penetrating Radar survey // *79th EAGE Conference and Exhibition 2017 / Paris: EAGE, 2017. – P. 1–5.*
22. Lutz P., Perroud H. Phased-array transmitters for GPR surveys // *Journal of Geophysics and Engineering*. – 2006. Vol. 3, No.1. P.35–42.

23. Huston D., Xia T., Zhang Y., Fan T., Razinger J., Burns D. Tri-band ground penetrating radar for subsurface structural condition assessments and utility mapping (2016) Transforming the Future of Infrastructure through Smarter Information // Proceedings of the International Conference on Smart Infrastructure and Construction / Cambridge: ICSIC, 2016. – P. 283-287.
24. Brunzell H. O., Ericsson A. Dual-antenna impulse radar for improved detection of buried land mines // Proceedings of SPIE - The International Society for Optical Engineering – 1998. – Vol. 3392. – P. 725-734.
25. Rachmana N., Hendrawan S., Suksmono A.B. Interpretation target pattern of a buried basic object on surface Ground Penetrating radar system // International Journal on Electrical Engineering and Informatics – 2009. – Vol. 1, No.1. P. 553-558.
26. Al-Nuaimy W., Huang Y., Nakhkash M., Fang M. T., Nguyen V. T., Eriksen A. Automatic detection of buried utilities and solid objects with GPR using neural networks and pattern recognition // Journal of Applied Geophysics – 2000. – Vol. 43, No.2–4. P. 157–165.
27. Shihab S., Al-Nuaimy W., Eriksen A. Image processing and neural network techniques for automatic detection and interpretation of ground penetrating radar data // Proceedings of the 6th International Multi-Conference on Circuits, Systems, Communications and Computers / Crete: WSEAS, 2002. – P. 1–4.
28. Ahmadi R., Fathianpour N. Estimating geometrical parameters of cylindrical targets detected by ground-penetrating radar using template matching algorithm // Arabian Journal of Geosciences – 2017. Vol. 10, No.6. P. 140.
29. Lanka M., Butler A., Sterling R. Use of approximate reasoning techniques for locating underground utilities // Tunnelling and Underground Space Technology – 2001. – Vol. 16. – P. 13-31.
30. Simi A., Bracciali S., Manacorda G. Hough transform based automatic pipe detection for array GPR: Algorithm development and on-site tests // In Proceedings of the 2008 IEEE Radar Conference / Rome: IEEE, 2008. – P. 1–6.

31. Dolgiy A., Dolgiy A., Zolotarev V. Optimal Radius Estimation for Subsurface Pipes Detected by Ground Penetrating Radar // 11 th International Conference on Ground Penetrating Radar / Columbus Ohio: IEEE, 2006. – P. 1–8.
32. O’Leary P., Zsombor-Murray P, Direct and specific least-square fitting of hyperbolae and ellipses // Journal of Electronic Imaging – 2004. – Vol. 13. P. 492–503.
33. Ristic A.V., Petrovacki D., Govedarica M. A new method to simultaneously estimate the radius of a cylindrical object and the wave propagation velocity from GPR data // Computers and Geosciences – 2009. – Vol. 35, No. 8. P. 1620-1630.
34. Shihab S., Al-Nuaimy W. Radius estimation for cylindrical objects detected by ground penetrating radar // Subsurface Sensing Technologies and Applications – 2005. – Vol. 6, No. 2. P. 151-166.
35. Jafrasteh B., Fathianpour N. Automatic extraction of geometrical characteristics hidden in ground-penetrating radar sectional images using simultaneous perturbation artificial bee colony algorithm // Geophysical Prospecting – 2017. – Vol. 65, No.1. P. 324-336.
36. Mertens L., Persico R., Matera L., Lambot S. Automated detection of reflection hyperbolas in complex GPR images with no a priori knowledge on the medium // IEEE Transactions on Geoscience and Remote Sensing – 2016. – Vol. 54. P. 580–596.
37. Liu T., Klotzsche A., Pondkule M., Vereecken H., Van Der Kruk J., Su Y. Estimation of subsurface cylindrical object properties from GPR full-waveform inversion // 2017 9th International Workshop on Advanced Ground Penetrating Radar, IWAGPR 2017 / Edinburgh: IEEE, 2017. – P. 1-6.
38. Vladov, M., Starovoitov, A. Introduction to the GPR. Publishing House of Moscow State University, 2004, 214 pp.
39. Grinev, A. Sub-surface radar issues. Moscow, Radiotekhnika, 2005, 416 pp.
40. Craddock, I. Antennas for Ground-penetrating Radar (Book Chapter) 2006, Ultra Wideband Antennas and Propagation for Communications, Radar and Imaging, pp. 413-435.

41. Z.B. Khakiev, V.A Bilalov, A.V Morozov and V.A. Yavna. Improving GPR monitoring of track ballast and railway structural integrity / Z.B // First break – 2009. V. 27. – P. 93-95.
42. Hai Liu, ,Motoyuki Sato. In situ measurement of pavement thickness and dielectric permittivity by GPR using an antenna array [Текст] // NDT & E International. Volume 64, June 2014, Pages 65–71.
43. M.U. Ahmed, R.A. Tarefder, A.K. Maji. Incorporating transmitter–receiver offset to interpret pavement layer thicknesses by GPR. Case Studies in Nondestructive Testing and Evaluation/ Volume 6, Part A, November 2016, Pages 94–104.
44. Shangguan, P., Al-Qadi, I.L., Lahouar, S. Pattern recognition algorithms for density estimation of asphalt pavement during compaction: A simulation study, 2014, Journal of Applied Geophysics 107, pp. 8-15
45. Tong, Z., Gao, J., Zhang, H. Recognition, location, measurement, and 3D reconstruction of concealed cracks using convolutional neural networks. Construction and Building Materials, 2017, 146, pp. 775-787
46. Xie, X., Qin, H., Yu, C., Liu, L. An automatic recognition algorithm for GPR images of RC structure voids, 2013, Journal of Applied Geophysics, 99, pp. 125-134
47. The development of a multi-channel GPR system for roadbed damage detection [Текст] / Xianlei Xu, Suping Peng, Yunhai Xia, Wanjun Ji // Microelectronics Journal. Volume 45, Issue 11, November 2014, Pages 1542–1555.
48. An innovative vehicle-mounted GPR technique for fast and efficient monitoring of tunnel lining structural conditions [Текст] / Yuewen Zana, Zhilin Lia, GuofengSua, XiyuanZhangb // Case Studies in Nondestructive Testing and Evaluation. Volume 6, Part A, November 2016, Pages 63–69
49. Evaluating the effectiveness of methods based on reflected GPR signal for determining the clogging of the ballast layer [Текст] / Khakiev Z.B., Yavna V.A., Ermolov K.M. // 12th Conference and Exhibition Engineering Geophysics 2016 12. 2016. C. 203-210.

50. Identification of type and degree of railway ballast fouling using ground coupled GPR antennas [Текст] / P. Anbazhagan, P.S. Naresh Dixit , T.P. Bharatha // Journal of Applied Geophysics. Volume 126, March 2016, Pages 183–190.
51. Benedetto, A., Tosti, F., Bianchini Ciampoli, L., (...), Brancadoro, M.G., Alani, A.M. Railway ballast condition assessment using ground-penetrating radar – An experimental, numerical simulation and modelling development. Construction and Building Materials, 2017, 140, pp. 508-520
52. Benchmarking large scale GPR experiments on railway ballast [Текст] /R. De Bold, G. O'Connor, J.P. Morrissey, M.C. Forde // Construction and Building Materials/ Volume 92, 1 September 2015, Pages 31–42. Railway Engineering-2013
53. GPR determination of physical parameters of motor road and railway structural layers [Текст] / Z. Khakiev, V. Shapovalov, A. Kruglikov, V. Yavna // Journal of Applied Geophysics 106 (2014) 139–145
54. Investigation of long term moisture changes in trackbeds using GPR [Текст] /Vladimir Shapovalov, Alexander Kruglikov, Andrey Morozov, Victor Yavna, Zelimkhan Khakiev//Journal of Applied Geophysics 110C, (2014), pp. 1-4.DOI:10.1016/j.jappgeo.2014.08.014
55. Determination of the complex permittivity and soil moisture by GPR [Текст] /Khakiev Z.B., Yavna V.A., Sulavko S.N., Kislitsa K. //12th Conference and Exhibition Engineering Geophysics 2016 12. 2016. C. 226-234.
56. Marecos, V., Solla, M., Fontul, S., Antunes, V. Assessing the pavement subgrade by combining different non-destructive methods. Construction and Building Materials, 2017, 135, pp. 76-85
57. Experimental study of soil compaction effects on GPR signals [Текст] / Ping Wang, Zhenqi Hu, Yanling Zhao, Xinju Li // Journal of Applied Geophysics. Volume 126, March 2016, Pages 128–137
58. Investigation of the freeze–thaw states of foundation soils in permafrost areas along the China–Russia Crude Oil Pipeline (CRCOP) route using ground-penetrating radar (GPR) [Текст] /Yongping Wang, Huijun Jin, , Guoyu Li//Cold Regions Science and Technology. Volume 126, June 2016, Pages 10–21.

59. Silvast, M., Nurmikolu, A., Wiljanen, B., Levomäki, M. Identifying frost-susceptible areas on Finnish railways using the ground penetrating radar technique, 2013, Proceedings of the Institution of Mechanical Engineers, Part F: Journal of Rail and Rapid Transit 227(1), pp. 3-9
60. Ameri, M., KashaniNovin, M., Yousefi, B. Comparison of the field measurements of asphalt concrete densities obtained by ground-penetrating radar, pavement quality indicator and the borehole coring methods. 2014. Road Materials and Pavement Design, 15(4), pp. 759-773
61. Dong, Z., Ye, S., Gao, Y., Fang, G., Zhang, X., Xue, Z., Zhang, T. Rapid detection methods for asphalt pavement thicknesses and defects by a vehicle-mounted ground penetrating radar (GPR) system. Sensors (Switzerland), 2016, 16(12), 2067
62. Estimation of in-situ density and moisture content in HMA pavements based on GPR trace reflection amplitude using different frequencies [Текст] / Christina Plati, Andreas Loizos // Journal of Applied Geophysics. Volume 97, October 2013, Pages 3–10.
63. GPR abilities in investigation of the pavement transversal cracks [Текст] / Lech Krysiński, Jacek Sudyka // Journal of Applied Geophysics. Volume 97, October 2013, Pages 27–36.
64. Trela, C., Wöstmann, J. Non-destructive imaging of reinforcement bars in circular concrete columns using radar technique | [Zerstörungsfreie Bewehrungsartung an runden Betonstützen mit Impulsradar], 2015, Beton- und Stahlbetonbau 110(8), pp. 511-520
65. Lachowicz, J., Rucka, M. Application of GPR method in diagnostics of reinforced concrete structures. Diagnostyka, 2015, 16(2), pp. 31-36
66. Wiwatrojanagul, P., Sahamitmongkol, R., Tangtermsirikul, S., Khamsemanan, N. A new method to determine locations of rebars and estimate cover thickness of RC structures using GPR data. Construction and Building Materials, 2017, 140, pp. 257-273
67. Robust adaptive detection of buried pipes using GPR [Текст] / Q. Hoarau, G.



- Ginolhac, A.M. Atto, J.M. Nicolas, // Signal Processing. Volume 132, March 2017, Pages 293–305.
68. A three dimensional approach for tracking cracks in bridges using GPR [Текст] /Andrea Benedetto //Journal of Applied Geophysics. Volume 97, October 2013, Pages 37–44.
69. Applications of ground penetrating radar (GPR) in bridge deck monitoring and assessment [Текст] /Amir M. Alania, MortezaAboutalebi, GokhanKilic // Journal of Applied Geophysics. Volume 97, October 2013, Pages 45–54.
70. Field observations and numerical models of GPR response from vertical pavement cracks [Текст] /Nectaria Diamanti, David Redman // Journal of Applied Geophysics. Volume 81, June 2012, Pages 106–116.
71. Hong, S., Lai, W.-L., Helmerich, R. Experimental monitoring of chloride-induced reinforcement corrosion and chloride contamination in concrete with ground-penetrating radar. 2015, Structure and Infrastructure Engineering 11(1), pp. 15-26
72. Hasan, M.I., Yazdani, N. An experimental study for quantitative estimation of rebar corrosion in concrete using ground penetrating radar, Journal of Engineering (United States), 2016,8536850
73. Kulizhnikov, A.M., Eremin, R.A. Dielectric values of various types of asphalt concrete pavements, 2015,Geophysics 2015 - 11th EAGE International Scientific and Practical Conference and Exhibition on Engineering and Mining Geophysics, pp. 34DUMMY
474. Porubiaková, A., Komačka, J. A comparison of dielectric constants of various asphalts calculated from time intervals and amplitudes. 2015, Procedia Engineering, 111, pp. 660-665
75. Rodríguez-Abad, I., Martínez- Sala, R., Mené, J., Klysz, G. Water penetrability in hardened concrete by GPR, 2014, Proceedings of the 15th International Conference on Ground Penetrating Radar, GPR 2014, 6970550, pp. 862-867
76. Rodríguez-Abad, I., Klysz, G., Martínez-Sala, R., Paul Balayssac, J., Mené-Aparicio, J. Application of ground-penetrating radar technique to evaluate the wa-

terfront location in hardened concrete. *Geoscientific Instrumentation, Methods and Data Systems*, 2016, 5(2), pp. 567-574

77. Xiao, X., Ihamouten, A., Villain, G., Dérobert, X. Use of electromagnetic two-layer wave-guided propagation in the GPR frequency range to characterize water transfer in concrete. *NDT and E International*, 2017, 86, pp. 164-174

78. Johnson, C.T., Evans, R.D. Non-destructive assessment of the rate of hydration and strength gain of concrete. 2014, *Proceedings of the 15th International Conference on Ground Penetrating Radar, GPR 2014*, 6970555, pp. 893-898

79. V. Lysyuk. Reliability of a railway track / V. S. Lysyuk, V. B. Kamensky, L. V. Bashkatova; ed. by V.S. Lysyuk. - M.: Transport, 2001. - 286 p.

80. V.L. Shapovalov, M.V. Okost, A.V. Morozov, V.A. Yavna, A.A. Vasilchenko. Monitoring the density of the subgrade soil by the GPR method. *Way and track facilities*. No. 9, 2018, pp. 7-13.

81. Pupatenko V.V. Density distribution in the bulk model of a railway subgrade. / Pupatenko V.V., Pazhentsev Ya.V. // *Bulletin of Rostov State Transport University*. 2011. № 1 (41). p. 153-159.

82. Lobanov G.V. Approaches to the study of the strength characteristics of soils as a factor of stability of floodplain-channel complexes (on an example of the basin of the upper Dniepr river). / Lobanov G.V., Polyakova A.V., Novikova M.A., Trishkin B.V., Kuznetsov D.S. // *Geographic Herald*. 2012. № 2. S. 14-21.

83. Neradovskiy L.G. Determination of the strength properties of sedimentary and intrusive rocks in the cryolithozone of southern Yakutia using the GPR method. / Neradovskiy L.G., Fedorova L.L. // *Mining information and analytical bulletin (scientific and technical journal)*. 2015. № 10. p. 201-210.

84. WANG Ping, Experimental study of soil compaction effects on GPR signals. / WANG Ping, HU Zhenqi, ZHAO Yanling, LI Xinju // *Journal of Applied Geophysics*. Volume 126, March 2016, Pages 128-137, doi: 10.1016/j.jappgeo.2016.01.019.

85. E. Forte, A new fast methodology to estimate the density of frozen materials by means of common offset GPR data. / E. Forte, M. Dossi, R.R. Colucci, M. Pipana // *Journal of Applied Geophysics* 99 (2013) 135–145
86. V.L. Shapovalov Approaches to the determination of the density of the sub-grade soil by means of a geradiolocation method during construction / V.L. Shapovalov, V.A. Yavna, M.V. Okost, Z.B. Khakiev, A.V. Morozov // *Bulletin of Rostov State Transport University*. 2018. №1.
87. Brandt A.A. Study of dielectrics at microwave frequencies. M., 1963. Moscow: Fizmatgiz, 1963. - 404 p.
88. Philippe Cosenza. Indirect determination of soil water content. E-UNSAT 2016, E3S Web of Conferences 9, 04004 (2016), DOI: 10.1051 / e3sconf / 20160904004
89. Gusev, Yu.A. Basics of dielectric spectroscopy. Tutorial. Kazan, 2008 -112 s.
90. Akhadov J.Yu., Dielectric properties of pure liquids, Moscow: Standards. 1972.- 412 p. The book is a reference manual for the dielectric properties of pure liquids.
91. Bogoroditsky NP, Volakobinsky Yu.M., Vorobev AA, Tareev VM, Theory of Dielectrics, Energy 1965. - 344 p.92. Michael Janezic. Dielectric Measurements and Resonators. Advanced Materials Metrology Project, National Institute of Standards and Technology (NIST), Boulder, Colorado, [citeseerx.ist.psu.edu](http://citeseerx.ist.psu.edu)
92. Molecular dielectrometry [Text] / A. A. Potapov; Ed. ed. P. I. Ostromensky; RAS. Siberian Branch, Dept. of Automation and Technical Physics, Irkutsk scientific center. - Novosibirsk: Science, 1994. - 284 p. - ISBN 5-02-030657-6: B. .93.
93. V. V. Volkov, V. Yu. Prischepenko, V. N. Semenov, M. A. Suslin. Microwave resonance method for the study of microwave losses in water droplets on a solid surface. *Condensed matter and interphase boundaries*, 2015, Volume 17, No. 3, P. 297—3066
94. Born, M., Wolf, E., 1999. Principles of Optics, 7th (expanded) edition Cambridge University Press, Cambridge (952 pp.).
95. Makeeva, T.G., Egorov, D.M. Dielectric properties of composite materials

based on cement of different genesis. Natural and Technical Sciences, 2013, №6, pp. 64-72.

96. Dane, J., Topp, G., 2002. Methods of Soil Analysis, Part 4 Physical Methods, Soil Science Society of America, Inc.

97. Benedetto, A. Water content evaluation in unsaturated soil using GPR signal analysis in the frequency domain, Journal of Applied Geophysics, Volume 71, Issue 1, May 2010, Pages 26-35, ISSN 0926-9851, <http://dx.doi.org/10.1016/j.jappgeo.2010.03.001>.]

98. Boyarsky, D., Tikhonov, V. The effect of coherent water on the dielectric constant of wet and frozen soils / M.: Preprint IKI RAS 2003.-48 p.

99. Tighe, S., N. Li, L. Cowe Falls and R. Haas 2000. Incorporating road safety into pavement management, Transportation Research Record, 1699:1-10.

100. A.I. Efimova, L.A. Golovan, P.K. Kashkarov, V.M. Senyavin, V.Yu. Tymoshenko. Infrared spectroscopy of low-dimensional systems: Tutorial. - St. Petersburg: "Lan" publishing house, p.2016. - 239

101. L.A. Apresyan, D.V. Vlasov, D.A. Zadorin, V.I. Krasovsky. On the model of an effective medium for particles with a complex structure. Journal of Technical Physics, 2017, V. 87, no. 1. P. 10-17.

102. Z. B. Khakiev, K.U. Kislitsa, V.A. Yavna. Efficiency evaluation of ground-penetrating radar by the results of measurement of dielectric properties of soils. Journal of Applied Physics, DOI: 10.1063/1.4770470, Vol. 112, Issue 12.

103. Topp, G.C., Davis, J.L., Annan, A.P. Electromagnetic Determination of Soil Water Content Using TDR: I. Applications to Wetting Fronts and Steep Gradients Soil Sci. Soc. Am. J. 1982. 46:672–678.  
doi:10.2136/sssaj1982.03615995004600040002x.

104. A. Kasprzhitskii, G. Lazorenko, A. Khater, V. Yavna. Mid-infrared spectroscopic assessment of plasticity characteristics of clay soils. Minerals. – 2018. – V. 8. – Issue 5. – №184 – P. 1-18.

105. V.A. Yavna, A.S. Kasprzhitsky, G.I. Lazorenko, S.N. Sulavko. Determination of the boundaries and plasticity number of clay soils using infrared spectroscopy.

10th EAGE Scientific Conference on Engineering Geophysics April 2014. DOI: 10.3997 / 2214-4609.20140358.

106. V.G. Savonenkov, E.B. Anderson, S.I. Shabalev. Clays as a geological environment for the isolation of radioactive waste “State Atomic Energy Corporation “Rosatom ”, V.G. Khlopin Radium Institute, St. Petersburg, 2012.

107. A.V. Kostin, L.V. Mostrygina, O.V. Filisteev, O.I. Bukhtoyarov Features of Silicon and Copper Ions Sorption on Bentonite Clay of the Zyryanovskoye Field of the Kurgan Region, SUSU Bulletin, No. 12, 2009.

108. B.V. Pokidko, I.A. Tutorsky, V.V. Bitt, N.M. Sklyarevskaya, P.L. Zhuravleva. The adsorption of alkyl dimethylphenylammonium chlorides and distearyl-dimethylammonium chlorides by layered silicates of various deposits and some properties of organobentonites. Colloid Journal, Vol. 71, No. 6, 2009

109. M.L.Kuleshova, V.I.Sergeev, T.G.Shimko, N.N. Danchenko. Absorbing properties of bentonite clays as a material for immobilization of radionuclides during the disposal of radioactive waste. Scientific Conference LOMONOSOV READINGS, MSU, April 2013, section of Geology <http://geo.web.ru/conf/>

110. G.M. Heydarzade, S.A. Mamedov, U.G. Osmanova, T.A. Salimova, A.I. Yagubov The use of Dash-Salakhlin sky bentonite in sorption processes. Science and world. 2016. № 11 (39). Vol. I. P46-48

111. Cherkasov A.S., Somin V.A., Komarova L.F., Kurtukova L.V. The study of the sorption properties of bentonite of the Milosky deposit and the material based on it. Polzunovsky Herald, № 3 2014, 254-259.

112. V.A. Smolko, E.G. Antoshkina. The kinetics of swelling of bentonite of Zyryanovskoe field. Bulletin of the South Ural State University. Series “Metallurgy” 2014, vol. 14, no. 2, pp. 89–91

113. V.A. Smolko, E.G. Antoshkina, Kinetics of swelling of bentonite from the Zyryanovskoye deposit, Bulletin of the Southern Urals State University. Series "Metallurgy" 2014

114. Specifications TU 5729-089-00284530-00. Kaolin dry enrichment deposit "Zhuraviny log." 2000-07-01

R. K. Taroo, B. R. Patel. Physico-Chemical Properties of Kutch Bentonite. Cryst.Res.Technol. 21, 1, 1986 p.141-144.

115. Mostalygina L.V., Elizarova S.N., Kostin A.V. Bentonite clays of Zauralye: ecology and human health: Monograph.–Kurgan: Publishing house of Kurgan State University, 2010. 148 pp.